DSPACE

https://dspace.org/

Development of protection measures for microinverters against lightning transients

Mosamane, Simisi

2022

https://hdl.handle.net/10539/35757

Downloaded from a DSpace repository. https://dspace.org/



Simisi Mosamane

Development of Protection Measures for Microinverters against Lightning Transients

Masters Dissertation

SUPERVISOR: Professor Chandima Gomes

A dissertation submitted to the Faculty of Engineering and the Built Environment, University of the Witwatersrand, Johannesburg, in fulfilment of the requirements for the degree of Master of Science in Engineering.

November, 2022

Declaration

I hereby declare that the contents of this dissertation are original, except where references are made, and was done following the registration of Master of Science in Engineering at the University of the Witwatersrand. It has not been submitted, in whole or in part, at any other institution for examination.



Simisi Mosamane, Johannesburg November, 2022

Abstract

The effects of lightning on electrical systems have been studied extensively in the past several years. Despite this establishment, lightning's induced, and indirect effects on microinverters used in photovoltaic installations (PVIs) have not been studied in detail. This includes induced overvoltages in the power cables of the solar cell arrays in the event of partial lightning currents. The lack of such information is a barrier to determining the voltage, current and energy characteristics when developing surge protection devices (SPDs) to protect photovoltaic (PV) systems with microinverter technology.

Overvoltages can destroy, degrade or cause malfunction of a PVI. Therefore, PVIs should be protected from this overvoltage risk. Furthermore, microinverters have lower voltage and current rating characteristics than central or string inverters, and therefore, on this basis, they become more sensitive to lightning stresses. Therefore, evaluation of the waveforms, representing the equivalent lightning surges, is essential in developing the necessary protection measures. This research explored this through experiment and simulation settings using COMSOL Multiphysics® and Power Systems Computer-Aided Design (PSCAD).

Induced overvoltage simulations, performed with COMSOL Multiphysics® software and validated experimentally, indicated the influence of electromagnetic coupling on PV systems caused by lightning transients. It was found that lightning currents flowing through lightning protection system (LPS) structures or the PV frame can cause transient overvoltages on the DC cabling of a PVI. The magnitudes and waveforms of these overvoltages varied as a function of several parameters, including the lightning current amplitude, protection scenario and mode of measurement. Furthermore, by injecting impulse currents at different positions using standard lightning current waveforms (8/20 μs and 10/350 μs), the induced electric field was caused by a time-varying magnetic field, which further induced an emf (electromotive force) on the DC cables of the PV panel. Based on these findings, the induced overvoltages on the DC cables of a solar panel, which can go up to several kilovolts in extreme impulse currents, can exceed the impulse withstand voltage of microinverters.

The protection of the microinverter against lightning transients was also investigated by simulation using PSCAD software, where surge protection in the form of Metal Oxide Varistor (MOV) was connected to the DC cables of the PV system with a microinverter. This

investigation measured the energy overload and the current flowing through the SPD caused by lightning-induced overvoltages. The results demonstrated that a class II internal SPD seems appropriate for PV installations with a microinverter with and without LPSs for impulse currents not exceeding 20 kA.

Keywords: microinverter, lightning protection system, PV system, lightning-induced overvoltage, impulse current, surge protection device (SPD)

Acknowledgements

This work would not have been possible without certain people who offered their generous assistance during the research.

And therefore, I would like to take this opportunity to thank Prof. Chandima Gomes, my primary academic advisor and supervisor, for his invaluable input and guidance throughout the study and writing process. And sincerest thanks to Prof. John Van Coller from the University of the Witwatersrand's Centre of Excellence in High Voltage Engineering for his inputs. Furthermore, it would be a disgrace not to acknowledge the University of the Witwatersrand High Voltage Laboratory team, Mr Sfiso Mtsweni and Mr Ronnet Diale, whose contribution to the laboratory experiments cannot go unnoticed. Finally, I thank the University of Witwatersrand's School of Electrical and Information Engineering staff for providing a suitable working environment and the necessary resources for this research.

On a more personal note, I am also profoundly grateful to my friends, whom I cannot mention individually, but have undeniably provided encouragement and laughter as needed. In addition, I would not forget Ms Mmasetshaba Tebele, to whom I am indebted to. And lastly, sincere gratitude to my family, from whom I sought strength and guidance most when I needed it.

Contents

Declaration ii

Abstract iii

Acknowledgements v

List of Figures xii

List of Tables xiv

Abbreviations xv

List of Symbols xvi

1 Introduction 1

1.1 Research Background 1

1.2 Research Problems 2

1.3 Research Objectives 3

1.4 Dissertation Outline 3

2 Microinverters in PV Systems 6

2.1 Introduction 6

2.2 Overview of Microinverters 6

2.3 Microinverter Topologies 7

2.3.1 Single-stage microinverters 8

2.3.2 Two-stage microinverters 9

2.4 Microinverter control mechanisms 12

2.5 Chapter Summary 12

3 Lightning Protection for PV systems 14

3.1 Introduction 14

3.2 Lightning Phenomenon 14

3.3 Lightning-induced Overvoltages . . . 17
3.3.1 Electromagnetic induction . . . 18
3.3.2 Electromagnetic field propagation model and coupling models . . . 19
3.3.3 Evaluations of lightning-induced voltages in PV systems . . . 22
3.4 Lightning protection . . . 25
3.4.1 IEC 62305 Standard . . . 25
3.4.2 Internal and External lightning protection . . . 26
3.5 Surge Protection Devices . . . 26
3.5.1 SPD technologies . . . 27
3.5.2 SPD protection distance to loads . . . 29
3.6 PV lightning-induced overvoltages and lightning Protection Studies . . . 31
3.7 Chapter Summary . . . 37

4 Research Methodology **38**
4.1 Introduction . . . 38
4.2 Case Studies . . . 39
4.3 Simulation 1: COMSOL Multiphysics® Simulation Software . . . 41
4.3.1 Components modelling . . . 41
4.3.2 Modelling of lightning currents . . . 43
4.4 Experimental Investigation . . . 44
4.4.1 Generation of high impulse current . . . 45
4.4.2 Experimental equipment . . . 47
4.4.3 Voltage and current measurements . . . 48
4.4.4 Test procedure . . . 48
4.5 Simulation 2: PSCAD . . . 49
4.5.1 Model development in PSCAD . . . 49
4.5.2 Protection performance . . . 56
4.6 Chapter Summary . . . 59

5 Simulation 1: Measurement of Induced Voltages (COMSOL Multiphysics® Simulation) **60**
5.1 Introduction . . . 60
5.2 Case Study 1 Simulation Results . . . 60
5.2.1 LPS one metre from the PV panel . . . 61
5.2.2 LPS two metres from the PV Panel . . . 63
5.2.3 LPS three metres from the PV Panel . . . 65
5.3 Case Study 2 Simulation Results . . . 66
5.4 The effect of wire lengths . . . 68

5.5 Chapter Summary 69

6 Experimental Validation **71**
6.1 Introduction 71
6.2 Case Study 1 Experimental Results 71
6.3 Case Study 2 Experimental Results 74
6.4 Twisted-pair Configuration 77
6.5 Validation 79
6.5.1 Measured values in experiment and simulation 79
6.5.2 Relative error 81
6.6 Chapter Summary 81

7 Simulation 2 Results: Protection Performance (PSCAD) **83**
7.1 Introduction 83
7.2 Simulation Results of PV Panel with microinverter at Steady State 83
7.3 Measurements of overcurrents appearing at the microinverter 84
7.3.1 Case 1: overcurrents appearing on the microinverter 85
7.3.2 Case 2: overcurrents appearing at the microinverter 88
7.4 Simulation Results with SPD connected on the DC cables 91
7.4.1 Case study 1 with SPD 91
7.4.2 Case study 2 with SPD 93
7.5 Chapter Summary 96

8 Discussion **97**
8.1 Introduction 97
8.2 Influence factors for induced overvoltages 97
8.2.1 The effect of changing current amplitude 99
8.2.2 The effect of changing LPS separation distance 99
8.2.3 The effect of changing protection scenario 100
8.2.4 The effect of mode of measurement 101
8.2.5 The effect of changing impulse current wave shape 102
8.2.6 The effect of wire lengths 104
8.2.7 The effect of twisting DC cables 104
8.2.8 Measurements with a microinverter 105
8.3 SPD energy overload and protection performance 105
8.3.1 Overcurrents appearing on the microinverter 105
8.3.2 SPD stress due to lightning currents 108
8.4 Recommendations 110
8.4.1 Lightning-induced overvoltages risk for microinveters 110

8.4.2 Lightning Protection Systems 110
8.4.3 SPDs for microinverters 111

9 Conclusion **114**
9.1 Conclusion 114
9.2 Principal Contributions 116
9.3 Suggested Future Work 116

Bibliography **118**

List of Publications **127**

List of Figures

2.1 Typical micro inverter circuit diagram [1] . . . 7
2.2 Classification of microinveter topologies [2] . . . 8
2.3 Typical micro inverter circuit [3] . . . 8
2.4 Single-Stage microinverter [4] . . . 9
2.5 Multi-Stage microinverter [3] . . . 9
2.6 Interleaved flyback dc-dc converter with an unfolding inverter [2] . . . 10
2.7 Push Pull topology with unfolding inverter [2] . . . 11
2.8 General scheme of the two-stage sliding-mode controlled microinverter [5] . . . 11
2.9 Transformerless PV microinverter general circuit configuration [6] . . . 12

3.1 Lightning occurrences . . . 15
3.2 Return stroke currents [7] . . . 15
3.3 Stages of lightning occurrences [8] . . . 16
3.4 Lightning waveform . . . 16
3.5 Electromagnetic propagation model [9] . . . 20
3.6 PV Inductive coupling equivalent circuit [10] . . . 23
3.7 Magnetic field values within a building in case of direct lightning strike [11] . . . 24
3.8 $I - V$ curve of a zinc oxide varistor [12] . . . 27
3.9 MOV equivalent circuit . . . 28
3.10 Protection for PV system with microinverters [13] . . . 30

4.1 Research methodology overview . . . 39
4.2 Case studies . . . 40
4.3 COMSOL Multiphysics® simulation process flow . . . 41
4.4 PV Panel . . . 42
4.5 Case study 1 COMSOL Multiphysics® simulation software setup . . . 43
4.6 Case study 2 COMSOL Multiphysics® simulation software setup . . . 43
4.7 Simulated impulse current waveforms . . . 44
4.8 Experimental Investigation Process flow . . . 45

4.9 High current impulse generator 46
4.10 Experiment Impulse current waveforms 46
4.11 Experimental setup 48
4.12 PSCAD simulation process flow 49
4.13 Microinverter block diagram [14] 50
4.14 Microinverter Model developed in PSCAD 50
4.15 PV panel model developed in PSCAD 51
4.16 Quadratic boost converter [16] 51
4.17 Boost Converter implementation on PSCAD 53
4.18 Boost converter control circuit implementation on PSCAD 53
4.19 Boost converter control - duty cycle process 53
4.20 Voltage Source Inverter [15] 54
4.21 Inverter model implemented in PSCAD 55
4.22 Inverter gate control circuit 55
4.23 DC-AC converter Controls 55
4.24 Induced voltage soruce on PSCAD 56
4.25 SPD selection process 57
4.26 Current and voltage characteristics for the selected MOV 58
4.27 Microinverter model with SPD connected on the DC cables 59

5.1 Simulation case study 1: Induced overvoltages DM, LPS 1 m 62
5.2 Simulation case study 1: Induced overvoltages CM, LPS 1 m 62
5.3 Simulation case study 1: Induced overvoltages DM, LPS 2 m 64
5.4 Simulation case study 1: Induced overvoltages CM, LPS 2 m 64
5.5 Simulation case study 1: Induced overvoltages DM, LPS 3 m, ... 65
5.6 Simulation case study 1: Induced overvoltages CM, LPS 3 m 66
5.7 Simulation case study 2: Induced overvoltages DM 67
5.8 Simulation case study 2: Induced overvoltages CM 67
5.9 Induced overvoltages with different DC cable lengths 69

6.1 Experimental case study 1: Induced overvoltages DM 72
6.2 Experimental case study 1: Induced overvoltages CM 73
6.3 Experimental case study 1: Induced overvoltages with a microinverter 73
6.4 Experimental case study 2: Induced overvoltages DM 75
6.5 Experimental case study 2: Induced overvoltages CM 76
6.6 Experimental case study 2: Induced overvoltages with a microinverter 76
6.7 Case study 1, DM Induced voltages: twisted-pair 78
6.8 Case study 2, DM Induced voltages: twisted-pair 78

6.9 Comparison of induced voltages in experiment and simulation, 20 kA 80
6.10 Relative error at different impulse currents 81

7.1 Boost converter waveforms 84
7.2 Inverter waveforms 84
7.3 Case study 1: Overcurrents at the microinverter, 5 kA 86
7.4 Case study 1: Overcurrents at the microinverter, 12.5 kA 86
7.5 Case study 1: Overcurrents at the microinverter, 20 kA 87
7.6 Case study 1: Overcurrents at the microinverter, 100 kA 87
7.7 Case study 2: Overcurrents at the microinverter, 5 kA 89
7.8 Case study 2: Overcurrents at the microinverter, 12.5 kA 89
7.9 Case study 2: Overcurrents at the microinverter, 20 kA 90
7.10 Case study 2: Overcurrents at the microinverter, 100 kA 90
7.11 Case study 1: SPD current and energy absorbed, 20 kA 92
7.12 Case study 1: SPD current and energy absorbed, 100 kA 93
7.13 Case study 2: SPD current and energy absorbed, 12.5 kA 94
7.14 Case study 2: SPD current and energy absorbed, 20 kA 95
7.15 Case study 2: SPD current and energy absorbed, 100 kA 95

8.1 The effect of changing LPS distance on induced overvoltage 100
8.2 The effect of changing the protection scenario 101
8.3 The effect of mode of configuration on induced overvoltage 102
8.4 The effect of changing current waveforms 103
8.5 The effect of twisting the DC Cables (10/350 μs Impulse) 104
8.6 Induced voltages, open DC cables vs with a microinverter, 5 kA 105
8.7 Case study 1 overrcurrents appearing at the microinverter, DM 106
8.8 Case study 1 overrcurrents appearing at the microinverter, CM 107
8.9 Case study 2 overrcurrents appearing at the microinverter, DM 107
8.10 Case study 2 overrcurrents appearing at the microinverter, CM 108
8.11 Currents flowing through the SPD, DM, 8/20 μs waveform 109
8.12 Energy absorbed by the SPD 110
8.13 Microinverter with SPD connected on the DC side. Concept adapted from [5] 112
8.14 AC side SPD recommendations for inverters [77] 113

List of Tables

2.1 Commercial microinverters. Data adapted from [16] 7

3.1 Characteristics of different strokes. Adapted from [11] 24
3.2 SPD protection recommendations 30
3.3 Summary of lightning-induced voltages studies 36
3.4 Summary of lightning protection studies 37

4.1 Material properties 42
4.2 Experimental components 47
4.3 PV panel parameters 51
4.4 Boost converter parameters 52
4.5 Insulation voltage for low voltage circuits. Data adapted from [17] 57
4.6 Characteristics of the selected MOV 57
4.7 IV Characteristics of the selected MOV 58

5.1 Maximum induced overvoltages when the LPS was placed one metre from the PV panel 63
5.2 Maximum induced overvoltages when the LPS was placed two metres from the PV panel 65
5.3 Maximum induced overvoltages when the LPS was placed three metres from the PV panel 66
5.4 Case study 2 simulation results 68
5.5 Maximum induced overvoltages for different DC cable lengths – Case Study 1 69
5.6 Maximum induced overvoltages for different DC cable lengths – Case Study 2 69

6.1 Case study 1 experiment results 74
6.2 Experimental case study 1 maximum induced overvoltages with a microinverter connected to the DC cables 74
6.3 Case study 2 experiment results 77

6.4 Experimental case study 2 maximum induced overvoltages with a microinverter connected to the DC cables 77
6.5 Experimental case study 1 maximum induced overvoltages with a twisted pair configuration 79
6.6 Experimental case study 2 maximum induced overvoltages with a twisted-pair configuration 79
6.7 Summary of induced overvoltages on open DC cables in DM 80
6.8 Summary of induced overvoltages on open DC cables in CM 80

7.1 Overcurrents at the microinverter in case study 1 88
7.2 Overcurrents at the microinverter in case study 2 91
7.3 SPD energy and current overload case study 1 93
7.4 SPD energy and current overload case study 2 96

8.1 Factors influencing lightning-induced overvoltages 98

Abbreviations

Name	Description
CCM	Continuous Current Mode
CM	Common Mode
DCM	Discontinuous Current Mode
DM	Differential Mode
EMF	Electromotive Force
IEC	International Electrotechnical Commission
LIO	Lightning-Induced Overvoltage
LPS	Lightning Protection System
LV	Low Voltage
MOSFET	Metal Oxide Semiconductor Field Effect Transistor
MOV	Metal Oxide Varistor
MPPT	Maximum Power Point Tracking
PSCAD	Power Systems Computer-Aided Design
PV	Photovoltaic
PVI	PV Installations
PWM	Pulse Width Modulation
SPD	Surge Protection Device

List of Symbols

Name	Description	Unit
V_{pv}	PV Voltage	V
L_{m1}	Magnetising inductance	H
P_o	Average output power	W
f_s	Switching frequency	Hz
v_s	Grid voltage	V
T_s	Switching period	s
I_{max}	Peak value of the current	A
B	Magnetic field density	T
Φ	Magnetic flux	Wb
H	Magnetic field strength	A/m
I_{spd}	Current flowing through the SPD	A
IV	Electrical current-voltage characteristics of the varistor	
τ_1, τ_2	the rise time constant, the decay time constant	s
E_{ind}	Induced electric field	V/m
e, U_{ind}, V_{ind}	Induced emf	V
E_z, E_r	Vertical electric field, Horizontal Electric Field	V/m
U_w, U_p	Impulse Withstand Voltage, Protection Level	V
U_c	Continuous Operating Voltage	V
V_{max}	Maximum induced voltage	V
V_{gate}	Gate Voltage	V
V_{ref}	Reference DC link voltage	V
V_{dx}	Forward voltage of the diode	V
V_H	DC link Voltage	V
V_{rms}	RMS voltage	V
V_{DC}	DC Voltage	V
ΔU	Voltage drop	V

1 Introduction

1.1 Research Background

The demand for photovoltaic (PV) systems is high and in line with the increasing importance of renewable energy. PV systems are, however, not immune to lightning strikes, and due to their outdoor setting, they become exposed to lightning transients that can damage their electrical components. Lightning transient-induced overvoltages are the most common effects experienced in electrical circuits through the electromagnetic induction concept. In addition, when lightning strikes metallic structures, the object affected develops an alternating magnetic field, inducing an electromotive force (emf) on the circuits [8]. Therefore, protection measures, including their choice and coordination, remain fundamental in electrical installations [18].

Microinverter technology is becoming increasingly popular compared to string or centralised inverter technologies in small and medium-sized PV systems [19]. The ability of microinverters to operate as plug devices on solar panels coupled with decentralised power point tracking techniques makes them an alternative approach in PV settings. In the centralised inverter method, one central inverter is connected to several series, parallel modules, and a single bus. However, the challenge on these systems is the dependency of a single inverter on several PV modules, which could bring the entire system or a majority of the system to a black-out if the inverter fails – a challenge that microinverter configurations have since overcome.

However, the installation configuration of microinverters brings several challenges to lightning protection; as they are installed close to the panel, they are more vulnerable to lightning strikes [20]. Without the necessary measures to protect the microinverters, the return on investment may be significantly affected.

Although lightning transient evaluation of PV systems has been conducted mainly on central and string inverter topologies, more research is required for developing effective lightning protection systems (LPSs) tailored for microinverters [19]. The current study aimed to analyse the lightning-induced overvoltage (LIO) stresses on microinverters in the event of lightning transients. The analysis of this voltage and the factors affecting their magni-

tude and waveforms will lead to the development of better-suited protection measures for microinverter applications.

Surge Protection Devices (SPDs) and their appropriate selection have emerged as efficient in the protection of lightning in low-voltage (LV) electrical systems. This is attributed to their non-linear current-voltage ($I - V$) characteristics and ability to absorb high energy during lightning transients. In the PV research area, the selection of these devices has been widely investigated for central and string inverter topologies; such selection has not been studied in microinverter topologies.

Both experimental and simulation studies were conducted. First, COMSOL Multiphysics® simulation software measured the induced voltages on a PV panel's DC cables through simulation to further assess the effect of wire lengths and LPS distance from the panel. Second, a microinverter was modelled using Power Systems Computer-Aided Design (PSCAD), and the resulting overcurrents on the microinverter were analysed. Following this, selected surge protection was introduced, and the energy overload and currents across the surge protection device (SPD) were analysed. Finally, the experimental work to validate the COMSOL simulation focused on the lightning-induced voltages measured on a PV panel's DC cables and was performed under different protection scenarios.

1.2 Research Problems

1. The voltage induced in the power cables of the solar cell arrays with microinverters in the event of partial lightning currents injected on the PV frame has not been studied in detail before. The lack of such information is a barrier to deciding the voltage, current and energy characteristics in developing SPDs to protect PV systems.

2. The difference between induced overvoltages under differential mode (DM; inner conducting loop) and common mode (CM; inner conducting loop and PV frame) settings in PV installations is not well understood and has not been investigated in detail. This is important for protection engineers to decide on the configuration mode for SPDs in PV installation.

3. The International Electrotechnical Commission (IEC) 62305-4:2010 [21] standard stipulates 'selection and installation of a coordinated SPD system' where the voltage protection level (U_p) of SPDs should be less than the impulse withstand voltage (U_w). However, the U_w of microinverters and the best-suited U_p of SPDs have not been investigated in detail in previous studies. This is a key issue encountered by engineers in selecting proper SPDs to protect microinverters.

4. SPDs have to be coordinated with the protective load by a certain maximum allowed

separation distance, which should be coordinated with the respective U_p and U_w. Considering this distance is crucial in reducing the probability of equipment damage. However, the correlation between the placement of SPDs and the distance between the PV panel and the microinverter is not fully understood. This information is essential to developing placement criteria for SPDs in microinverter systems.

1.3 Research Objectives

The objectives of the current study were:

1. To develop a simulation model to analyse the voltage and current distribution, energy content of transients, effects of wire lengths of the transient overvoltages and overcurrents appearing at microinverters of PV systems in the event of lightning strikes.

2. To validate the simulation model using a laboratory experiment design with a solar panel (with open DC terminals), thus predicting the lightning effects for a wide range of transient voltage and current waveforms.

3. To propose the characteristics and parameters of SPDs that can protect microinverters from possible lightning effects.

1.4 Dissertation Outline

This dissertation comprises nine chapters, each rendering the desired purpose to achieve the research objectives. The dissertation, broadly outlined, will be:

1. **Chapter 1:** The **Introduction** describes the background, objectives and justification for undertaking the study.

2. **Chapter 2: Microinverters in Photovoltaic Systems** presents the first part of the literature review. This includes an overview of microinverters and their topologies used in PV systems.

3. **Chapter 3: Lightning Protection for PV Systems**, as the concluding section of the literature review, outlines lightning and its parameters and lightning protection in PV systems, which forms an integral part of this research.

4. **Chapter 4: Research Methodology** presents the methodology, including the experimental setup and simulations. In addition, the relevance of test methods and selection of testing and simulation equipment is evaluated in this chapter.

5. **Chapter 5: Simulation 1: Measurement of Induced Voltages (COMSOL Multiphysics® Simulation)** investigates the indirect LIOs on a PV panel's DC cables using COMSOL Multiphysics® simulation software under different protection scenarios and impulse currents. Simulations were performed to obtain:

   - Induced overvoltages on the open DC cables when an impulse current is injected on the LPS for different distances between the LPS structure and PV panel,
   - Induced overvoltages on the open DC cables when an impulse current is injected on the PV frame,
   - Induced overvoltages for different wire lengths.

6. **Chapter 6: Experimental Validation** covers, in detail, the findings from the experimental investigation, including a thorough interpretation of the measured results to assess the risk of overvoltages under different protection scenarios. Measurements were performed to obtain:

   - Induced overvoltages on the open DC cables when an impulse current is injected on the LPS,
   - Induced overvoltages on the open DC cables when an impulse current is injected on the PV frame of the panel,
   - Induced overvoltages on the DC terminals when the microinverter is connected to the DC cables when an impulse current is injected on the LPS,
   - Induced overvoltages on the DC terminals when the microinverter is connected when impulse current is injected on the frame of the PV panel,
   - Induced overvoltages on the DC terminals with twisted pair configuration.

7. **Chapter 7: Simulation 2: Protection Performance (PSCAD)** presents the SPD's protection performance and development to protect the microinverter simulated in PSCAD. In this chapter, the obtained overvoltages from COMSOL Multiphysics® were tested in a practical scenario connected to a microinverter model developed in PSCAD. The evaluation of the resulting SPD energy overload and currents is described in this chapter. The simulations were performed to obtain:

- Overcurrents appearing at the microinverter caused by induced overvoltages when an impulse current is injected on the LPS without surge protection,
- Overcurrents appearing at the microinverter caused by induced overvoltages when an impulse current is injected on the frame of the PV panel without surge protection,
- SPD energy overload and current caused by induced overvoltages when an impulse current is injected on the LPS,
- SPD energy overload and current caused by induced overvoltages when an impulse current is injected on the frame of the PV panel.

8. **Chapter 8:** The **Discussion** discusses the simulations and experimental investigations in line with the research problem being investigated.

9. **Chapter 9:** The **Conclusion** concludes the study's findings and highlights the principal contributions of this research. This chapter further highlights probable future research related to this topic.

2 Microinverters in PV Systems

2.1 Introduction

Solar energy, and its conversion to electricity through the PV process, have gained momentum in research. Moreover, in line with the inversion process, microinverter application and design have been one of the topics of interest in designing PV systems [22]. Over the years, several different topologies and configurations have been presented for microinverters to improve efficiency, costs and optimal control. These configurations have been the focus of research in recent years. This chapter is a review, beginning with a rapid introduction to microinverter technologies and their configurations in PV system applications.

2.2 Overview of Microinverters

While inverters for large solar plants are becoming bigger, residential inverters are becoming smaller. This is attributed to the microinverter technology [20, 23], which is on a surge to replace the conventional central and string inverter methods [24].

The first microinverter, the Module Integrated Converter, or simply MIC deriving the name microinverter, was designed in the 1990s. In microinverter configurations, each module is connected to the grid through microinverters, offering efficient peak power tracking and improving the overall energy output [5]. The AC sides of the inverters are synchronised and connected to a single AC bus. A power flow diagram of a microinverter can be seen in figure 2.1.

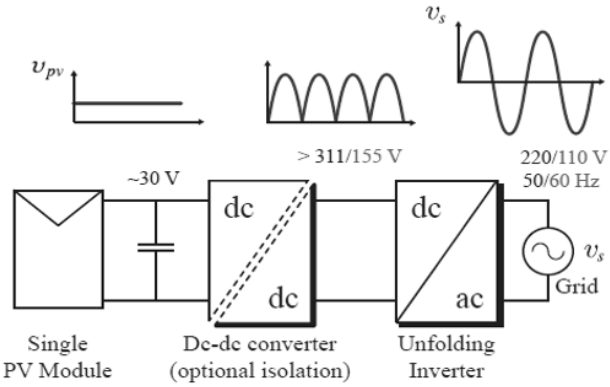


Figure 2.1: Typical micro inverter circuit diagram [1]

Several manufacturers are developing and manufacturing microinverters competitively to attain segmentation (Table 2.1). As a result, most microinverters usually offer efficiencies that exceed 90% [24,25] and can perform current shaping waveforms that are as close to sine waves as possible.

Table 2.1: Commercial microinverters. Data adapted from [16]

Manufacturer	Maximum Efficiency (%)	Nominal Power (W)	Input Voltage (V)	Power Factor
APS	95.5	250	22 – 45	>0.99
Siemens	96.3	215	16 - 36	>0.95
Aurora	95.5	300	25 – 60	>0.95
ABB	96.5	250	25 – 60	>0.95
Enecsys	94	200	27 – 54	>0.95

Microinverters have an expected service life of more than 25 years, in line with the PV system warranty [26]. This implies that reliability-orientated designs are paramount in the design of microinverters. However, like any electrical equipment, they are subjected to failures that may arise before the expected lifespan. Overvoltages have been identified as one of the top five risks of microinverter failures [27].

2.3 Microinverter Topologies

Recently, engineers have had the flexibility of selecting the preferred design to improve module efficiency and reliability while reducing costs. Power conversion in microinverters usually occurs in a single or two-stage approach (Figure 2.2).

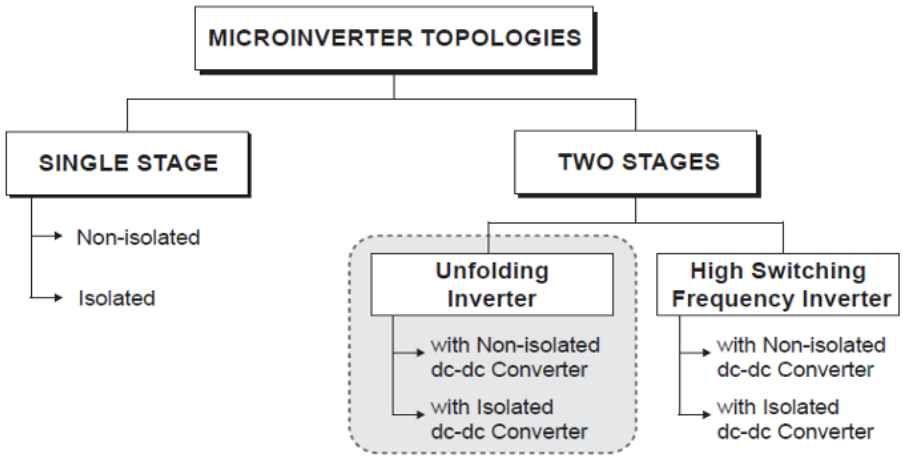


Figure 2.2: Classification of microinveter topologies [2]

2.3.1 Single-stage microinverters

Single-stage microinverters employ a DC-DC stage input modulated to produce the required output waveform, see figure 2.3 [3]. Many designs have been proposed in the literature; for example, Shimizu *et al.* [4] proposed a flyback utility-interactive inverter using film capacitors (Figure 2.4). The authors proposed an improvement, especially in high temperatures, thus improving the system's lifespan. Furthermore, low harmonic distortion can be achieved through the flyback.

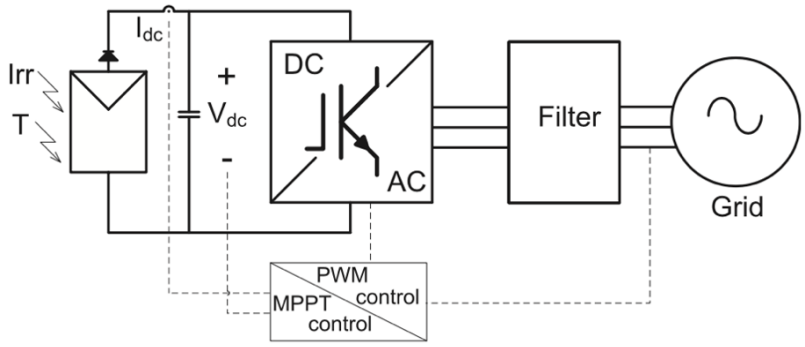


Figure 2.3: Typical micro inverter circuit [3]

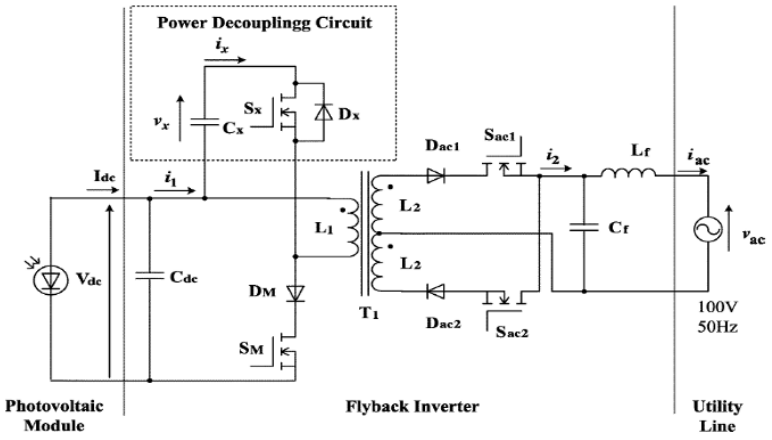


Figure 2.4: Single-Stage microinverter [4]

Other single-stage inverters proposed in the literature are: Li and Oruganti [28] developed a flyback-based inverter that operates at continuous conduction mode; Jain and Agarwal [29] developed single-stage inverter configurations for grid-connected PV systems; Sahan *et al.* [30] designed a single-stage topology microinverter using a low power current source inverter; Kerekes *et al.* [31] investigated a single-stage inverter based on the H-bridge with a new AC bypass circuit.

2.3.2 Two-stage microinverters

A two-stage microinverter is configured in a multistage topology with an isolated DC-DC input followed by a pulse width modulation (PWM) stage, and then a sine wave output (figure 2.5).

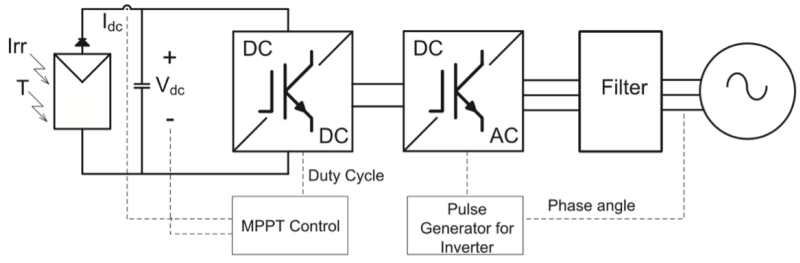


Figure 2.5: Multi-Stage microinverter [3]

For most commercial purposes, an interleaved flyback converter is often used (Figure 2.6) [2]. In this topology, the interleaved converter is connected to the input and the output of the two flyback converters. This topology further allows the size of the high-frequency transformer to be reduced. The flyback converter operates in two modes, the continuous

current mode (CCM) and the discontinuous current mode (DCM), where the magnetising current is zero in each switching period.

The peak value of the primary current can be expressed by:

$$i_{p,(DCM))}(t) = \frac{v_{pv}}{L_{m_1}} d_{DCM}(t) T_s \tag{2.1}$$

where d_{DCM} is the duty cycle in discontinuous current mode, $L_{m_1}$is the magnetizing inductance, T_s is the switching period, and v_{pv} is the PV voltage. The duty cycle can be expressed as:

$$d_{DCM} = \frac{2}{v_{pv}} \sqrt{(P_o L_{m_1} f_s)} |\sin \omega t| \tag{2.2}$$

where P_o is the average output power.
In the push-pull topology (Figure 2.7), there are two switches, S_a and S_b, two diodes and a transformer. A double-tapped centre transformer is used. Similarly, this setting can operate on both the DCM and CCM with the duty cycles expressed as:

$$d_{ccm}(t) = \frac{|v_s|}{2 n v_{pv}} \tag{2.3}$$

$$d_{dcm}(t) = \sqrt{\frac{L f_s i_l ink |v_s|}{(n v_p v (n v_p v - |v_s|)}} \tag{2.4}$$

where L is the inductor, f_s is the switching frequency, i_{link} is the current, and v_s is the grid voltage.

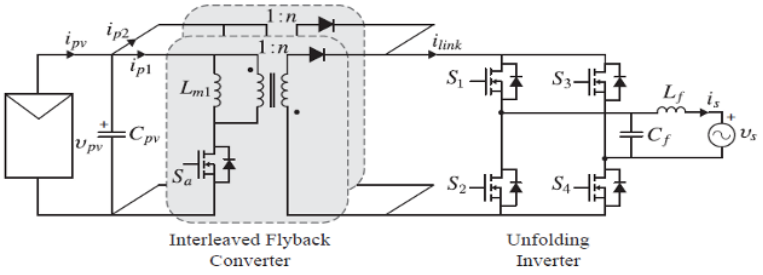


Figure 2.6: Interleaved flyback dc-dc converter with an unfolding inverter [2]

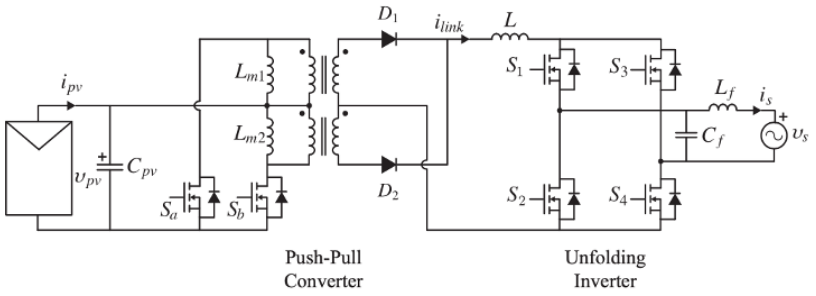


Figure 2.7: Push Pull topology with unfolding inverter [2]

Several contributions for two-stage microinverters have been previously reported in the literature. Jiang *et al.* [23] proposed a two-stage inverter using a linear phase infinite impulse response filter controlled by a plug-in repetitive current controller connected to the grid. Ahmed *et al.* [32] proposed a cascaded inverter using a high voltage gain switch inductor with a current shaping circuit and an H-bridge. Hasan *et al.* [33] proposed a similar inverter using a full bridge, and it employs an active-clamp circuit to limit the voltage stress. Evran [34] also proposed a multistage flyback configuration.

The use of transformers in microinverter topologies has also been well investigated. However, transformers introduce more weight, and subsequently more costs [16,35]. Transformer-less topologies have been proposed while achieving a trade-off between efficiency and power density. A power flow diagram of a transformer-less microinverter can be seen in figure 2.8 [5], and the configuration with components can be seen in figure 2.9 [6]. It must be noted that these transformer-less topologies cannot cover all microinverter requirements to boost a voltage of less than 30 V to 400 V DC. And as a result, transformer topologies are the most utilised. Several transformer-less topologies have been reviewed in the literature [35–37].

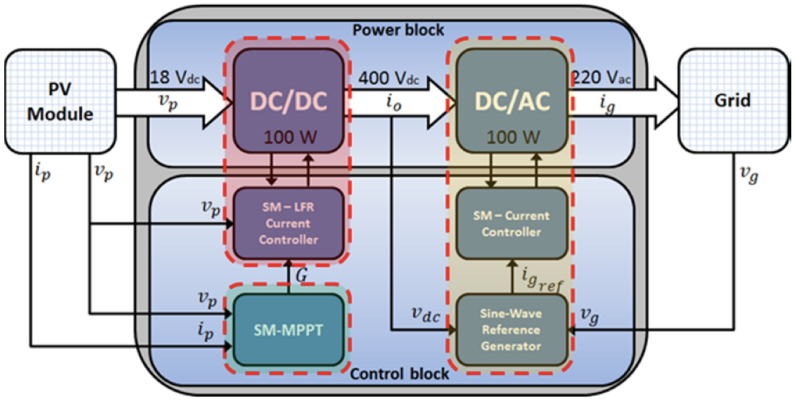


Figure 2.8: General scheme of the two-stage sliding-mode controlled microinverter [5]

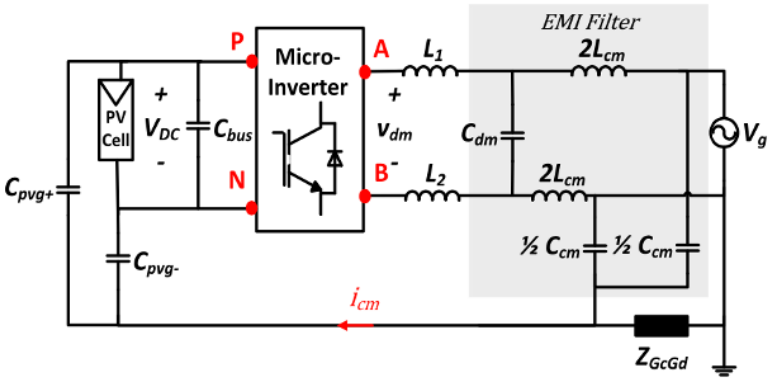


Figure 2.9: Transformerless PV microinverter general circuit configuration [6]

2.4 Microinverter control mechanisms

Although PV systems are strategically placed in positions where the maximum irradiance can be obtained, some conditions can render this process inefficient. These include shading by clouds, birds, or dust on panels. Despite these conditions, any PV system has an optimal power point in the inverter's voltage-current (VI) characteristics. Therefore, maximum power point tracking (MPPT) schemes offer maximum power extraction by tracking the highest achievable power. This is applicable in partial shading conditions and dynamic weather conditions [38, 39].

Many MPPT control strategies are used for PV inverters, each with benefits and drawbacks. Li [40] classifies them into three categories: the conventional methods (Constant Voltage Tracker, Pertube and Observe, IncCond); the intelligent methods (Genetic Algorithms, Fuzzy Logic Controller, Neural Network, Sliding Mode Controller); the hybrid methods that use two or more MPPT methods. In addition, other methods using MPPT techniques, such as the Current Sweeping the Variable Weather Parameter methods, have been utilised.

Two main PWM techniques are employed in the control of microinverters. The first system employs the PWM collectively to the inverter and the DC-DC converter. To prevent the DC input from being affected by the ripple, the power flow in the two stages is decoupled with a constant voltage DC-link. The second method controls the DC-DC converter using a quasi-sinusoidal PWM method to generate the required sinusoidal current at the inverter's DC link [23].

2.5 Chapter Summary

The power conversion in microinverters occurs either in a single or two-stage approach, each with advantages and drawbacks. This chapter has reviewed microinverters and their different

topologies used in PV systems. Since this research aimed to develop microinverter protection, a thorough review of microinverters was vital.

3 Lightning Protection for PV systems

3.1 Introduction

The previous chapter provided an introduction to microinverter technologies. As a follow-up from the set objectives, this chapter examines, in detail, the protection of PV systems - more precisely, against lightning transients. This chapter reviews lightning and its parameters in alignment with the study's objectives. Understanding the fundamentals of lightning, including the research trends in lightning protection, can establish a path for better protection against lightning transients.

3.2 Lightning Phenomenon

Despite being one of the most well-known phenomena, lightning has been investigated since Benjamin Franklin's experiments. Franklin demonstrated that lightning was a manifestation of electricity using an iron rod and a ground wire. The study was succeeded by Thomas Francois Dalibard's study [41]. And it was towards the end of the nineteenth century, when inventions of photography and spectroscopy became available, that more research on this concept was done. Frederich Pockels measured the first lightning current in Germany by analysing residual magnetic fields in rocks induced by nearby lightning transients. Other researchers like Charles Wilson, who worked on high-energy particles and was later awarded a Nobel prize, also played critical roles in lightning research. Many subsequent experiments were performed in many countries such as South Africa, Switzerland, England, and the United States of America in the 19th century. These studies, through advancements in measuring systems, have contributed significantly to our current knowledge of the physics of this phenomenon [41, 42].

Lightning is observable in the clouds and has been estimated to occur 30 to 100 times per second globally [42]. It is an electrical spark, typically longer than a kilometre. These electrical sparks are characteristically produced by thunderstorms usually greater than two kilometres in length.

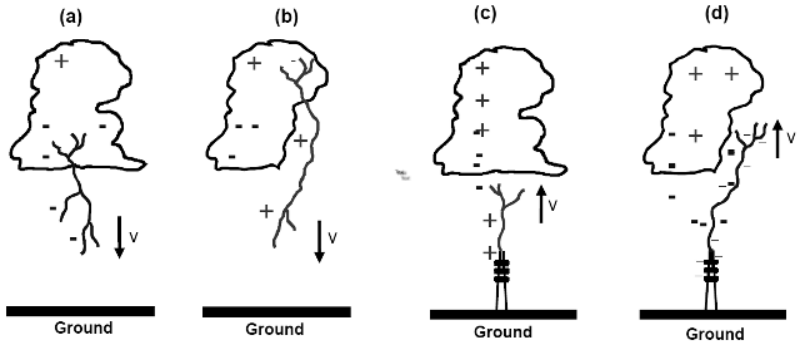


Figure 3.1: Lightning occurrences: (a) negative downward (b) positive downward (c) negative upward (d) positive upward lightning [7]

Lightning occurrences are illustrated in figure 3.1 [7]. The leader mechanism is widely used to describe the occurrence of lightning. In negative and positive downward lightning with the negative and positive downward leaders, respectively, the leader travels to the ground, and the connection between the ground charges objects when the electric field attains a certain level. In upward lightning, the top of the structure experiences the most electric field as it intensifies with height. The upward leader, being negative or positive, propagates to the cloud, creating a connecting channel (figure 3.2) [7].

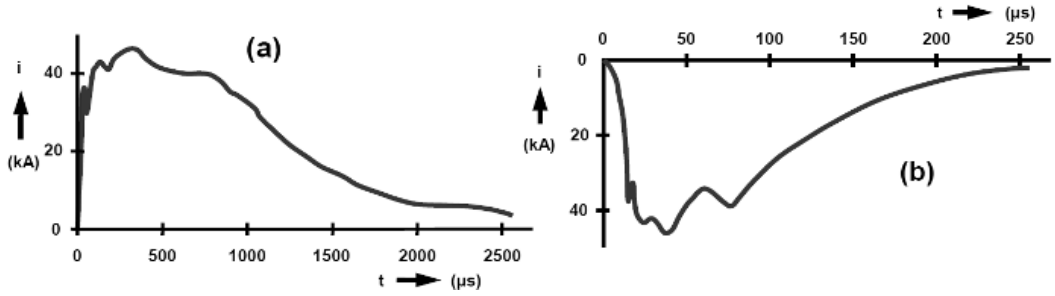


Figure 3.2: Return stroke currents [7]

A lightning stroke consists of two processes: the leader and the return stroke; the downward-moving stroke (figure 3.3) [8].

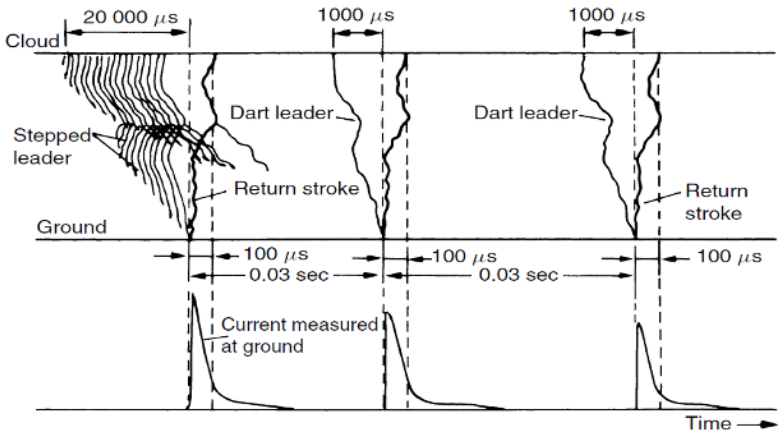


Figure 3.3: Stages of lightning occurrences [8]

Studying the lightning current parameters is essential in developing protection measures [43, 44]. The return stroke current has a relatively high peak, followed by slow decay (figure 3.4) [43]. The time taken from zero to achieve the peak value is defined as the front time, and the subsequent decay time is called the tail time. Each of these parameters renders an important aspect when designing protection systems. However, in the earthing system, the highest value of the stroke or the maximum peak current is crucial, as well as the total charge for the melting points of the attachment. The specific flash energy is responsible for mechanical forces, and the derivative of the lightning flash or the maximum rate of rising is also responsible for the maximum induced voltage of electronics [7].

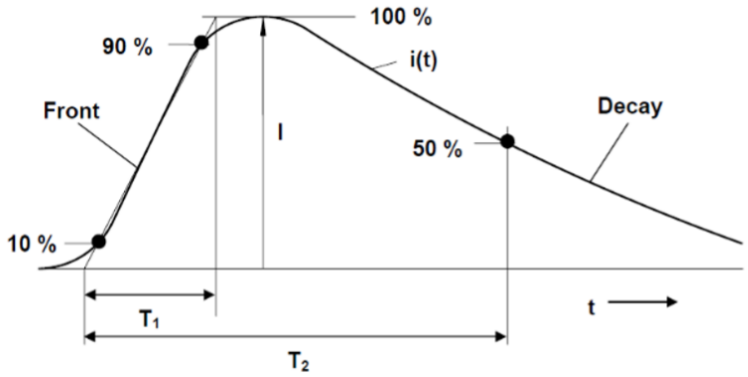


Figure 3.4: Lightning waveform. The fast front time (τ_1) followed by a slow decay (τ_2) [43]

Spatial-temporal distribution calculations are based on the current appearing at the bottom of the channel [45]. In the design of LPSs, mathematical modelling is used to determine the magnitude of the currents and voltages associated with lightning. Several current return-stroke models are found in literature [46]. The double exponential model and the Heidler

function are commonly used waveforms.

The return-stroke current can be numerically expressed using two equations, the first being the double exponential formula [47]:

$$i = \frac{i_{max}}{k}.\left(e^{\frac{t}{\tau_1}} - e^{\frac{t}{\tau_2}}\right) \tag{3.1}$$

where i_{max} is the peak current, k is the peak current correction, τ_2 is the decay time constant and τ_2 is the rise time constant.
The Heidler function, presently the standard for the current model, has been used extensively in lightning research and is expressed by the following equation [48]:

$$i(t) = \frac{i_0}{\eta}\frac{\left(\frac{t}{\tau_1}\right)^n}{1+\left(\frac{t}{\tau_1}\right)^n} exp(-\frac{t}{\tau_2}) \tag{3.2}$$

where i_0 is the peak current, η is the peak current correction, τ_1 is the rise time constant, τ_2 is the decay time constant, and n is the steepness factor.
From equation 3.2, the peak current correction can be expressed as:

$$\eta = exp\left(\frac{-\tau_1}{\tau_2\left(\frac{n\tau_2}{\tau_1}\right)^{\frac{1}{n+1}}}\right) \tag{3.3}$$

3.3 Lightning-induced Overvoltages

Lightning transients can have unfavourable effects on equipment and structures, including the failure of electronic equipment. A direct lightning strike occurs when the lightning energy is directed through the equipment. For example, lightning can strike the phase conductor in an electrical network, allowing the overvoltage to propagate through the conductor and subsequently damaging the connected electrical equipment. An indirect lightning strike can occur in two ways: through a ground current when lightning strikes the ground and travels until it reaches an object or as a side flash passing through the air to the second object.

Lightning transients commonly induce overvoltages on electrical circuits through the electromagnetic induction concept. When lightning strikes metallic structures, the affected object develops an alternating magnetic field, inducing an emf on the circuits [8, 49]. This phenomenon was first explained by the bound charge theory, which was accepted in the 20th century for lightning-induced overvoltages. The latest theories explain the process: the lightning channel between the clouds and the ground contains a subsequent return stroke. During

the return stroke, the radiated electromagnetic fields induce overvoltages [20, 49].

3.3.1 Electromagnetic induction

For a long time, electricity and magnetism were considered unrelated entities. This, however, changed when Faraday, Ampère, and others concluded, through research, that there was an indisputable relation between these phenomena. Faraday concluded that changing magnetic fields induce electric currents in closed coils. And therefore, time-varying currents produce induced electric fields, which are accompanied by magnetic fields.

The induced electric field ($\mathbf{E}_{ind}$) for a charged moving particle with a velocity v with respect to the source of the magnetic field can be expressed as [50]:

$$\mathbf{E}_{ind} = v \times \mathbf{B} \tag{3.4}$$

where $\mathbf{B}$ is the magnetic flux density.
The equation can also be expressed with the current distribution of density ($\mathbf{J}$) in vacuum, localized inside a volume v as:

$$\mathbf{E}_{ind} = \frac{\partial}{\partial t}\left(\frac{\mu_0}{4\pi}\int_V \frac{\mathbf{J}dV}{r}\right) \tag{3.5}$$

where r is the distance of the point where the induced electric field is being determined from the volume element dV.

Faraday's law of electromagnetic induction can be used to determine the total emf induced in a closed loop due to an electric field:

$$de = \mathbf{E}_{ind}.dI \tag{3.6}$$

Therefore, the emf induced can be determined as follows:

$$e = \oint_C \mathbf{E}_{ind}.d\mathbf{I} \tag{3.7}$$

$$e = \oint_C \mathbf{v} \times \mathbf{B}.d\mathbf{I} \tag{3.8}$$

In any case, whether time-varying currents or contour motion, the induced electric field can be calculated as:

$$e = \oint_C \mathbf{E}_{ind} d\mathbf{I} = \frac{d\Phi}{dt} = -\frac{d}{dt}\int_s \mathbf{B}.d\mathbf{S} \tag{3.9}$$

where Φ is the magnetic flux.

3.3.2 Electromagnetic field propagation model and coupling models

The evaluation of lightning-induced voltages is commonly conducted by this sequence of steps [51]:

- The lightning return-stroke current model as a function of time and height is employed on several points by considering the lightning return stroke electromagnetic field change.
- A selected coupling model is used to calculate lightning-induced voltages based on the interaction between the line conductors and the field.

Lightning Induced Overvoltages (LIOs) are composed of the electrostatic and electromagnetic components, namely, the horizontal and the vertical components, respectively [49]. The electromagnetic propagation model as shown in figure 3.5 [9] can be described using the vertical electric field (E_z) the horizontal electric field (E_r) and the vertical field, and the horizontal magnetic field (H_r):

$$E_z(r,z,t) = \frac{1}{4\pi\varepsilon_0}\left(\int_{-H}^{H} \frac{2(z-z_0)^2 - r^2)}{R^5} \int_0^t i(z_0,\tau) - \frac{R}{c}\right) d\tau dz_0$$
$$+ \int_{-H}^{H} \frac{(2(z-z_0)^2 - r^2)}{cR^4} i(z_0, \tau - \frac{R}{c})\, dz_0 - \int_{-H}^{H} \frac{r^2}{c^2R^2} \frac{di(z_0, \tau - \frac{R}{c})}{dt} dz_0 \quad (3.10)$$

$$E_r(r,z,t) = \frac{1}{4\pi\varepsilon_0}\left(\int_{-H}^{H} \frac{3r(z-z_0)^2 - r^2)}{R^5} \int_0^t i(z_0,\tau) - \frac{R}{c}\right) d\tau dz_0$$
$$+ \int_{-H}^{H} \frac{(3r(z-z_0)^2 - r^2)}{cR^4} i(z_0, \tau - \frac{R}{c})\, dz_0 - \int_{-H}^{H} \frac{r^2}{c^2R^2} \frac{di(z_0, \tau - \frac{R}{c})}{dt} dz_0 \quad (3.11)$$

$$E_z(r,z,t) = H_z(r,z,t)\frac{1}{4\pi}\left(\int_{-H}^{H} \frac{r}{R^2} i(z_0, \tau - \frac{R}{c})\, dz_0 - \int_{-H}^{H} \frac{r}{cR^2} \frac{di(z_0, \tau - \frac{R}{c})}{dt} dz_0 \right. \quad (3.12)$$

where r is the distance from the observation point to the leader channel, z_0 is the height of the object being calculated, τ is the variable of time in integration, R is the distance between the calculating point and the observing point.

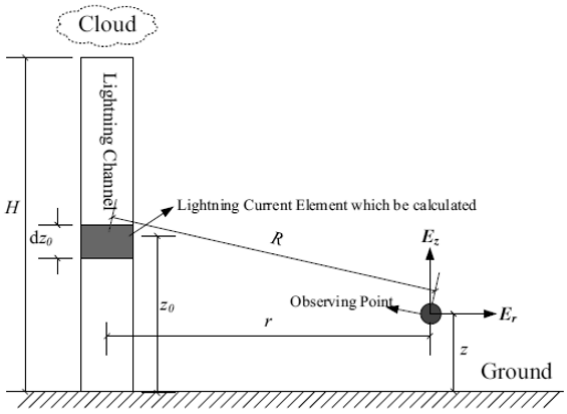


Figure 3.5: Electromagnetic propagation model [9]

Most recently, the simulation of electromagnetic transients has been very popular. As such, models performing these calculations have been developed; these include the Rusck Model, Chowdry Model, Agrawal Model and many others [52]. These models mainly focus on the physical process of the return stroke.

The Rusck model [53] can be expressed as:

$$\frac{\partial \phi(x,t)}{\partial x} + L' \frac{\partial i(x,t)}{\partial t} = 0 \tag{3.13}$$

$$\frac{\partial i(x,t)}{\partial x} + C' \frac{\partial}{\partial t}\left[\phi(x,t) - \phi^i(x,t)\right] = 0 \tag{3.14}$$

where C' and L' are the line capacitance and inductance per unit length respectively, and ϕ is the induced scalar potential.
The total induced voltage can be expressed as:

$$v(x,t) = \phi(x,t) + \int_0^h \frac{\partial A_z^e(x,z,t)}{\partial t} dz \tag{3.15}$$

where A_z^e is the vertical component of the incident vector potential and h is the conductors height.

The equations describing the transmission line coupling using the Agrawal model [54] are expressed as:

$$\frac{\partial}{\partial t}[u_i^s(x,t)] + [R'_{ij}].i_i(x,t) + [L'_{ij}].\frac{\partial}{\partial x}[i_i(x,t) = [E_x^i(x,h_i,t)] \tag{3.16}$$

$$\frac{\partial}{\partial t}[i_i(x,t)] + [G'_{ij}].u_i^s(x,t) + [C'_{ij}].\frac{\partial}{\partial x}[u_i^s(x,t) = 0 \tag{3.17}$$

where $[E_x^i(x,h_i,t)]$ is the vector of the horizontal component of the incident electric field along the x axis at the conductor's height h, $[L'_{ij}]$, $[R'_{ij}]$,$[C'_{ij}]$,$[G'_{ij}]$, are inductance, resistance, , capacitance, and conductance matrices respectively.
The total line voltage $[u_i(x,t)]$ can be expressed as:

$$[u_i(x,t)] = [u_i^s(x,t)] + [u_i^i : (x,t)] = [u_i^s(x,t)] - \left[\int_0^{h_i} E_z^i(x,z,t)dz\right] \tag{3.18}$$

where $E_z^i(x,z,t)$ is the incident (or inducing) vertical electric field.

The Chowdy-Gross model [55] which has also been used in lightning literature can be expressed as [56]:

$$\frac{\partial u(x,t)}{\partial x} + L' \frac{\partial i(x,t)}{\partial t} = 0 \tag{3.19}$$

$$\frac{\partial i(x,t)}{\partial x} + C' \frac{\partial}{\partial t} \left[u(x,t) - u_i(x,t) \right] = 0 \tag{3.20}$$

where the incident voltage $u_i(x,t)$ is expressed as:

$$u_i(x,t) = \int_0^{h_i} E_z^i(x,z,t) dz \tag{3.21}$$

Bazelyan and Raker [8] estimates the induced overvoltages to be expressed as:

$$E_{emf} \approx S \frac{(dB_{av})}{dt} \tag{3.22}$$

where $B_a v(t)$ is the average magnetic induction averaged over a cross-section (S). This overvoltage can also be calculated when the length of the current conductor is much longer than the distance to the circuit:

$$E_{emf} \approx (\mu_0 S)/(2\pi r_c) \frac{di}{dt} \tag{3.23}$$

where μ_0 is the magnetic permeability of vacuum, r_c is the distance to the circuit. The parameter of di/dt can also be expressed in the form of the maximum rate of current impulse (A_{max}) which equates to 10^{11} A/s, thus the formula being:

$$E_{emf} \approx (\mu_0 S)/(2\pi r_c) A_{max} \tag{3.24}$$

3.3.3 Evaluations of lightning-induced voltages in PV systems

For PV settings, research on induced voltages surged in the 1990s; this brought about a new branch of research where induced voltages were measured and calculated in PV loops by associated magnetic fields [57]. Through this surge of research, it was observed that the connections of the cells inside PV modules form geometric loops. These loops are collective of all the cells from the positive to the negative poles [10]. Furthermore, the module's metal frame creates another loop in addition to the internal loop. And therefore, the induced voltages are caused by the magnetic field passing through the loops. An inductive coupling equivalent circuit of the PV modules can be seen in figure 3.6.

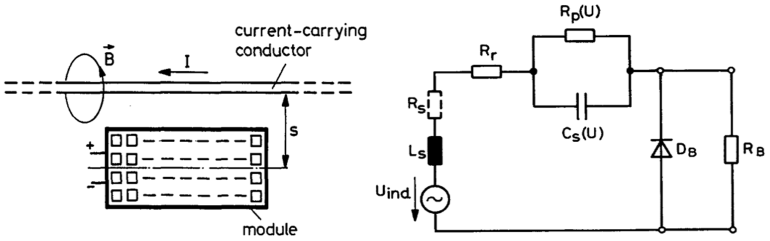


Figure 3.6: PV Inductive coupling equivalent circuit [10]

Given this loop arrangement, the resulting induced overvoltages can be analysed through Faraday's law:

$$U_{ind} = -\frac{\partial \Phi}{\partial t} = -M\frac{\partial I}{\partial t} \tag{3.25}$$

where M is the mutual inductance and Φ is the magnetic flux.

Assuming an infinite current-carrying conductor, the magnetic flux density from distance s from the conductor is given by:

$$B = \frac{I.\mu_o}{2\pi s} \tag{3.26}$$

where I is the current.

The mutual inductance between the current carrying conductor and the internal conductor loop can be expressed as:

$$M = \frac{\mu_0.l}{2\pi}.ln\frac{2s+b}{2s-b} \tag{3.27}$$

where l is the length of the loop and b is the width of the loop.

Assuming a finite current-carrying conductor, the magnetic flux density at a distance (s) to the conductor can be expressed as:

$$B = \frac{I.\mu_o}{2\pi s}\frac{1}{\sqrt{1+4\left(\frac{s}{l_i}\right)}} \tag{3.28}$$

And finally, the mutual inductance is given by:

$$M = \frac{\mu_0.l}{2\pi}.ln\frac{\frac{l_i}{2}+\sqrt{\frac{l_i}{4}+(s-2b)}}{\frac{l_i}{2}+\sqrt{\frac{l_i}{4}+(s-2b)}}.\frac{2s+b}{2s-b} \tag{3.29}$$

The Biot-Savart law can be used to include the effect of the metal frame by calculating the magnetic field strength in a distance (r) as:

$$\overrightarrow{H_p} = \frac{1}{4\pi}. \int_c \frac{d\overrightarrow{s}.d\overrightarrow{r}}{|\overrightarrow{r}|^3} \tag{3.30}$$

where I is the conductor current, r is the distance to a path increment (ds) of the conductor

For PV systems installed and using IEC 62305-4:2010 [21] standard, the lightning electromagnetic pulse can be calculated based on the lightning strike location [11]. This can be calculated with a direct lightning strike to the external LPS (figure 3.7), where the magnetic field strength (H_1) is calculated as:

$$H_1 = k_h.I_0.\frac{w_m}{dw.\sqrt{d_r}} \tag{3.31}$$

where k_h is the configuration factor $\frac{1}{\sqrt{m}}$, w_m is the the mesh width of the grid-like shield, and I_0 (kA) is the peak value of the lightning impulse.

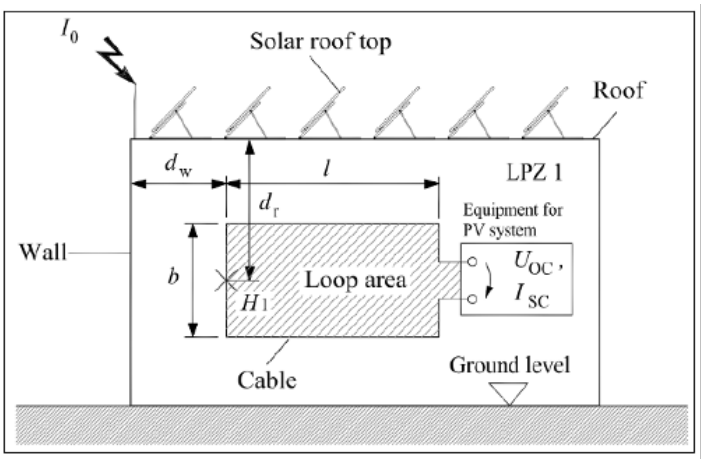


Figure 3.7: Magnetic field values within a building in case of direct lightning strike [11]

I_0 can be determined using characteristics of different strokes as per table 3.1.

Table 3.1: Characteristics of different strokes. Adapted from [11]

Symbol	Description	Time(τ_1)
$I_{0-F/MAX}$	The first positive stroke	10 μs
$I_{0-FN/MAX}$	The first negative stroke	1 μs
$I_{0-S/MAX}$	The subsequent stroke	0.25 μs

The induced overvoltage can be expressed as:

$$U_{ip} = k_c.L_m.\frac{di}{dt} \tag{3.32}$$

where k_c is the repartition of the coefficient of the lightning current amongst the air termination and the down conductors, L_m is the mutual inductance between the lightning current along the downward conductor, and di/dt is the steepness of the subsequent current.

Since the conventional circuit theory-based techniques cannot accurately simulate fast surge phenomena on three-dimensional structures [58], numerical methods have been previously used to solve electromagnetic problems, including lightning problems. These methods include the Finite-Difference Time-Domain method, Partial Element Equivalent Circuit (PEEC) method, Method of Moments, and others [59].

3.4 Lightning protection

Many PV systems are not adequately protected against lightning, accounting for about 26% of failures [60]. Surges could occur as transients for a very short time, typically from a few hundred microseconds to a few milliseconds, with amplitudes as high as several kilovolts. Nevertheless, the protection measures against lightning should be adequate to reduce the risk to a tolerable level in both indirect and direct lightning strike risk [61, 62].

An increase in the number of PV installations has been observed globally. PV systems are usually installed on rooftops or in an outdoor area. Due to this setting, they become exposed to the possibility of being struck by lightning, which can affect the system and its electronics. Damages caused by lightning on PV systems can be seen on the module where bypass diodes and the glass can be damaged, the cables can incur damage and holes can be observed on the insulation, the inverter can be damaged on the input and the output, and PV systems with a solar tracker can have their power supply, sensors and drive train damage.

Lightning protection measures, including external lightning protection, internal lightning protection, SPDs, grounding and equipotential bonding, may be employed on electrical systems [44]. These systems act like Faraday cages for buildings to disperse the lightning effect by providing a low resistive path to the ground.

3.4.1 IEC 62305 Standard

The IEC 62305-2010 lightning protection standard expedites the increase in technology and the research on lightning to recommend improved lightning measures. Part 1 [63], termed 'General Principles', introduces the current parameters, the types and sources of damage, including the types of losses. Part 2 [64] provides a comprehensive methodological process to assess the risk due to lightning strikes. Part 3 [65] concerns the LPS. Part 4 [21] provides recommendations for protection against lightning electromagnetic pulse.

3.4.2 Internal and External lightning protection

The internal lightning protection, consisting of equipotential bonding and electrical insulation, and SPDs (discussed in detail in the next section), aims to deprive dangerous spark formation inside the system. The equipotential bonding prevents dangerous potential differences by connecting the LPS to the metal installations and electrical or electronic systems. The grounding system distributes the lightning discharge to the ground. The grounding geometry should be carefully implemented for this process to be effective. Exposed conductive parts should be kept at the same potential bonding by maintaining continuity of the equipment grounding path to avoid an electrical shock under fault conditions [66].

External lightning protection measures intercept and divert the lightning strikes near the protected object to the ground. This is done using down conductors, air termination and grounding systems. By performing a risk analysis, as suggested by the IEC 62305-2:2010 [64] standard, the location of the air terminals can be determined by the rolling sphere method, the protective angle method, or the mesh method.

The protective angle method works on the principle of installing multiple air termination rods coordinated around the PV system, while the rolling sphere method ensures that the PV system's supporting structure does not come into contact with a sphere of a certain radius (R) [61]. The external LPS can either be designed to be isolated in high risk cases or otherwise non-isolated.

3.5 Surge Protection Devices

SPDs have proved to be very effective in protecting lightning transients due to their non-linear current-voltage ($I-V$) characteristics and their energy absorption mechanisms [67–72]. In normal operating voltages, the SPD has a high impedance value, but when a transient is present in a line, the SPD switches itself to a low impedance mode for a short duration, thus giving the transient opportunity to pass to the ground. Following this, the SPD should switch back to high impedance mode [18]. In addition, various lightning protection standards have evaluated the installation coordination of these devices.

SPDs are selected based on numerous criteria, including the withstand voltage of equipment, impulse current, maximum continuous operating current and response time [18, 73]. The key parameter in the design of an SPD is the U_p, which is related to the equipment's U_w. Failure of protection devices can occur if the U_p of the SPDs is greater than the U_w of the equipment or when the energy content associated with the current is greater than the maximum energy that the SPD can absorb. The selection and test methods of SPDs in lower voltage systems has been described in detail in IEC61643-11:2011 [74] and IEC61643-12:2008 [75], and in IEC 61643-31:2017 [76], and IEC 61643-32:2017 [77] standards for PV

systems.

3.5.1 SPD technologies

An SPD can contain one of the non-linear components, with Metal Oxide Varistors (MOV) and spark gaps being the most utilised types. Class I SPDs are installed at the most exposed zone and should withstand higher current handling capacity; class II and class III SPDs have sequentially reducing values of current handling capacity [18]. Class I SPDs are mainly based on spark gap technology, being able to withstand about 100 kA 10/350 μs impulse current, whilst class II SPDs can withstand about 10 kA 8/20 μs impulse current and are mainly based on MOV technologies [78].

MOVs consist of semiconductor materials made of metal oxide. The MOV's structure is formed by series and parallel p-n junctions connected and separated by zinc oxide grains. Other additives such as antimony oxide, and bismuth oxide are combined with these zinc oxide grains. An interconnected mesh is created using a bismuth-rich phase coating the zinc oxide grains throughout the microstructure [12].

MOVs are voltage-dependent devices, meaning, at lower voltages, the conduction is blocked, while at higher voltages, their impedance changes from open circuitry to a very high conductive value. When exposed to lightning surges, varistors can absorb much higher transient voltages. The $I - V$ characteristic curve of the varistor is illustrated in figure 3.8.

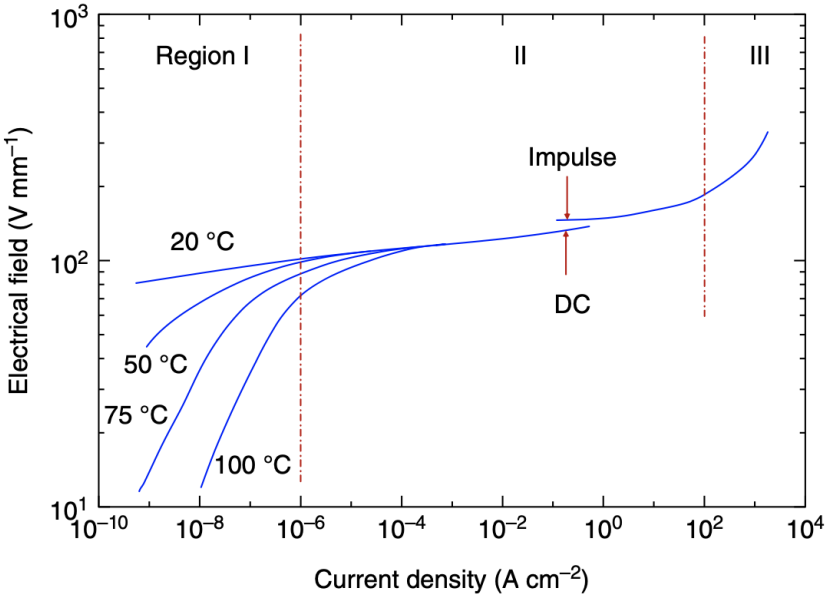


Figure 3.8: $I - V$ curve of a zinc oxide varistor [12]

As seen from figure 3.8, the varistor's $I - V$ relation is characterised by three regions (Region I, II, II). In region I, the varistor is in a pre-breakdown region when the leakage

current changes as a function of temperature. Region II is the breakdown region, where the non-ohmic properties of the varistor are now in play. In region III, the non-ohmic properties slowly decay, and the varistor becomes ohmic. These regions are sometimes referred to as the low-current, medium-current and high current regions, respectively.

The non-linear ohmic properties of a varistor can be expressed by a logarithmic relation using the nonlinear coefficient (α) as:

$$\alpha = \frac{V}{I}\frac{dV}{dI} \tag{3.33}$$

The equation is simplified to:

$$I = \left(\frac{V}{C}\right)^{\alpha} \tag{3.34}$$

where C is a constant.

The equivalent circuit of the varistor in different regions can be seen below;

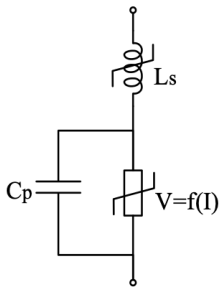


Figure 3.9: MOV equivalent circuit

The energy absorbed by the SPD can be calculated by the following expression [79]:

$$E = \int_{t_0}^{t} u(t)i(t)\,dt \tag{3.35}$$

where $u(t)$ is the instantaneous voltage across the SPD and $i(t)$ is the instantaneous current across the SPD.

Other SPD technologies include spark gap technology, gas discharge tube technology, and silicon avalanche diodes. Spark gap technology uses two sets of electrodes separated by a set distance in a medium such as air. When the voltage between the electrodes exceeds the electric strength of air, an electric arc will form. The Gas Discharge Tubes technology employs ceramic body electrodes with a mixture of gas. Silicon Avalanche Diode use silicon-based diodes as a form of protection. Numerous studies from the literature have developed

strategies to make proper selections for SPDs [68, 70, 80–83].

3.5.2 SPD protection distance to loads

The installation of SPDs is highly dependent on the distance between the devices and the load protected. If this distance is neglected, the loads will be at risk of damage despite the coordination of the SPDs [84]. The IEC standards provide such protection distance guidelines. The IEC 62305-4:2010 [21] standard stipulates the 'selection and installation of a coordinated SPD system' using U_p. The probability of SPDs to minimise the risk is one of the major considerations in selecting and developing coordination of these devices.

The zonal concept of protection highlighted standards that guide the coordination of SPDs. Per the IEC 62305-4:2010 [21] standard, SPDs in zone 1 may be subjected to higher energy surges and should therefore have higher energy handling capabilities. Zones-2 and 3 SPDs are subjected to a portion of the induced voltages with low durations.

The proper selection of SPDs can be achieved by considering voltage drop ΔU of the connecting conductors and the SPDs U_p. For voltage limiting SPDs, the total voltage protection level (U_{pf}) is given by [21]:

$$U_{pf} = U_p + \Delta U \tag{3.36}$$

And for voltage switching SPD's, it is given by:

$$U_{pf} = max(U_p, \Delta U) \tag{3.37}$$

The system is protected if the following conditions are met [21]:

1. $U_{p/f} < U_w$ When the circuit length between the SPD and the equipment is negligible.
2. $U_{p/f} <= 0.8U_w$: When the circuit length is not greater than 10 meters.
3. $U_{p/f} <= (U_w - U_i)/2$: When the circuit length is more than 10 meters.

The IEC further emphasises the energetic coordination of the SPDs, where SPDs connected on the same circuit should share the energy based on their energy absorption capabilities. This energy coordination can be seen as a typical multistage combination, where classes I, II, and II SPDs are used collectively so that the quick responsive SPDs take the first portion of the discharge current.

In PV systems, SPDs may be installed in buildings with and without external lightning protection; the risk analysis determines this process. The SPDs can be installed on the AC

and the DC side of the system, depending on the configuration; refer to Table 3.2. The IEC 61643-32:2017 [77] standard provides a technical description of the principles for selecting, locating, and coordinating SPDs connected to PV installations.

Table 3.2: SPD protection recommendations

Standard or Manufacturer	Protection Scenario	SPDs configuration
IEC 61643-32:2017 [77]	PVI without external LPS	DC: SPD 1(Class II) and SPD2 (Class II) (l <10m) AC: SPD 3 Class II) and SPD 4 Class II) (l<10m)
IEC 61643-32:2017 [77]	PVI with external LPS when the separation distance is kept	DC: SPD 1 Class II) and SPD2 (Class II) (l <10m) AC: SPD 3 (Class I) and SPD 4 Class II) (l <10m)
IEC 61643-32:2017 [77]	PVI with external LPS when the separation distance is not kept	DC: SPD 1 Class I) and SPD2 (Class I) (l <10m) AC: SPD 3(Class I) and SPD(Class I) 4 (l <10m)
DEHN [13]	Protection for PV system with microinverters	DC: No SPD (Space Limitation)AC: SPD 3 Class II) and SPD 4 Class II) (l <10m)

*l is the distance between the PV panel and the inverter

Without standardised microinverter protection, some SPD manufacturers such as DEHN have recommended microinverter protection scenarios. According to the DEHN (Lightning and Surge Protection – White Paper) [13], PV systems with microinverters do not need protection on the DC side but only on the AC side (Figure 3.10), citing space limitations.

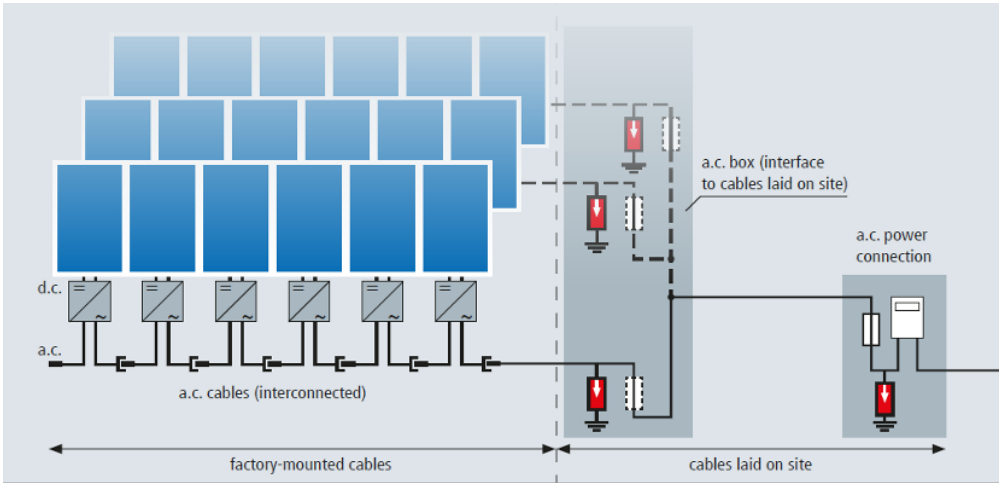


Figure 3.10: Protection for PV system with microinverters [13]

3.6 PV lightning-induced overvoltages and lightning Protection Studies

Researchers have carried out the evaluations of lightning-induced voltages on PV modules and strings through simulations and experiments. These studies have shown that the induced voltages on the DC cables caused by nearby lightning transients are caused by the electromagnetic coupling between the lightning channel, the internal loop created by the interconnection of the cells, and the metal frame of the PV module. Such studies and their contribution are highlighted in Table 3.3.

Several research studies have concluded that lightning striking closer to the panel may be destructive to the inverters due to the high voltages associated with the lightning surges [20, 85–87]. However, most studies in this area have mainly focussed on Differential Mode (DM) measurements. Common Mode (CM) induced voltage effects, however, have not widely been studied [88].

1. Stern and Karner [10] were among the first to show the linear increase in induced voltages with impulse current. Their study has experimentally shown the presence of induced voltages using an oscillating current injected on a conductor near the PV panel with and without the frame effect. The induced voltages, measured with an injection of an oscillating current of 0.5 kA/μs went as high as 40 V at a distance of 0.5 meters. The study further projected that at 120 kA/μs oscillating waveform, the projected induced voltage was 3.5 kV with a separation distance of 1 meter. The following observations are made:

    - Based on experimental results and projected values, high induced overvoltages were recorded on the DC cables of the PV panel.
    - The induced effects of lightning may create insulation voltages of live parts to ground, and thus the risk of insulation failure.
    - The inductive interference may damage bypass diodes, thus increasing the risk of overheating and ignition.

2. Ahmad *et al.* [91], using a simulation model, injected a 10/350 μs impulse current waveform which was developed using the Heidler function with amplitudes as high as 169 kA nearby a PV battery energy storage system using an electromagnetic transient program. In this study, the lightning-induced voltages were measured for distances from 20 to 100 meters from the system. The following observations are made from this study:

- The induced voltages caused by lightning currents nearby a PV-Energy storage system increased with current amplitude
- Differences in cables lengths showed no significant change in induced voltages due to low voltage drops

3. Rahim *et al.* [89] investigated the influence of lightning current at different distances experimentally. The study, however, used an impulse voltage generator of 1.2/50 μs waveform with an amplitude of 66 kV in a lab setting to measure induced voltages on the DC cables of the panel. In this study, the mean values of the induced voltages reduced as the distance between the panel and the striking point increased. The following observation was made from the study:

   - The induced voltage caused by lightning is proportional to the distance of the striking point.

4. Sun *et al.* [86] also noticed increased induced voltages as the striking distance between the panel and the PV was reduced. In this simulation, the induced voltages were measured for a PV system installed in a mountain and developed using three-dimensional modelling. This was further validated through experiences by Stern and Karner [10]. The authors simulated the 6/350 μs lightning current using the Heidler function with amplitudes as high as 110 kA. The highest induced voltage measured was 4.29 kV on the open DC cables. The following observations are made from this study:

   - The lightning-induced voltages were different with different parameters, such as the oblique angle, the lightning striking spot, and the lightning channel geometry.
   - The presence of the metal frame can cause a short circuit current and thus reduce induced voltage across the DC cables of a PV panel.

5. The increase in DC cable lengths from the inverter to the panel was investigated by Zaini *et al.* [90] who concluded that the induced voltage was insignificant in different DC cable wire lengths for string inverters. This study used PSCAD/EMTDC software to model a PV farm. The lightning current waveshapes for this study were modelled using the Heidler Function in 8/20 μs and 10/350 μs waveshapes with amplitudes from 2 kA to 200 kA. The induced voltages were measured in two case studies (with and without the SPDs). The following observations are made:

   - The increase in wire lengths does not influence the induced voltages.
   - Due to high induced voltages, the SPDs connected to the DC and AC cables may be damaged.

- The direct lightning strikes contribute to high induced voltages on the electronics of a PV system.
- Surge protection should be installed in PV farms, where one will be closer to the inverter of the PV system.

6. Tu *et al.* [87] assessed the induced voltages on a rooftop PV system with and without external lightning protection. The impulse current injected in different spots on the PV system was modelled using the Heidler function with a peak value of 20 kA and 50 kA. The absolute induced voltages and induced voltages across the DC cables were recorded. The voltage across the DC cables when lightning strikes different point range from 0.5 - 14 kV given the striking distance, and hundreds of kilovolts were recorded as absolute induced voltages. The following observation is made from this work:
   - Lightning-induced voltages are affected by several parameters, including peak amplitude, lightning striking spot, and soil resistivity.
   - Both relative induced voltages were directly proportional to the lightning current amplitude.
7. Vangala *et al.* [85], using an experimental method, a highspeed datalogger to perform voltage measurements between the two PV terminals of the two PV arrays to measure the LIOs. The following observation is made:
   - DC protection for a PV system is important to protect against lightning strikes
8. Charalambous *et al.* [61], through simulation and experiment, a scaled laboratory experiment was designed to measure the induced overvoltages on PV DC cabling loops. The system tested consisted of a 2 kW PV system consisting of 9 modules. Two case studies were considered in this model (isolated and non-isolated LPS). The injected lightning current amplitude of 10kA (10/350 μs) was injected. The highest induced voltage was 475 V for non-isolated LPS and 680 V for isolated LPS with eternal lightning protection. The following observations are made:
   - The results indicate that induced voltages in a non-isolated LPS are higher compared with an isolated LPS.
   - Induced overvoltages varied with the distance between the striking point and the measurement point.
9. Formisano *et al.* [88] studied induced overvoltages in PV systems in DM and CM using a simulation and concluded that the latter is slightly greater under the same conditions. The authors proposed a three-dimensional semi-analytical numerical method.

The lightning currents were modelled using the Heidler function of 0.2/100 μs with peak amplitudes of 20 kA. With a strike distance of about 5 metres, the induced voltage averaged 205 V and 2.6 kV in common mode. The following observations are made:

- The lightning strike hitting point plays an important role in the induced voltages recorded in differential mode and common mode
- Induced voltages in common mode were higher than induced voltages in differential mode

10. Fuangfung *et al.* [11] contributed by developing software for rooftop PV systems to calculate induced overvoltages and currents. The software applies principles laid out by IEC 62305-4

Other studies have further developed or recommended surge protection measures for PVIs against lightning transients in addition to induced voltage calculations. These studies and their contribution can be seen in Table 3.4. These studies have mainly focused on central [20, 92, 93] and string inverters [90]. No studies on lightning protection for microinverters were found in the literature.

1. Zhang *et al.* [20] introduced a PEEC method, slightly modified with the vector fitting technique to measure lightning-induced effects on a PV system. This, too, was performed by way of simulation and experiment. The simulated impulse current had a maximum peak current of 100 kA with a waveshape of 1/200 us rise and fall times, respectively. The induced voltages without SPDs were measured to be 8.75 kV and 6.75 kV across the two bypass diodes using a resistivity of 2000 ohm/m. This study further explored the inclusive ferromagnetic properties of steel. The following observations are made from this research:

   - The induced voltages on the DC cables have a short waveform and are unaffected by soil resistivity
   - Overvoltages observed on the bypass diodes may exceed the breakdown strength of the bypass diodes
   - Induced voltages measured with one SPD may still be greater than the withstand voltage of the SPD, and an additional SPD may be installed between the DC cables.

2. Tu *et al.* [87], through an experimental investigation and simulation, performed a study on PV systems to measure the magnitude and effects of induced overvoltage through different cases. A selected coupling model is used to calculate lightning-induced voltages based on the interaction between the line conductors and the field. The following observations are made:

- Lightning-induced voltage on PV systems depends on parameters such as the position of the lightning strike, the soil resistivity, the current amplitude and the distance from the external LPS.
- The lightning return-stroke current model as a function of time and height can be employed on several points by considering the lightning return stroke electromagnetic field change.

3. Mohammed *et al.* [93] assigned voltage protection levels for SPDs connected in a hybrid PV-Wind Farm on central inverters based on the CENELEC 50539 standard. This study assessed a 4.1 MW PV wind system with direct impulse current waveforms modelled using the Heidler function with maximum amplitudes of 45 kA and 90 kA. in negative first stroke and positive strokes. The following observations are made:
   - PV-Wind systems without SPDs will be at risk of damage due to lightning effects.
   - Proper SPD selection at different points in PV systems may reduce the effects of lightning on PV-Wind farms.
4. Pons and Tommasini [92] estimated the lightning-induced overvoltages and overcurrents to determine the necessity of a lightning protection system. Surge overcurrents expected on the PV system were measured by considering the effect of direct and indirect lightning strikes. The following observation is made:
   - The need for protection systems in PV systems should be evaluated following a risk assessment as suggested by IEC 62305-2.

Table 3.3: Summary of lightning-induced voltages studies

Ref	Type of System	Methods	Contribution
[85]	PV System	Experiment	Used a highspeed datalogger to perform voltage measurements between the terminals of the two photovoltaic arrays to measure the lightning-induced overvoltage.
[87]	PV System	Experiment Simulation	Through an experimental investigation and simulation, performs a study on PV systems to measure the magnitude and effects of induced overvoltage through different cases using a modified mesh current method.
[61]	PV System	Experiment Simulation	Designed a scaled laboratory experiment to measure the induced overvoltages on PV dc long cabling loops.
[11]	PV System	Software tool	Presents a software tool for rooftop PV systems to calculate induced overvoltages and currents.
[90]	PV System	Simulation	Used PSCAD software to model a solar PV farm and analysed induced overvoltages and overcurrents with different lightning strike positions.
[89]	PV System	Experiment	Performs an experiment to measure the effect of induced voltages on PV systems in different distances.
[88]	PV System	Simulation	Studied induced overvoltages in PV systems in DM and CM using a three-dimensional (3D) semi-analytical numerical method and concluded that the latter is slightly greater under the same conditions.
[91]	Hybrid PV System	Simulation	Assessed the impacts of lightning-induced overvoltages on a hybrid PV-energy storage system.
[86]	PV System	Simulation	Analysed the induced voltages on PV arrays installed on a mountain through a three-dimensional modelling technique.

Table 3.4: Summary of lightning protection studies

Ref	Type of Inverter System	Contribution
[92]	Central Inverter	Estimated the lightning-induced overvoltages to determine the necessity of a LPS using risk analysis prescribed by IEC 62305-2 [64] standard.
[90]	String Inverters	Assigned a proper location SPD to protect the solar PV modules and inverter.
[93]	Central Inverter	Studied the protection of PV systems by simulation using PSCAD software. The study further analysed the effects of with and without lightning protection. Considering these two case studies play a major role in determining the need for a protection system. Furthermore, using the CENELEC standard, lightning protection recommendations were designed to analyse the equipment's required ratings and specifications.
[20]	Central Inverter	Introduced a PEEC method, slightly modified with the vector fitting technique to measure lightning-induced effects on PV systems. This, too, was performed by way of simulation and experiment. This study further explored the inclusive ferromagnetic properties of steel and suggested SPDs to protect the inverter

3.7 Chapter Summary

Lightning has been a subject of research for many years. Many excellent studies have been conducted in this regard. These studies, which among other things, define and classify the nature of this phenomenon, have provided the foundation of how best to develop protection systems against lightning transients. It was also essential to form a review of studies specific to PV systems, which include a foundational background to the research. This chapter concludes the literature review of studies performed on lightning protection PV systems.

4 Research Methodology

4.1 Introduction

The development of protection measures for microinverters follows a procedural approach. This chapter presents the methodological process employed to achieve the main objectives of this research. In this quest, it is important to understand the lightning-induced voltages caused by impulse currents on the PV circuit. Therefore, this chapter details the experimental and simulation methodologies while highlighting some considerations that could affect the measurements.

The scope of this research involves two clearly defined components, namely, the experimental study and the simulation. The first simulation to measure induced overvoltages was conducted using COMSOL Multiphysics® simulation software, where induced voltages were measured with a solar panel with and without external lightning protection. By injecting impulse currents at different positions and protection scenarios, the induced overvoltage on the power cables of the solar panel was measured. This was further validated by an experiment designed in the High Voltage Laboratory at the University of the Witwatersrand. The second simulation used PSCAD to select parameters for SPDs to protect microinverters. Finally, the simulation results recommended effective protection measures for microinverters. A research methodology overview is illustrated in figure 4.1.

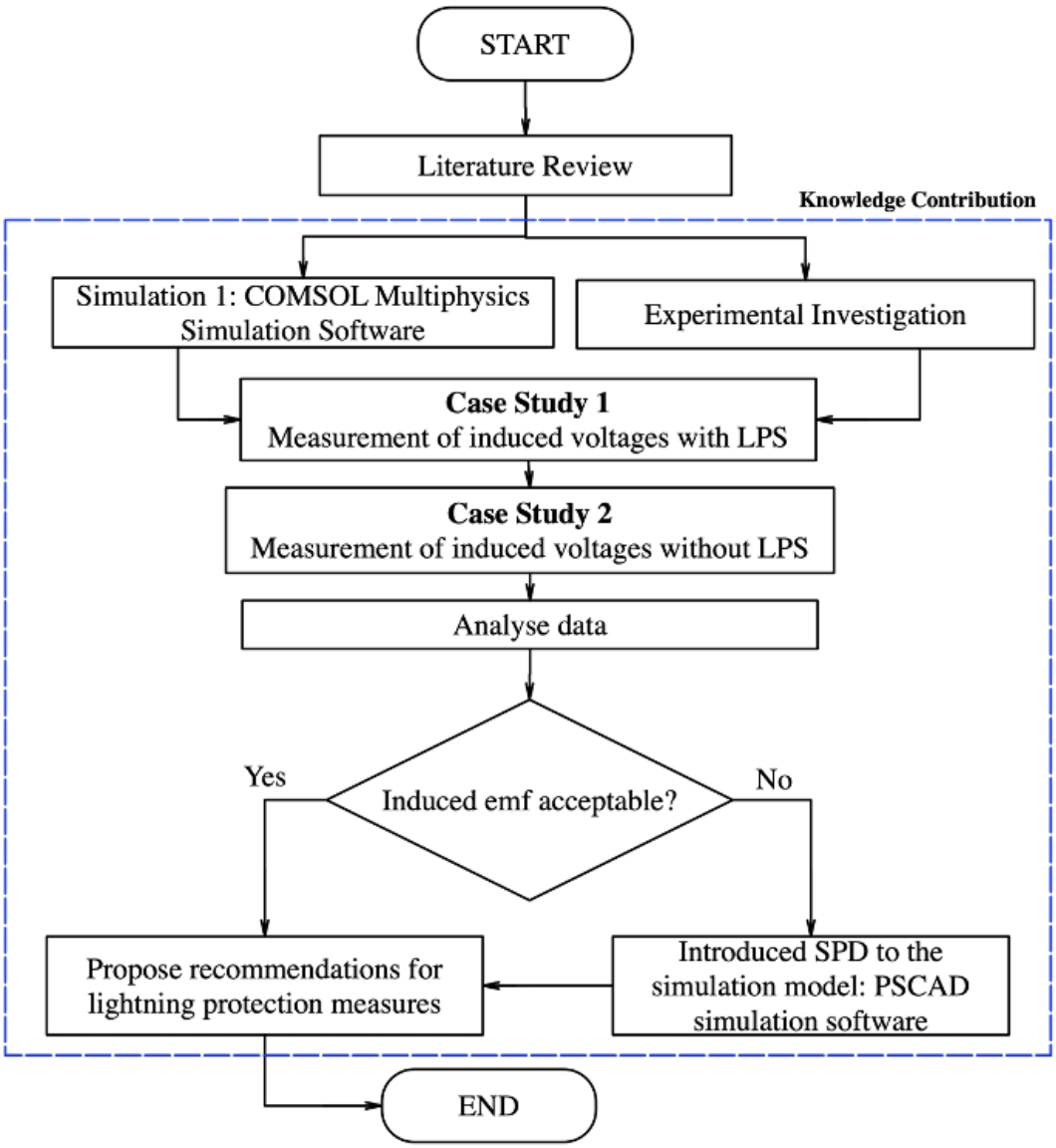


Figure 4.1: Research methodology overview

4.2 Case Studies

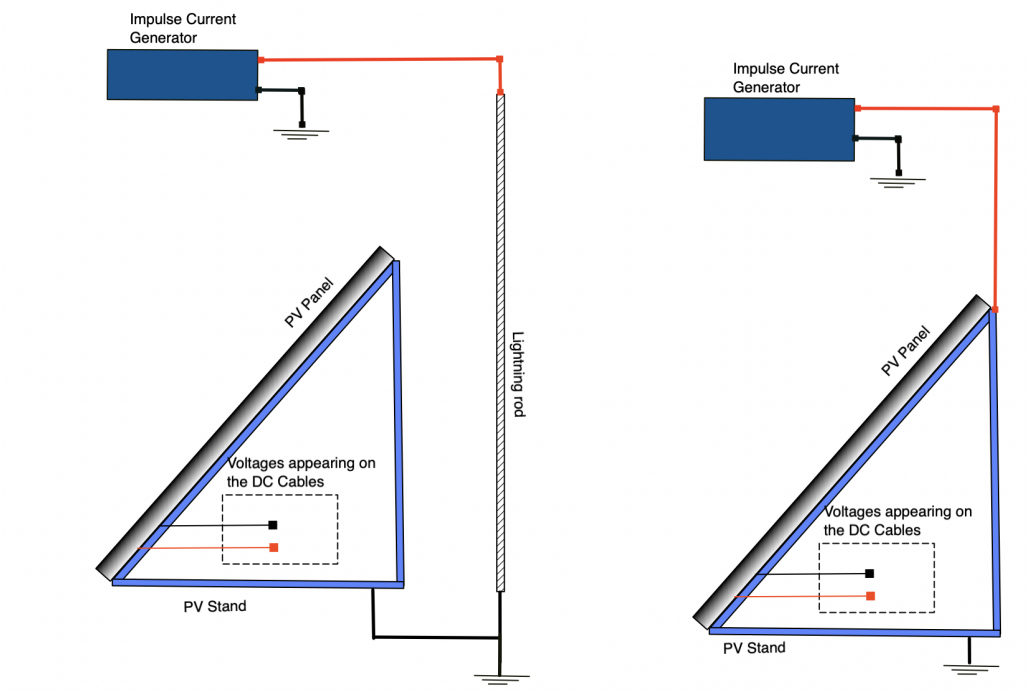
The following case studies were performed in sequential order:

1. **Case Study 1**: This study involved injecting impulse current onto a lightning rod that formed part of the external lightning protection system (Figure 4.2a). An oscilloscope measured the induced overvoltage on the PV cables resulting from this strike on the open DC wires in CM and DM. The maximum current injected did not exceed 20 kA for experimental work and 100 kA for simulations.

   In the experimental setting, the PV panel was situated near the impulse generator to maintain the shortest delivery circuit of the current. A support structure was created to carry the PV panel and connected to a low inductance copper foil used as a return path to the ground.

   The simulation model in this case study made it possible to measure the influence of the distance between the LPS and the PV panel. This was achieved by measuring induced voltages at different distances (1 metre, 2 metres, and 3 metres)

2. **Case Study 2**: In the second study case, impulse current was injected directly on the frame of the PV panel, and overvoltages were measured on the DC cables (Figure 4.2b). Similarly, injection currents did not exceed 20 kA for experiments and 100 kA for simulation.



(a) Design of case study 1

(b) Design of case study 2

Figure 4.2: Case studies

An experimental investigation was also performed with a microinverter connected to the DC cables. Induced voltages from lightning currents of 1 kA, 2 kA and 5 kA were measured across the microinverter.

4.3 Simulation 1: COMSOL Multiphysics® Simulation Software

The first simulation used COMSOL Multiphysics® simulation software, which can solve electromagnetic problems by coupling several physics problems in three dimensions, and components can be assigned with material properties. The simulation model measured the induced voltages in different case studies described in section 4.2, including the effects of LPS distance and the DC cables' wire lengths. The simulation process is outlined in figure 4.3.

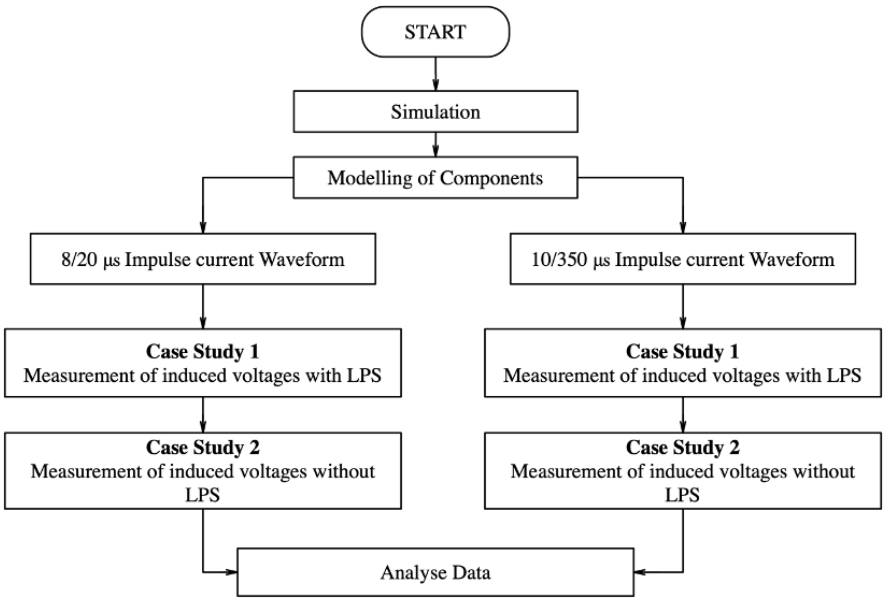


Figure 4.3: COMSOL Multiphysics® simulation process flow

4.3.1 Components modelling

The panel components, including the aluminium frame, tempered glass, Encapsulate-EVA, back sheet and DC cable, were modelled to represent a PV panel (figure 4.4). As required for numerical solutions, boundary conditions are specified as the space where the electromagnetic field is achieved. The correct modelling of the equipment is crucial as the slightest mistake in the measurements and parameters can significantly influence the results. A voltage measuring device was connected between the DC cables to measure the induced overvoltages caused by the lightning currents. Using the software's capabilities, the electrical circuit (AC/DC) module was coupled with the magnetic modules function to provide an interaction between the circuit and electromagnetic fields. The material properties can be seen in table 4.1.

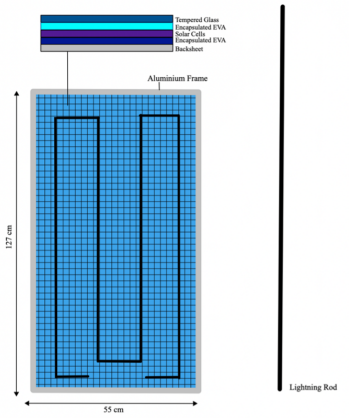


Figure 4.4: PV Panel

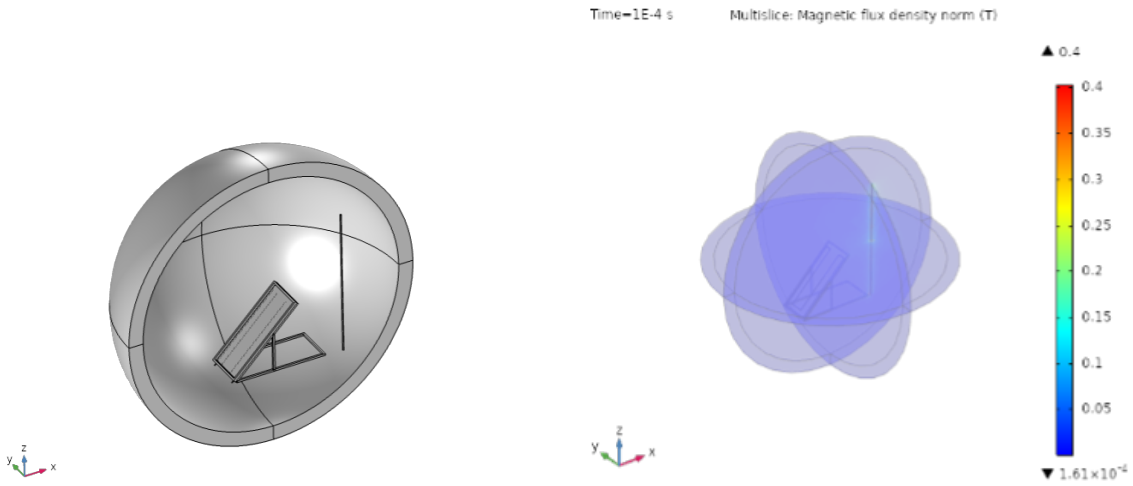
Table 4.1: Material properties

Material	Relative permeability	Relative permittivity	Electrical conductivity (S/m)
Steel	750	1	$4.032\text{x}10^{6}$
Aluminium	1	1	$3.77\text{x}10^{7}$
Air	1	1	$3\text{x}10^{-15}$
Glass	1	4.2	$1\text{x}10^{-14}$
Copper	0.99	1	$5.99\text{x}10^{7}$
Silicon	1	11.68	$1.56\text{x}10^{-3}$
Ethylene Vinyl Acetate	1	1	$3.45\text{x}10^{-9}$

To solve electromagnetic problems, Maxwell's equations are used on a macroscopic level under boundary conditions in COMSOL Multiphysics®. These equations state the relationships in electromagnetic quantities.
For general time-varying fields, Maxwell's equations, in differential form, can be written as:

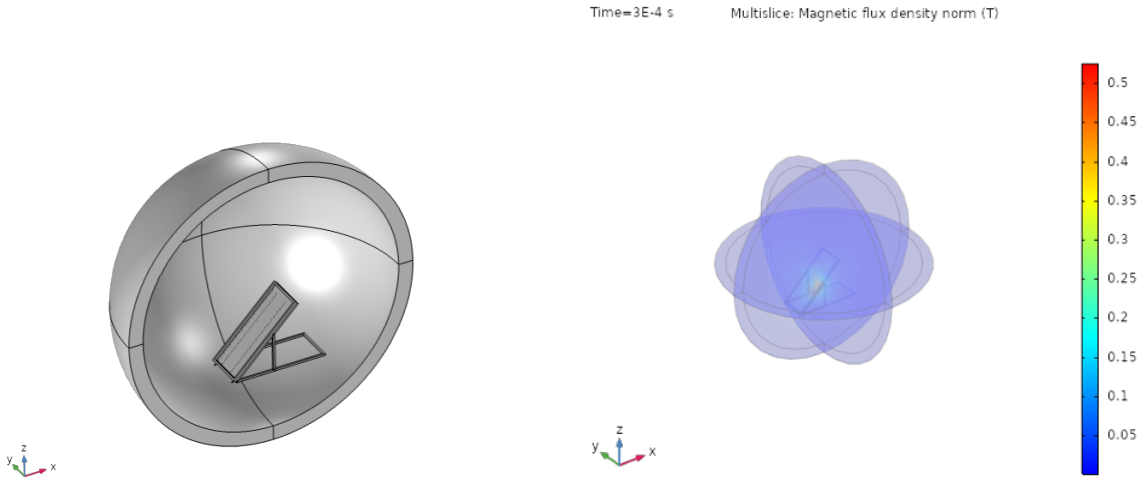
$$\begin{aligned} \frac{\partial \mathbf{D}}{\partial t} &= \nabla \times \mathbf{H}, && \text{(Faraday's Law)} \\ \frac{\partial \mathbf{B}}{\partial t} &= -\nabla \times \mathbf{E}, && \text{(Ampère's law)} \\ \nabla \cdot \mathbf{B} &= 0, && \text{(Gauss's Law for magnetism)} \\ \nabla \cdot \mathbf{D} &= 0. && \text{(Coulomb's Law)} \end{aligned} \tag{4.1}$$

Figures 4.5 and 4.6 illustrate the simulation setup in COMSOL Multiphysics® simulation software for case studies 1 and 2, respectively.



(a) Pre-computation. **(b)** During computation

Figure 4.5: Case study 1 COMSOL Multiphysics® simulation software setup



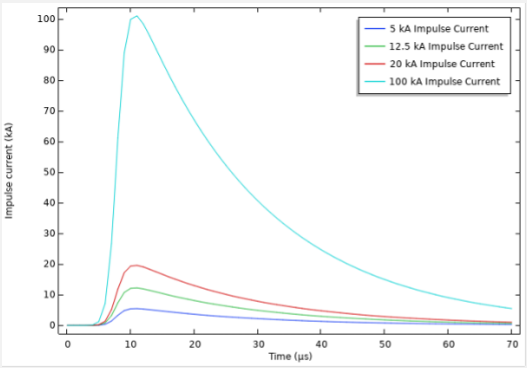
(a) Pre-computation. **(b)** During computation

Figure 4.6: Case study 2 COMSOL Multiphysics® simulation software setup

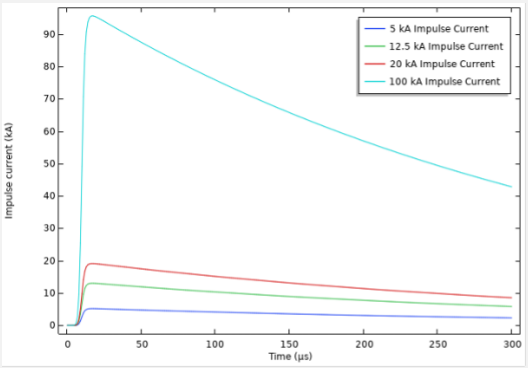
4.3.2 Modelling of lightning currents

The lightning stroke was simulated as an impulse current generator. To generate high impulse currents, the Heidler function, which has been used extensively in lightning research, was used as an analytical function on COMSOL Multiphysics® in two current waveforms (8/20 μs and the 10/350 μs standard lightning waveforms) [63]. Using analytical functions of the COMSOL Multiphysics® module, the rise and the fall times were adjusted to produce the

required waveforms. The waveforms were plotted and used as the current source connected directly to the stroke location. The equation for the Heidler function has been described in section 3.2 (equation 3.2). Figures 4.7 (a) and (b) show the simulated current waveforms in magnitudes of 20 kA (current peak value (I_{max})).



(a) 8/20 µs standard lightning current waveform



(b) 10/350 µs standard lightning current waveform

Figure 4.7: Simulated impulse current waveforms

4.4 Experimental Investigation

A laboratory experiment was conducted at the High Voltage Laboratory at the University of Witwatersrand. The experimental study, performed under different case studies, aimed to determine the electromagnetic influence of lightning on PV systems within the vicinity of the lightning strike and was used as a primary validation method. The induced voltages were measured experimentally for the different case studies as described in section 4.2, including the influence of DC cables twisted-pair configuration. The experimental investigation process flow is outlined in figure 4.8.

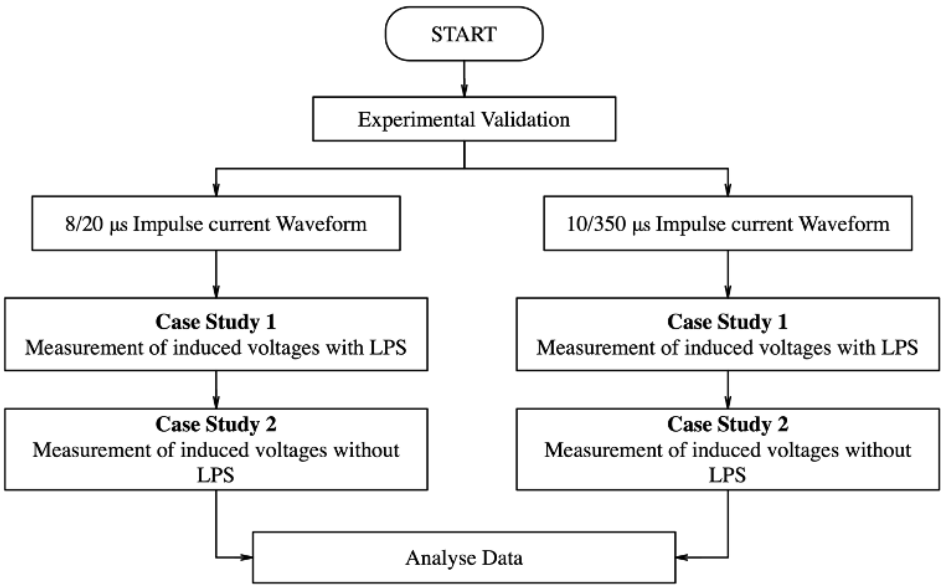


Figure 4.8: Experimental Investigation Process flow

4.4.1 Generation of high impulse current

(a) **Lightning stroke model**

The waveshape adopted for this experiment had a rapid rise to the peak and a decline to zero. Two standard lightning current waveforms were adopted: the 8/20 μs impulse current waveform with $\tau_1 = 8\ \mu s$ and $\tau_2 = 20\ \mu s$, rise and fall times, respectively, and the 10/350 μs lightning current waveform with $\tau_1 = 10\ \mu s$ and $\tau_2 = 350\ \mu s$. The generator had a tolerance of $\pm 10\%$ for the peak and $\pm 20\%$ for the fall time, while the polarity reversal of the current did not exceed 30% of the peak value of the current.

(b) **Impulse generator**

The impulse current generator, consisting of multiple capacitors charged by a high voltage direct source and then connected in series to a test object (dependent on the case study) through spark gaps, was used to generate high impulse currents for the experiments. The circuit parameters of the impulse generator can be adjusted to give the impulse current of the desired shape. The circuit diagram of the high impulse current generator consisting of a DC changing set with non-inductive charging resistors, charging and discharging capacitors, waveshaping resistors is illustrated in figure 4.9.

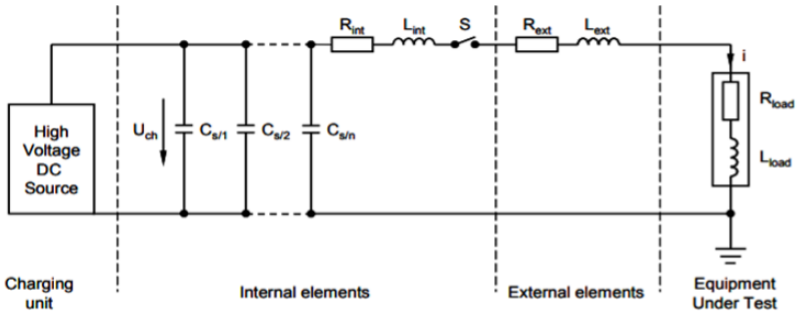


Figure 4.9: High current impulse generator

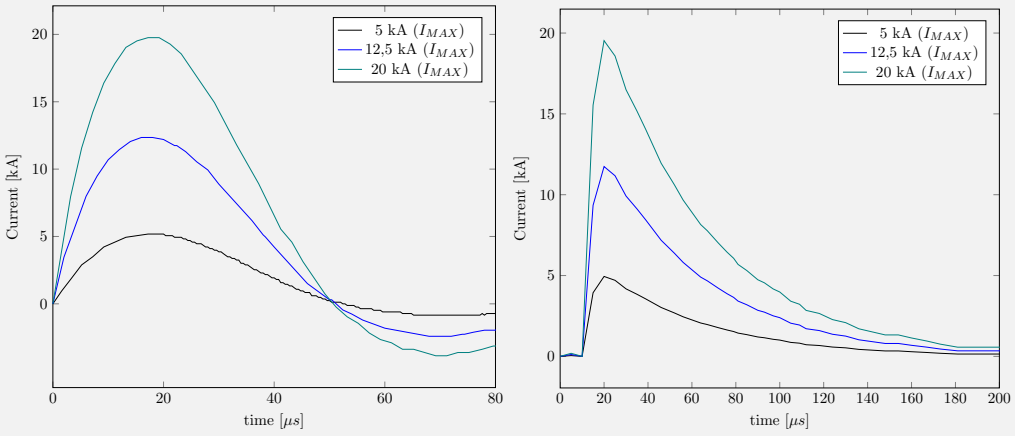
The impulse generator used in the experimental study had sufficient capacity to deliver the required waveform within the tolerances set. The charge of the impulse current is defined as the time integral over the absolute value of the waveform:

$$Q = \int_0^\infty |i(t)|\, dt \tag{4.2}$$

The joule integral, defined as the time integral of the square of the impulse current is calculated as:

$$W = \int_0^\infty i^2(t)\, dt \tag{4.3}$$

The impulse current waveforms measured in the laboratory are shown in figures 4.10 (a) and (b).



(a) 8/20 μs Impulse current waveform **(b)** 10/350 μs Impulse current waveform

Figure 4.10: Experiment Impulse current waveforms

(c) **Inductance considerations**

Lightning current, having a similar behaviour to a current source, can generate high voltages at the point of the strike to the circuitry impedance of the structure. This voltage can be described with the following equation:

$$V = IR + L\frac{di}{dt} \tag{4.4}$$

where I is the peak current, R is the resistance and L is the inductance. Lightning is usually in high values of peak current; it is to be expected that the voltages at the strike points can be in megavolts across the conductors. Increasing the circuit's total inductance can decrease the total peak current, increase the undershoot value and affect the rise time. Considering this, the results would be affected by the magnitude of the inductance of the total circuit.

4.4.2 Experimental equipment

The components used for the experiment are outlined in table 4.2, and the experimental setup is illustrated in figure 4.11.

Table 4.2: Experimental components

Component	**Specification**
PV Panel	300 W PV Panel
Implulse Generators	8/20 μs (20 kA I_{max}), 10/350 μs (20 kA I_{max})
High Voltage Output	Spellman SA501P4, 50 kV, 208Vac±10%, 50 or 60Hz
Oscilloscopes	2*Rigol DS1064B 60 MHz Oscilloscopes, Rise Time 5.8 ns Input, Impedance 1 M Omh——18 pF, Timebase Range 5 ns/div 50 s/div, Vertical Sensitivity 2 mV/div 10 V/div
Pulse Current Transformer	Pearson Model 301X, Volt Per Amp 0.01
Microinverter	Input power - 300 -350 W, Operating Voltage - 29 - 48 Maximum Input Current 10.5 A
Lightning Rod	Steel, height 1,5 m, diameter 16 mm, situated 1 metre from the panel
PV Stand	Steel - Specifically designed to fit the PV panel

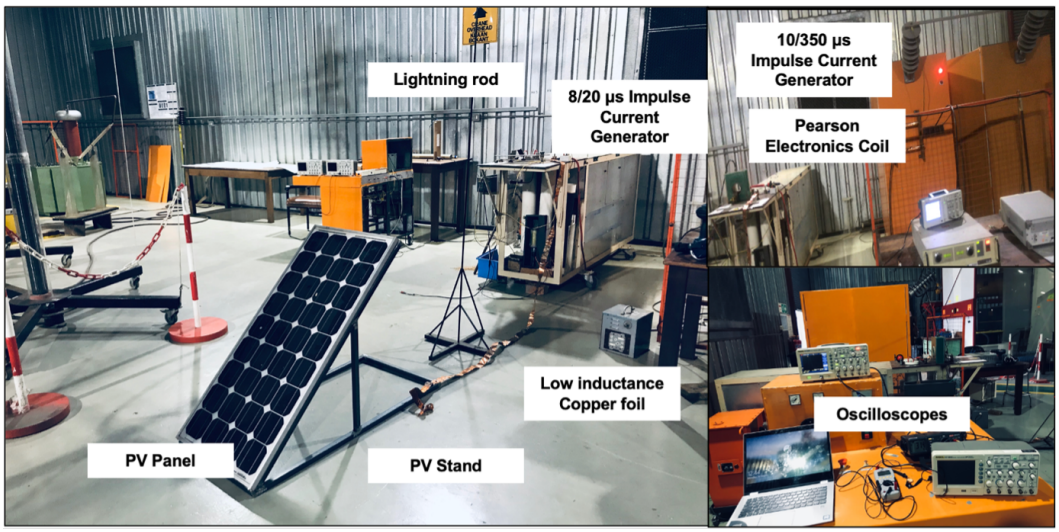


Figure 4.11: Experimental setup

4.4.3 Voltage and current measurements

The impulse current was measured using a Pearson Electronics coil (current transformer). The output received from the oscilloscope is a voltage proportional to the current on the device, this value being 0.01 V for 1 A. The protection circuit was connected to the oscilloscope via a coaxial cable. The differential voltage across the shunt resistor was measured by the oscilloscope. The induced voltages on the DC cables of the PV panel were measured using an oscilloscope triggered to measure the rising edge of the voltage waveform.

4.4.4 Test procedure

The test procedure of the experiment was:

(a) The reference waves were established using short circuit modes of the impulse generators and recorded on the oscilloscopes.

(b) The initial test impulse current was applied to the test object, and induced overvoltages were measured across the DC cables of the PV panel.

(c) The peak current level was increased incrementally using 5 kA, 12.5 kA, and 20 kA (I_{max}) for the open DC configuration and 1 kA, 2 kA and 5 kA (I_{max}) for a microinverter configuration.

(d) The voltage waveform of the impulse was recorded on an oscilloscope.

(e) The process was conducted for the case studies described in section 4.2.

4.5 Simulation 2: PSCAD

The second simulation was performed in PSCAD, allowing component modelling and visualisation flexibility. To correctly select protection measures, an SPD was connected to the DC cables of a PV system with a microinverter. The induced voltages measured on the DC cables from the COMSOL Multiphysics® simulation were introduced to the PSCAD model. Further analysis was performed, including the development of protection measures and protection performance (Figure 4.12).

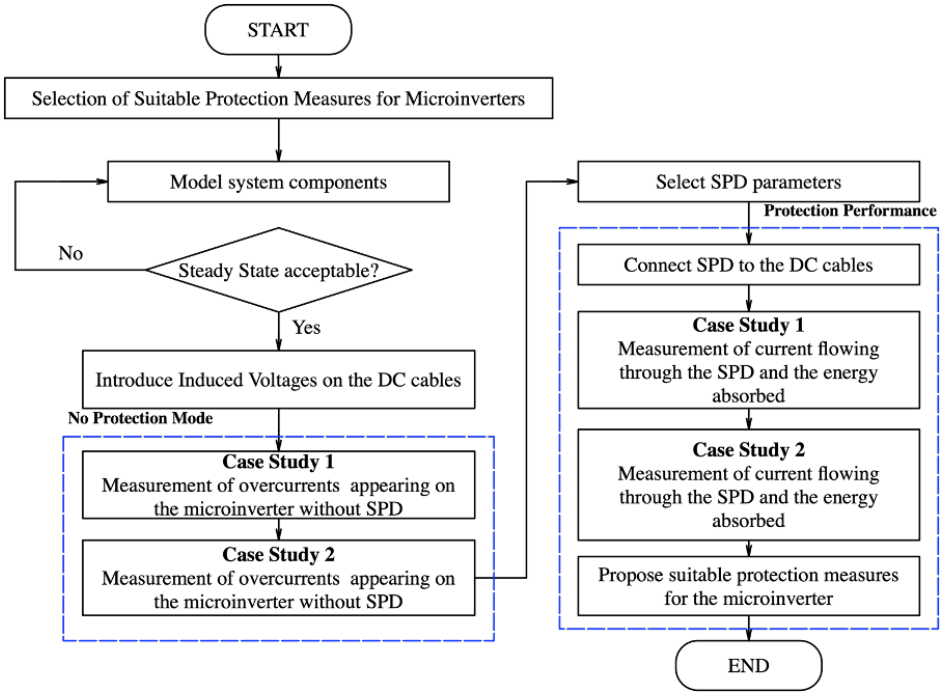


Figure 4.12: PSCAD simulation process flow

4.5.1 Model development in PSCAD

A simple block diagram of the microinverter can be seen in figure 4.13. The microinverter PV model consisting of the DC-DC and DC-AC converter stages was modelled on PSCAD. The microinverter model was composed of the power circuit and the control circuit. The power conversion occurred with DC-DC and DC-AC converter stages (Figure 4.14). The DC-DC converter stage used a boost converter, and a full-bridge converter was used for the DC-AC stage. The control circuit mainly controlled the voltage at the DC link and the inverter output through amplitude and references.

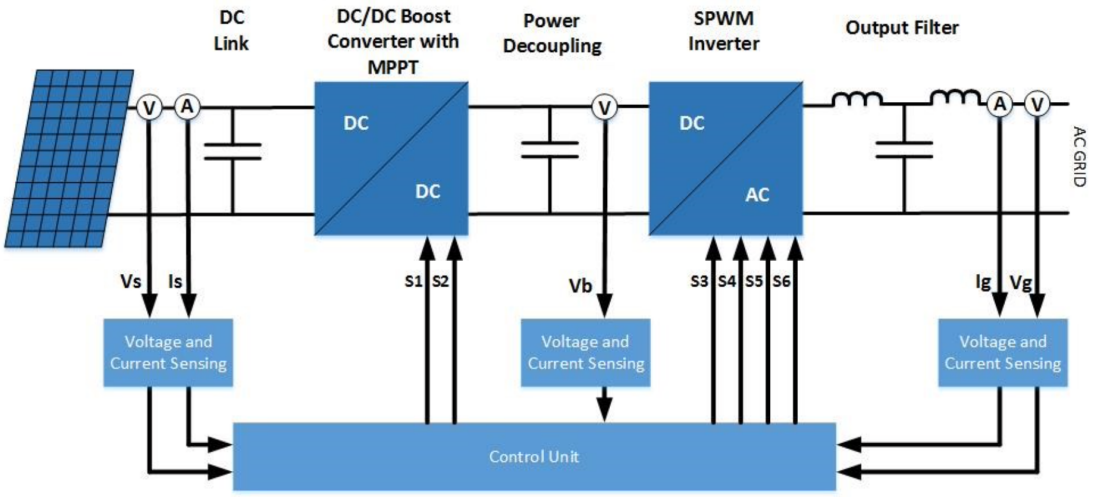


Figure 4.13: Microinverter block diagram [14]

The panel fed the boost converter with an input voltage of 30 V from the PV panel. The output voltage of the boost converter was 400 V, which was subsequently the input to the inverter stage to give an output voltage of 230 V to the grid.

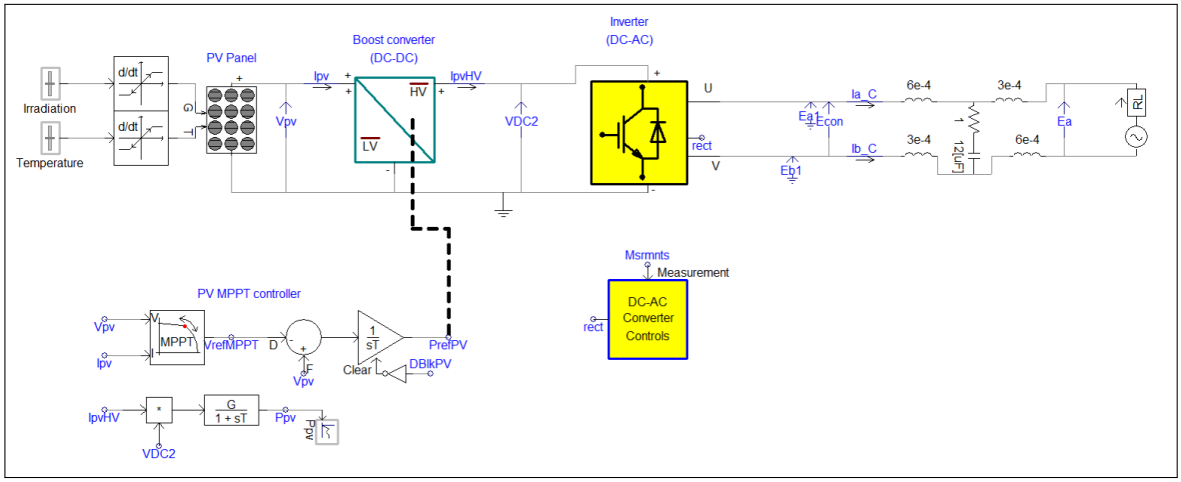


Figure 4.14: Microinverter Model developed in PSCAD

(a) PV panel

The PV panel implemented was created from the PSCAD library with fixed temperature and irradiation of 25°C and 1000 W/m2, respectively (Figure 4.15). Table 4.3 shows the default parameters of the PV panel.

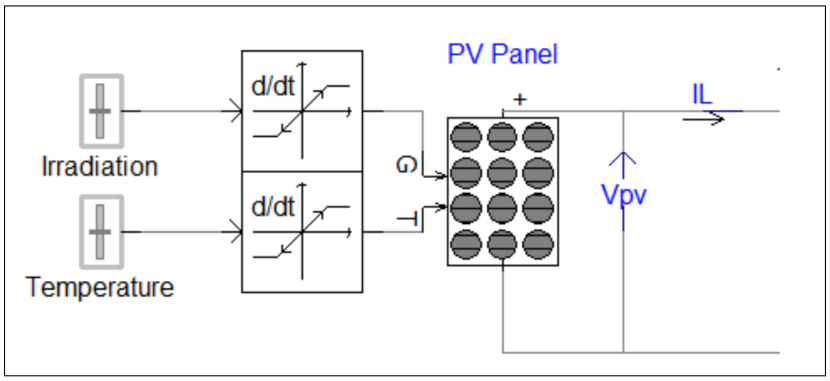


Figure 4.15: PV panel model developed in PSCAD

Table 4.3: PV panel parameters

Name	Value
Series Resistance Per Cell	0.02 Ω
Diode Ideality Factor	1.5
Shunt Resistance per Cell	1000 Ω
Band Gap Energy	1.103 eV
Effective Area per Cell	0.01
Number of Cells connected in series	36
Temperature coefficient of photo Current	0.001

(b) **Boost converter: DC-DC stage**

DC-DC converters are widely employed in PV system microinverter technologies. The voltage required at the inverter stage greatly exceeds the input voltage of the panel, and therefore a high gain. Models reviewed have shown that both transformer models and transformer-less models are employed. However, for this research, a transformer-less topology was implemented.

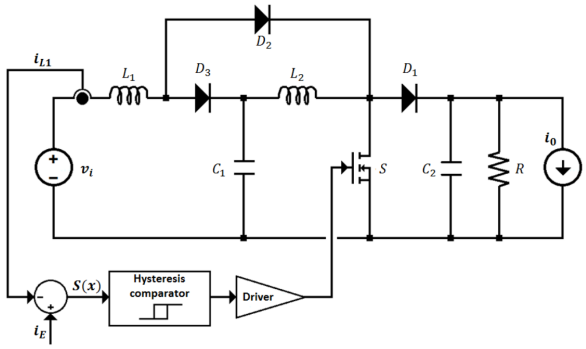


Figure 4.16: Quadratic boost converter [16]

As shown in figure 4.16, the boost converter operated under two modes, on-state and off-state, where the switch was turned on and off, respectively, using control circuitry. In the on-state, the inductor was charged, increasing the current. In the off-state, the inductor discharged and charged the capacitor through the diode. This energy can be expressed as:

$$W_L = \frac{Li^2}{2} \tag{4.5}$$

This energy is therefore converted to electric field energy of the capacitor:

$$W_c = \frac{Cu^2}{2} \tag{4.6}$$

The required capacitance and inductance can be calculated as:

$$L = (U_2 - U_1)\frac{{U_1}^2}{{U_2}^2}\frac{T}{2I_2} \tag{4.7}$$

$$C > \frac{TI_{2max}}{U_2} \tag{4.8}$$

where U_1 and U_2 are the input and output voltages to the converter, I_2 is the current, and T is the duty cycle.

The component parameters are listed in table 4.4 [16].

Table 4.4: Boost converter parameters

Element	Parameter	value
Inductor 1	L1	120 μH
Inductor 2	L2	4.7 mH
Capacitors	C1 and C2	10 μF
MOSFET	M1	$V_{gate} = 12$ V
Diodes	D	$V_{dx} = 0.75$ V

The input side of the boost converter shown in figure 4.17 consisted of a low pass filter. The control circuit shown in figure 4.18 used a combination of measurement principles and a PI controller constantly monitoring the error signal to generate the converter duty cycle. The PI controller coefficients (i.e., KpBoost and TiBoost) and its output limit (DmaxBoost) were adjusted to provide an accurate required output voltage. The reference voltage (Vref) is compared with the DC-link voltage (VH) during this process. Figure 4.19 illustrates the duty cycle process.

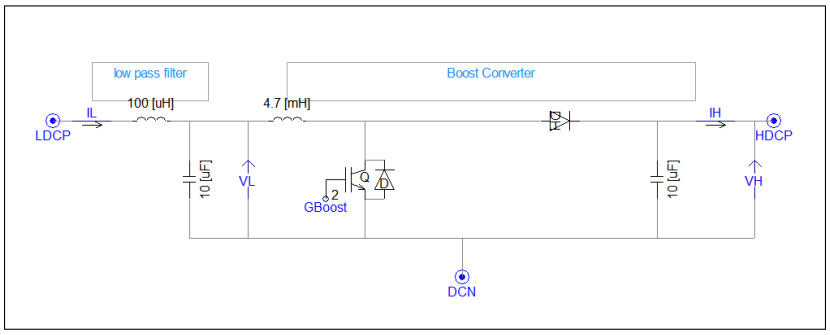


Figure 4.17: Boost Converter implementation on PSCAD

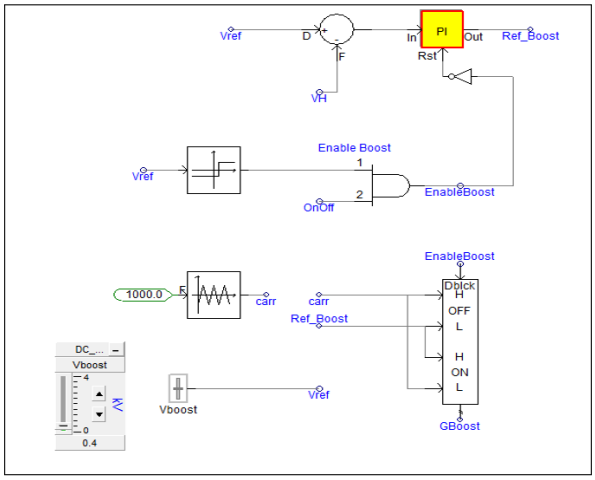


Figure 4.18: Boost converter control circuit implementation on PSCAD

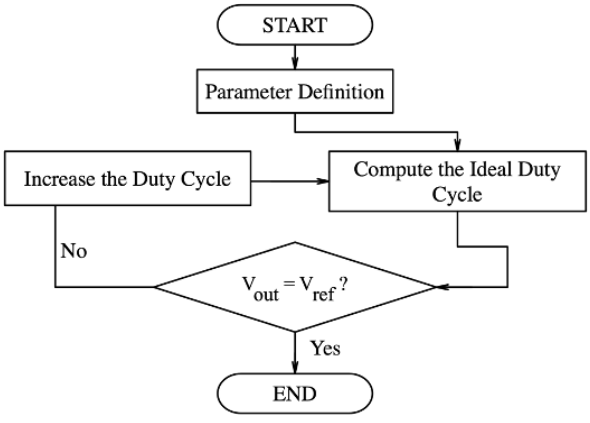


Figure 4.19: Boost converter control - duty cycle process

(c) Inverter: DC-AC Stage

A Full bridge converter is often applied in grid applications to provide the required

voltage and waveshapes to meet the grid requirements (figure 4.20). The full-bridge converter operating as an inverter works with an energy source always available on the DC side. In microinverter applications, the DC side of the inverter is fed with a 400 V DC link voltage source. The control circuit applies a current tracking loop combined with other algorithms to meet the control objectives.

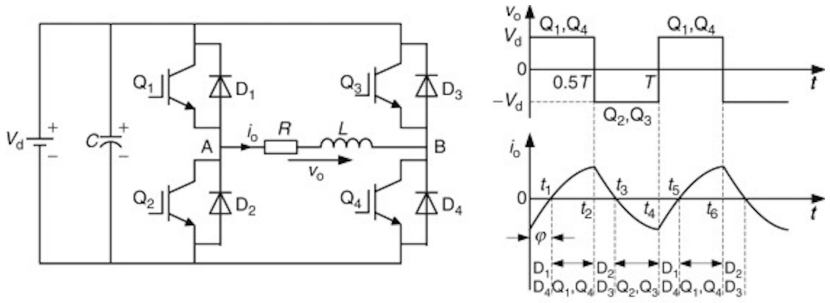


Figure 4.20: Voltage Source Inverter [15]

Q_1 and Q_4 operate as pairs, as do Q_2 and Q_3. The load was connected in the middle of the bridge circuits. The four diodes (D_1 to D_4) provided a current path for the energy stored in the load inductor. Initially, Q_1 and Q_4 were closed until t_1; this process allowed the current to flow while voltage was applied at the load (Figure 4.23). At t_1, Q_1 and Q_4 are reopened; this stops the flow of current and removes the voltage. During this time, Q_2 and Q_3 are closed to change the load's polarity of the voltage, thus allowing the current to flow in the opposite direction. At a certain time, t_2, Q_2 and Q_3 are reopened and Q_1 and Q_4 are re-closed. This process continues [15]. The full-bridge modelled in PSCAD is shown in figure 4.21 the control circuit is shown in figure 4.22, and DC-AC controls circuit is shown in figure 4.23.

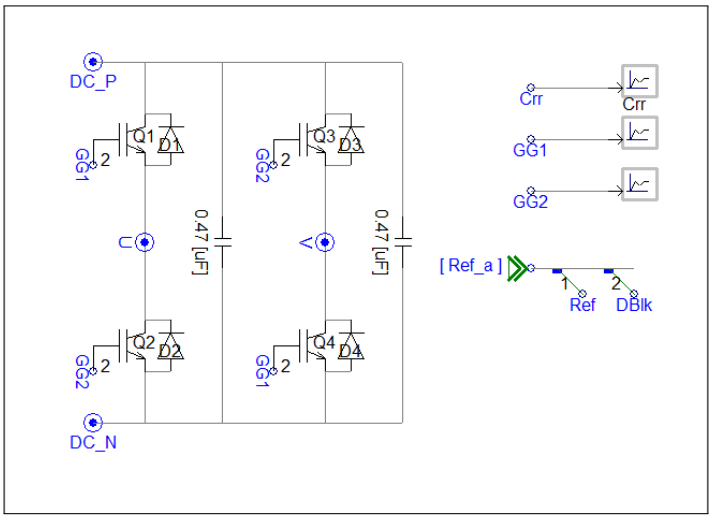


Figure 4.21: Inverter model implemented in PSCAD

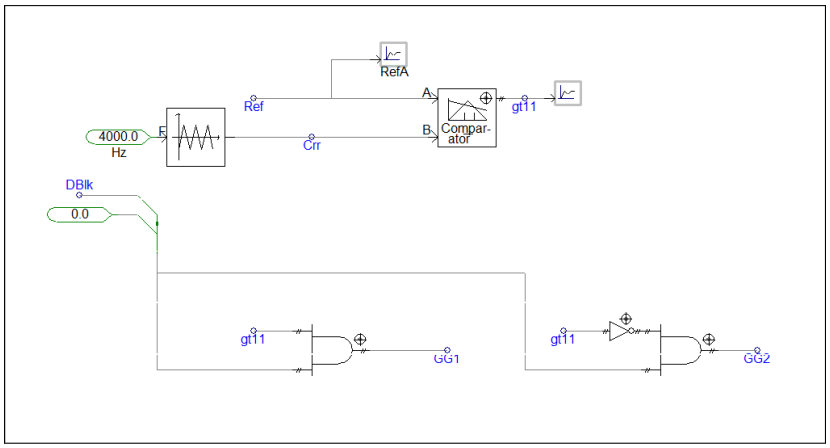


Figure 4.22: Inverter gate control circuit

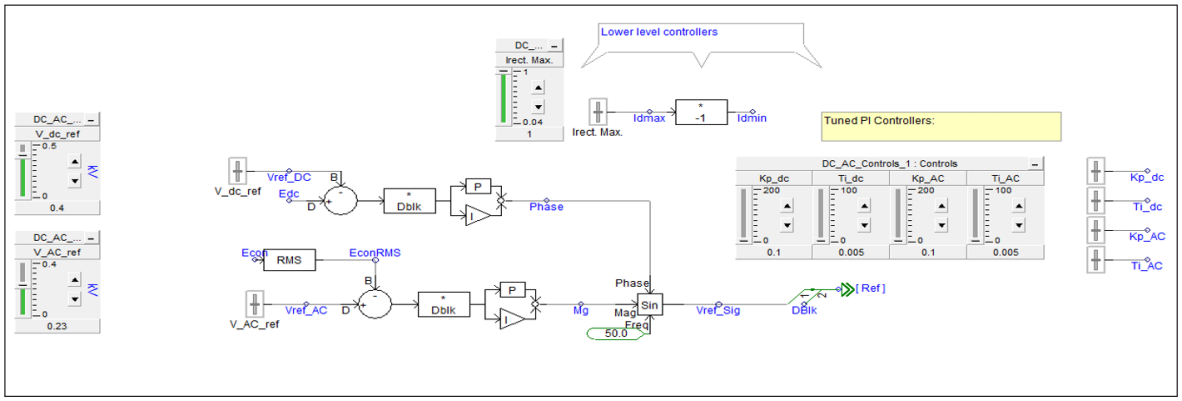


Figure 4.23: DC-AC converter Controls

4.5.2 Protection performance

The induced voltages measured on the open DC terminals on the COMSOL Multiphysics® model were taken as the voltages that microinverters were subjected to and applied to the PSCAD model. The data points as measured were transferred to a voltage source in PSCAD. Figure 4.24 demonstrates how this voltage was connected to the DC terminals of the model.

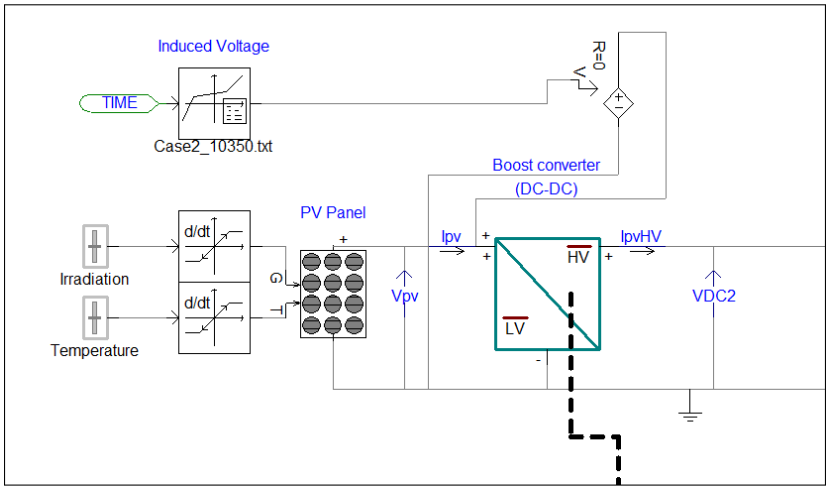


Figure 4.24: Induced voltage soruce on PSCAD

A protection measure based on an SPD connected to the DC cables was employed to mitigate transient overvoltage under withstand voltage of the microinverter and reduce the risk of failure. The IEC 61643-32:2017 [77] and IEC 61643-31:2018 [76] standards, along with surge protection standards, were used as guidance. The SPD was connected between the PV DC cables and the microinverter while the induced voltages measured on the open DC terminals on the COMSOL Multiphysics® simulation were applied. The process of selecting the characteristics of the SPD is outlined in figure 4.25.

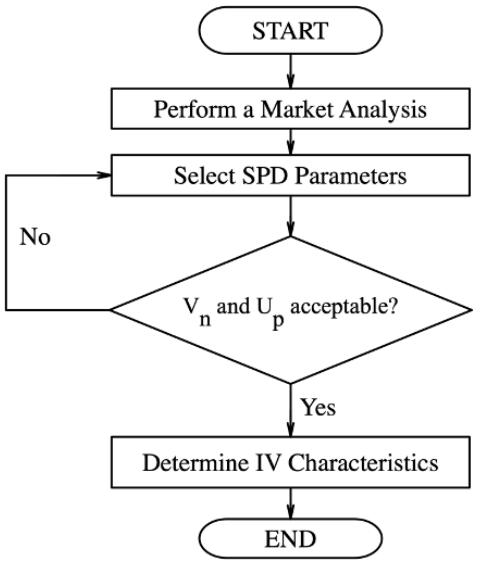


Figure 4.25: SPD selection process

The selection of the U_w of the microinverter was based on IEC 61442 – 2010 [17] standard, where impulse withstands levels in a low-voltage system are specified (Table 4.5). Since microinverters operate in voltages lower than 50 V, an overvoltage category II U_w of 500 V was selected for the DC protection.

Table 4.5: Insulation voltage for low voltage circuits. Data adapted from [17]

System Voltage (V)	Impulse Withstand Voltage (V)			
	Overvoltage Category			
	I	II	III	IV
50 Vrms or 71 Vdc	330	500	800	1500
100 Vrms or 141 Vdc	500	800	1500	2500
150 Vrms or 213 Vdc	800	1500	2500	4000
300 Vrms or 424 Vdc	1500	2500	4000	8000

The parameters of the MOV selected and used in the investigation are given in table 4.6.

Table 4.6: Characteristics of the selected MOV

Model	Max Line to Line Voltage (V)	SPDs Protection Level (U_p) (V)	Recommended MCOV or Uc (V)
SPV48-V-S/C	48	400	85

The $I - V$ characteristics of the SPD were selected based on typical manufacturer data. These values were simulated using an Interactive V-I Characteristic Curve Generator de-

veloped by Woodworth and Limburg [94]. Table 4.7 shows the V-I characteristics for the selected MOV. The resulting characteristic curves of the selected MOV for the MCOV and an MCOV adjusted by 12% can be seen in figure 4.26.

Table 4.7: IV Characteristics of the selected MOV

Current (kA)	Voltage (P.u)
0.01	0.425
0.125	0.498
0.5	0.531
1	0.5616
1.5	0.581
3	0.6122
5	0.6425
10	0.6881
20	0.7564
40	0.85
100	1.0625

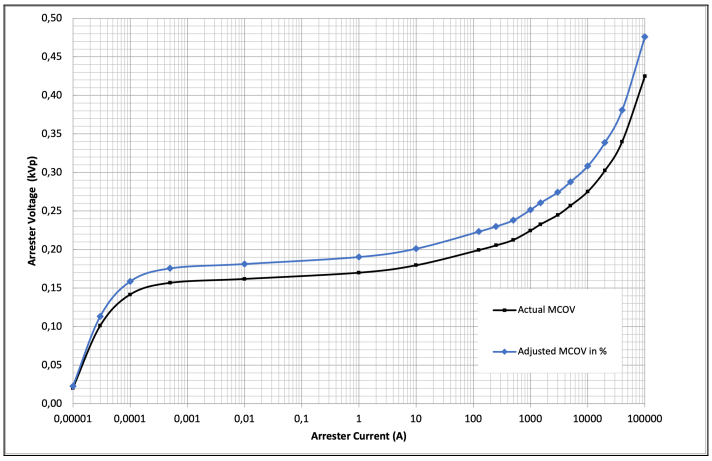


Figure 4.26: Current and voltage characteristics for the selected MOV

Figure 4.27 shows the configuration of SPD installation for the DC cable.

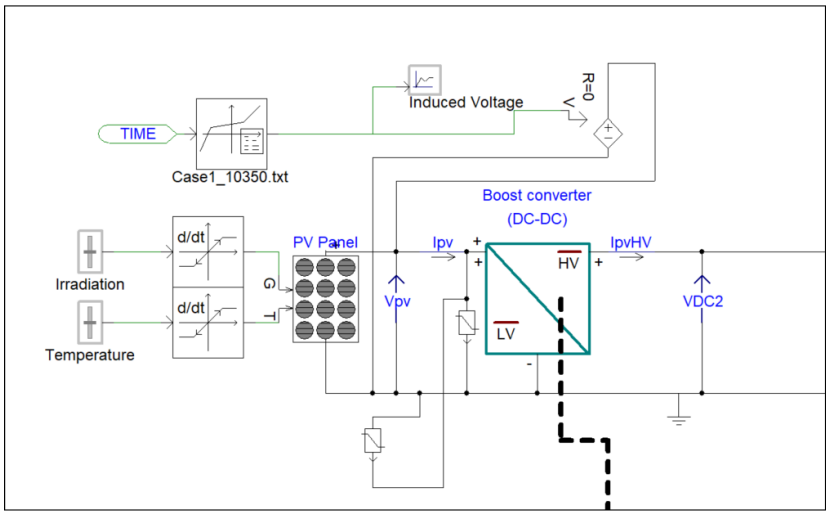


Figure 4.27: Microinverter model with SPD connected on the DC cables

The simulations focused on the influence of the SPD connected between the DC cables were performed with induced voltages measured from the COMSOL Multiphysics® simulation in different protection scenarios. Maximum currents across the SPD and the energy absorbed by the SPD (Equation 3.35) were used as performance criteria for assessing protection performance.

4.6 Chapter Summary

This chapter has introduced the experimental setup and the simulations. First, the method of generating the impulse current using an impulse generator was discussed. Specifics of the impulse generator and the test object were also discussed. Furthermore, some considerations for performing the experiment were discussed, including inductance, voltage and current measurements. Finally, and similarly, the simulation setup and considerations were discussed.

5 Simulation 1: Measurement of Induced Voltages (COMSOL Multiphysics® Simulation)

5.1 Introduction

Evaluating lightning-induced voltages has been one of the most important factors in designing and coordinating protection measures in electrical systems. In PV systems, these induced voltages may damage sensitive electronic equipment, including the inverter connected to the DC cables. Therefore, the magnitude and waveforms of these voltages may be used to develop, design or select surge protection devices in PV systems. Simulations have been performed through research to determine the magnitudes of these lightning-induced voltages for several electrical systems over the years.

This section investigated the induced overvoltages on the DC cables of a PV panel using a simulation. The investigation was carried out using COMSOL Multiphysics® simulation software. The measurements were carried out using the two simulated current waveforms (10/350 µs and 8/20 µs using the Heidler function) injected at different positions, as described in Chapter 4. The lowest impulse current magnitude adopted in the simulation was 5 kA, and the highest was 100 kA. Despite having a low probability of occurrence, the highest impulse current is favourable in regard to the most severe circumstance.

5.2 Case Study 1 Simulation Results

In this simulation case study, the impulse current was injected on the external LPS. The resultant induced voltages were measured between the DC cables with distances of one, two and three metres between the LPS and the panel. The impulse currents of 8/20 μs and 10/350 μs represented by the Heidler function as specified by IEC 62305-1:2010 [63] standard with peak currents of 5 kA, 12.5 kA, 20 kA and 100 kA were simulated. In this investigation, it was observed that the maximum induced overvoltages depend on the impulse current amplitude

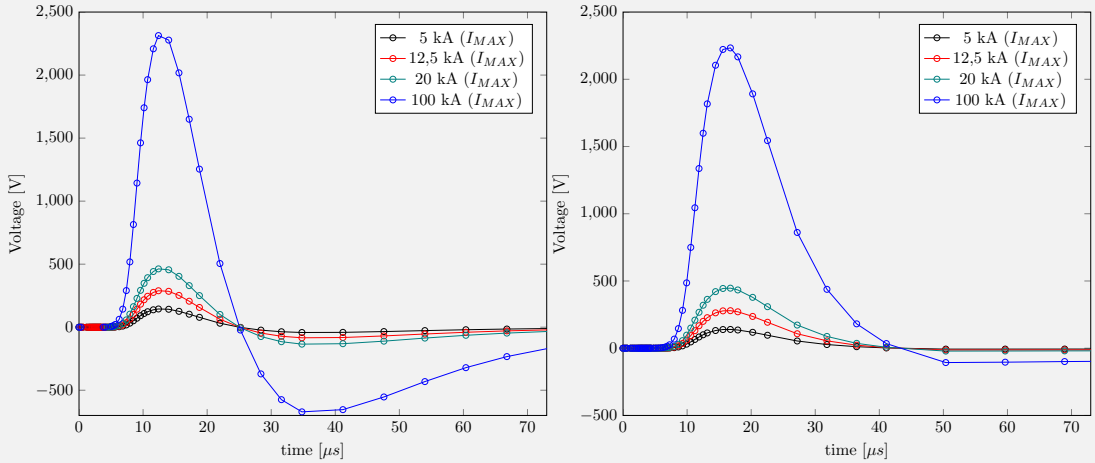
and the distance between the LPS and the PV panel.

5.2.1 LPS one metre from the PV panel

DM voltage waveforms when the LPS was one metre from the panel can be seen in figures 5.1 (a) and (b) under 8/20 μs and 10/350 μs impulse current waveforms. This is the transient voltage transmitted to the microinverter during a lightning strike. When a 100 kA impulse current was injected on the external LPS, the overvoltages measured on the DC cables in DM configuration under 8/20 μs waveform was 2.31 kV. In addition, 462 V was measured for a 20 kA impulse current and 289.12 V for a 12.5 kA impulse current. For the 10/350 μs impulse waveform, the maximum induced voltages were 113.25 V, 280.70 V, 448.54 V, and 2.2 kV for 5 kA, 12.5 kA, 20 kA, and 100 kA impulse currents, respectively. The waveforms show a linear increase in voltage and impulse current.

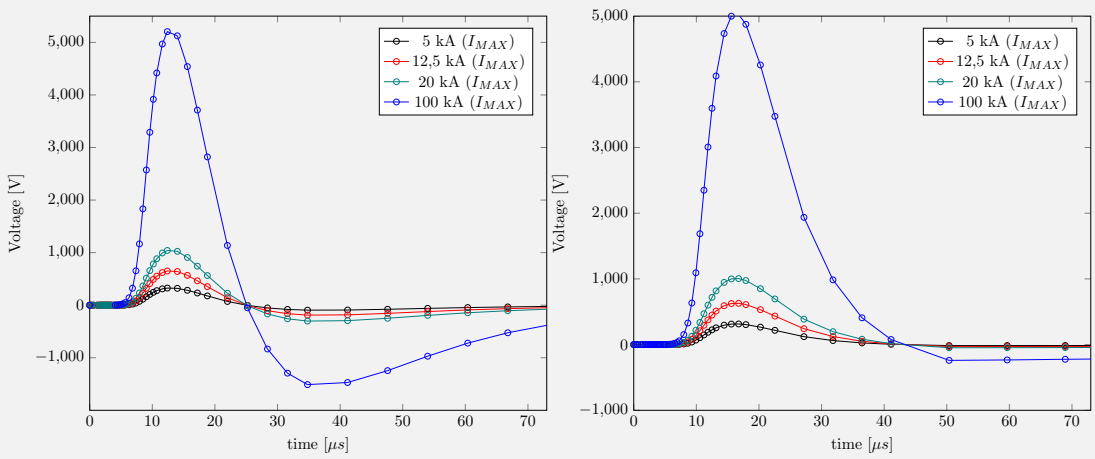
Figures 5.2 (a) and (b) show the induced voltages measured in CM configuration under 8/20 μs and 10/350 μs impulse currents, respectively. Under extreme lightning currents (100 kA), it was observed that these voltages might exceed the minimum withstand voltage for PV inverters at extreme currents as prescribed by IEC 61643-31:2017 [76] standard. The results with the rod connected under 8/20 μs impulse waveform indicated induced overvoltages (V_{max}) as high as 1040 V when exposed to an impulse current (I_{max}) of 20 kA injected on the rod. When the system was tested with a 5 kA impulse current, 260 V was measured on the DC cables. When the system was exposed to a 12.5 kA impulse current, 650 V appeared on the lines. Using a 100 kA extreme current, the induced overvoltage rose significantly to 5.2 kV on the DC cables. For the 10/350 μs impulse waveform, the maximum induced voltages in CM were 252 V, 631.07 V, 1.01 kV, and 5.04 kV for 5 kA, 12.5 kA, 20 kA, 100 kA impulse currents respectively. These findings are important for developing protection measures for microinverters against lightning transients. A summary of maximum induced voltages when the LPS was placed one metre from the PV panel is given in table 5.1.

The LIO maximum amplitudes differed slightly for the 8/20 μs and 10/350 μs impulse currents. Maximum amplitudes with an 8/20 μs waveform were slightly higher than those recorded for a 10/350 μs waveform due to the current differential. The other difference between induced voltage waveforms was the rise and fall times, which may affect the energy when an SPD is connected. For the 8/20 μs impulse current, the induced overvoltage waveforms had a polarity reversal caused by the quick rise and fall times and thus a higher peak to peak voltage. On the other hand, for the 10/350 μs impulse current, the induced overvoltage waveforms had a longer duration with minimal polarity reversal. Based on these results, it is inevitable that even when the lightning rod is installed on a PV residential, microinverters are still subjected to induced overvoltages, which could damage the internal components.



(a) Induced overvoltages, 8/20 μs impulse **(b)** Induced overvoltages, 10/350 μs impulse

Figure 5.1: Simulation case study 1: Induced overvoltages DM, LPS 1 m



(a) Induced overvoltages, 8/20 μs impulse **(b)** Induced overvoltages, 10/350 μs impulse

Figure 5.2: Simulation case study 1: Induced overvoltages CM, LPS 1 m

.

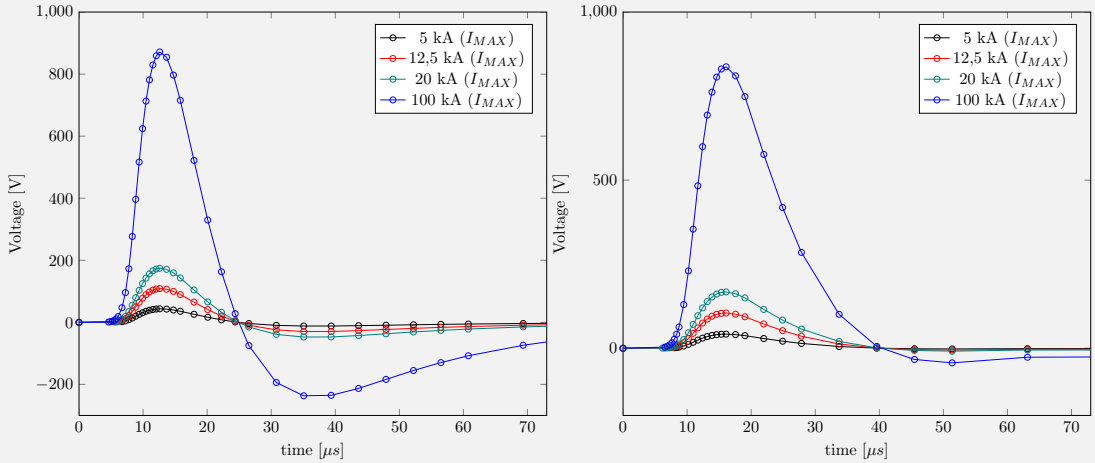
Table 5.1: Maximum induced overvoltages when the LPS was placed one metre from the PV panel

Impulse Current (I_{max})	**Induced Overvoltages (V_{max}) LPS 1m**			
	DM		**CM**	
	8/20 μs	**10/350 μs**	**8/20 μs**	**10/350 μs**
5 kA	115,65 V	113,25 V	260 V	252 V
12,5 kA	289,12 V	280,70 V	650 V	631.07 V
20 kA	462 V	448.54 V	1040 V	1.01 kV
100 kA	2.31 kV	2.24 kV	5.2 kV	5.04 kV

5.2.2 LPS two metres from the PV Panel

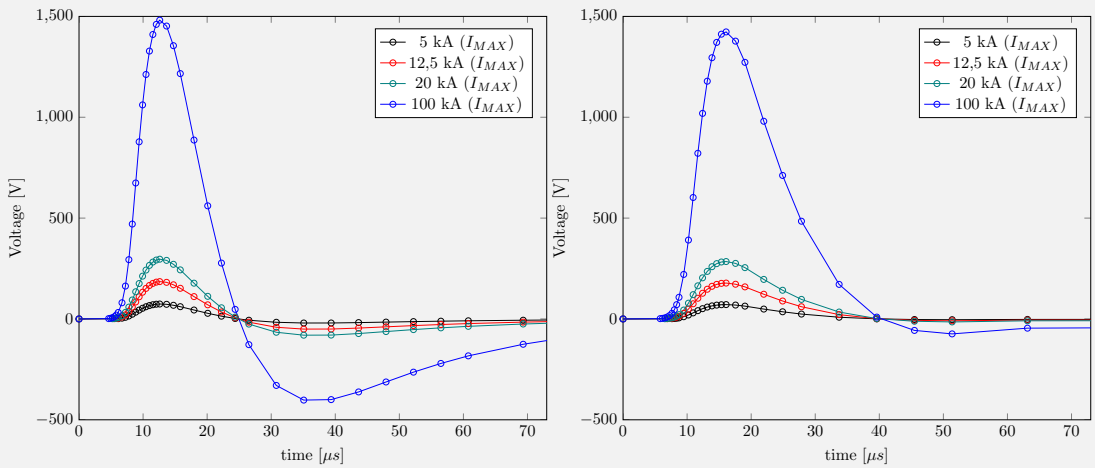
The incremental increase in the distance between the PV panel and the LPS indicated a reduction in induced overvoltages (Figures 5.3 (a) and (b) compared to Figures 5.1 (a) and (b)). When a 100 kA impulse current was injected, an induced overvoltage of 850 V for 8/20 μs impulse currents in the DM configuration was observed. For a 20 kA and 12.5 kA impulse current, the induced overvoltage was 462 V and 289.12 V, respectively (Figure 5.3 (a)). For the 10/350 μs impulse waveform, the maximum induced voltages were 40.64 V, 101.59 V, 162.54 V, and 812.73 V for 5 kA, 12.5 kA, 20 kA, and 100 kA impulse currents respectively (Figure 5.3(b)).

The voltage waveforms for CM configuration are illustrated in figures 5.4 (a) and (b). The highest overvoltage measured for a 100 kA in 8/20 μs impulse current was 1.42 kV, and when the same current waveforms with a 20 kA peak were injected, an overvoltage of 284 V was measured. Similarly, a low overvoltage of 177 V was measured when a 12.5 kA impulse current was injected into the external LPS. For the 10/350 μs impulse waveform, the maximum induced voltages in CM were 68.93 V, 171.84 V, 275.72 V, and 1.38 kV for 5 kA, 12.5 kA, 20 kA, 100 kA impulse currents respectively. A summary of the induced overvoltages when the LPS was placed two metres from the PV panel is given in table 5.2.



(a) Induced overvoltages, 8/20 μs impulse **(b)** Induced overvoltages, 10/350 μs impulse

Figure 5.3: Simulation case study 1: Induced overvoltages DM, LPS 2 m



(a) Induced overvoltages, 8/20 μs impulse **(b)** Induced overvoltages, 10/350 μs impulse

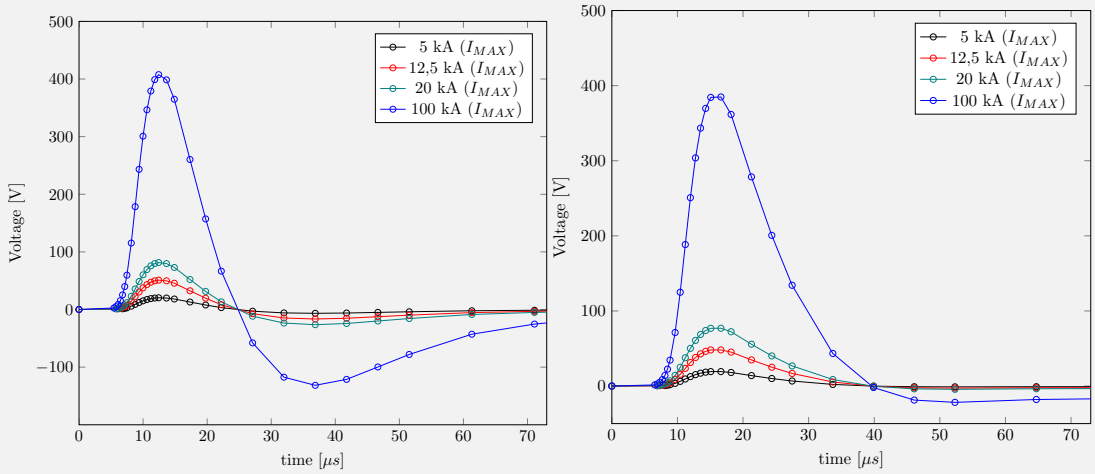
Figure 5.4: Simulation case study 1: Induced overvoltages CM, LPS 2 m

Table 5.2: Maximum induced overvoltages when the LPS was placed two metres from the PV panel

Impulse Current (I_{max})	**Induced Overvoltages (V_{max}) LPS 2m**			
	DM		**CM**	
	8/20 μs	**10/350 μs**	**8/20μs**	**10/350 μs**
5 kA	41.86 V	40.64 V	71 V	68.93 V
12,5 kA	104.64 V	101.59 V	177 V	171.84 V
20 kA	167.42 V	162.54 V	284 V	275.72 V
100 kA	837.12 V	812.73 V	1423 V	1.38 kV

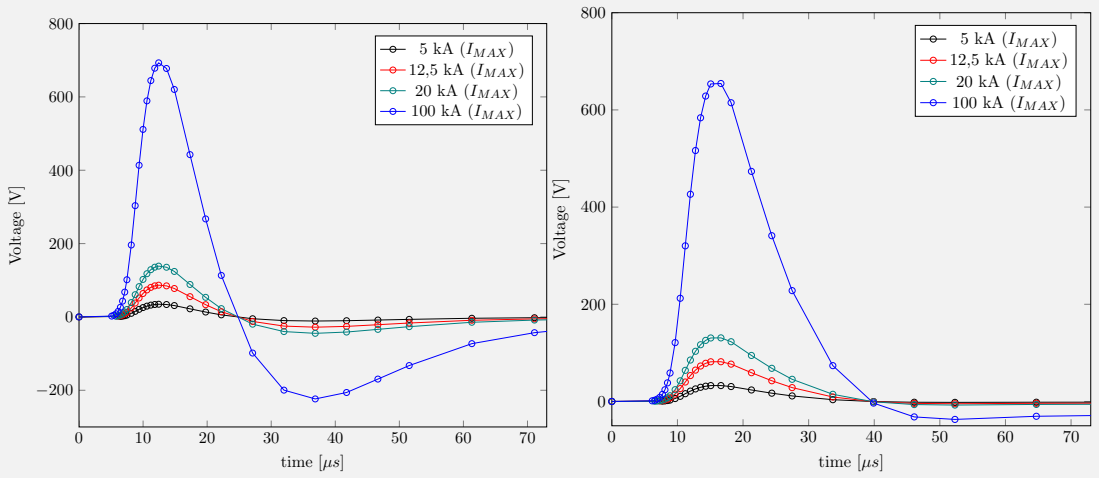
5.2.3 LPS three metres from the PV Panel

Further increase in the LPS-PV panel distance indicated a further reduction in overvoltages; for example, in DM configuration, the overvoltage measured for an 8/20 μs waveform reduced to 384.9 V and 654.33 V in CM for a 100 kA impulse current (Figures 5.5 and 5.6). A summary of the induced overvoltages when the LPS was placed three metres from the panel is given in table 5.3.



(a) Induced overvoltages, 8/20 μs impulse **(b)** Induced overvoltages, 10/350 μs impulse

Figure 5.5: Simulation case study 1: Induced overvoltages DM, LPS 3 m,



(a) Induced overvoltages, 8/20 μs impulse

(b) Induced overvoltages, 10/350 μs impulse

Figure 5.6: Simulation case study 1: Induced overvoltages CM, LPS 3 m

Table 5.3: Maximum induced overvoltages when the LPS was placed three metres from the PV panel

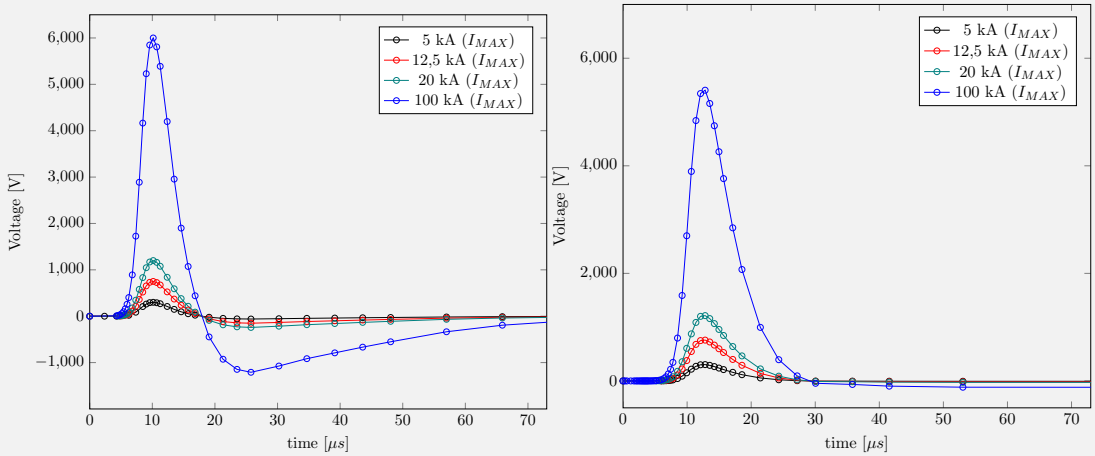
Impulse Current (I_{max})	**Induced Overvoltages (V_{max}) LPS 3m**			
	DM		**CM**	
	8/20 μs	**10/350 μs**	**8/20μs**	**10/350 μs**
5 kA	19.25 V	18.69 V	32.72 V	31.77 V
12,5 kA	48.11 V	47.71 V	81.79 V	79.40 V
20 kA	76.98 V	74.73 V	130.87 V	127.05 V
100 kA	384.90 V	373.68 V	654.33 V	635.27 V

5.3 Case Study 2 Simulation Results

In the second case study, the impulse current was injected into the PV panel's frame, and the resultant induced overvoltages were measured on the DC cables. The highest magnitude of induced overvoltages in DM was observed with a 100 kA injected current, where the induced overvoltage was 5.8 kV using an 8/20 μs impulse waveform. Using an injection current of 5 kA and 12.5 kA, induced overvoltages of 275 V and 687 V were measured on the DC cables, respectively. For 20 kA, an induced overvoltage of 1.1 kV was measured (Figures 5.7 (a) and (b)). The results further confirm that having a protection system for a PV system is important. The induced voltages measured for the CM configuration when the impulse current was injected into the PV panel's frame are shown in figures 5.8 (a) and (b). The highest induced overvoltages were 9.1 kV in 8/20 μs waveform when a 100 kA impulse current

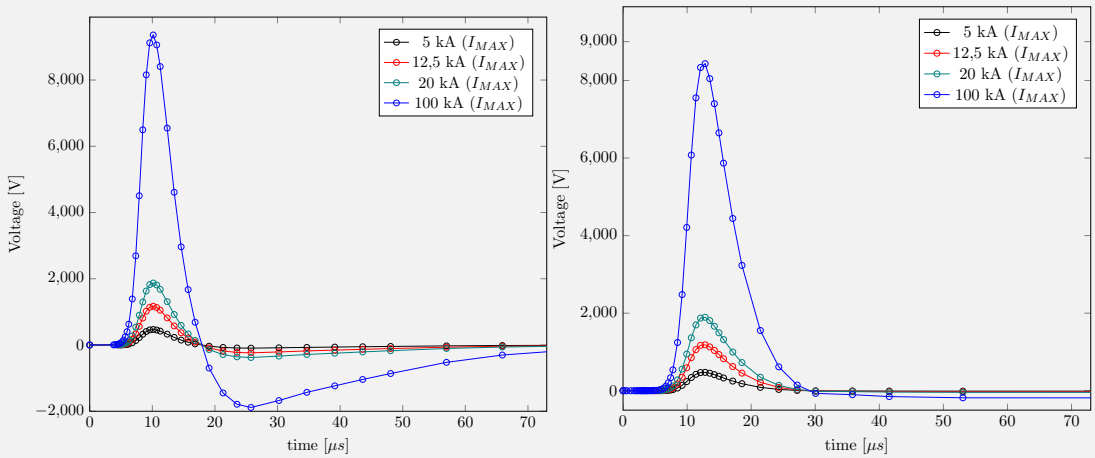
was injected. When a 20 kA maximum impulse current was applied, the voltage measured was 1.82 kV. The case study 2 simulation results are summarised in table 5.4.

Since the distance between the lightning surge to the DC cables is shorter compared to case study 1, the overvoltages appear to be higher and almost double the previous case study. It is important to note that this case study indicates a PV system without external lightning protection and represents one of the worst-case scenarios for induced overvoltages.



(a) Induced overvoltages, 8/20 μs impulse **(b)** Induced overvoltages, 10/350 μs impulse

Figure 5.7: Simulation case study 2: Induced overvoltages DM



(a) Induced overvoltages, 8/20 μs impulse **(b)** Induced overvoltages, 10/350 μs impulse

Figure 5.8: Simulation case study 2: Induced overvoltages CM

Table 5.4: Case study 2 simulation results

Impulse Current (I_{max})	**Induced Overvoltages** (V_{max})			
	DM		**CM**	
	8/20 μs	**10/350** μs	**8/20**μs	**10/350** μs
5 kA	275 V	244.75 V	455 V	404.95 V
12,5 kA	687.5 V	611.85 V	1.14 kV	1.01 kV
20 kA	1.1 kV	0.99 kV	1.82 kV	1.61 kV
100 kA	5.8 kV	5.16 kV	9.1 kV	8.1 kV

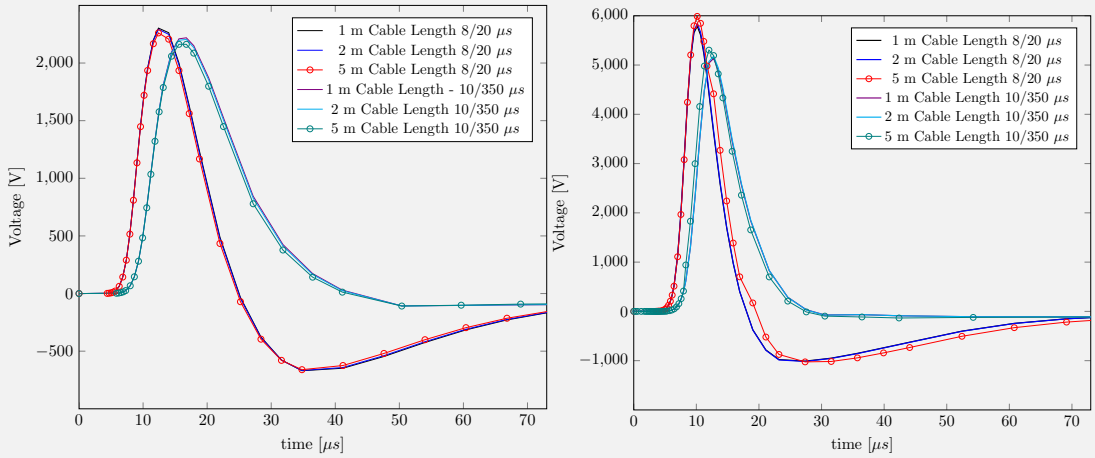
5.4 The effect of wire lengths

To investigate the influence of wire lengths, the length of the DC cables was increased from one metre to two and five metres. The length of the wires can affect the resistance of the circuit since the resistance of a wire may be represented by:

$$R = \rho \frac{L}{A} \tag{5.1}$$

where ρ represents the resistivity of wire material, L is the length of the wire, and A is the cross-sectional area of the wire.

The induced overvoltages measured with a 100 kA impulse current are represented in figure 5.9 (a) and (b) for case study 1 and case study 2, respectively. PV systems with microinverters usually have little DC wiring; therefore, the effect of wiring was tested with cable lengths of one, two and five metres. The maximum induced overvoltages for different cable lengths in different case studies at 100 kA are summarised in Tables 5.5 and 5.6 for case studies 1 and 2, respectively. It can be observed that the maximum induced voltages during this investigation change only slightly for all three cable lengths (1, 2, and 5 metres). These differences are almost negligible with small cable lengths. Since the voltage drop of the cables is little, it doesn't affect the induced voltages across the DC cables.



(a) Case study 1: Induced overvoltages **(b)** Case study 2: Induced overvoltages

Figure 5.9: Induced overvoltages with different DC cable lengths

Table 5.5: Maximum induced overvoltages for different DC cable lengths – Case Study 1

Induced Overvoltages (V_{max}) Case study 1		
Cable Length	**8/20 µs**	**10/350 µs**
1 m	2302.90 V	2210.78 V
2 m	2292.5 V	2200.6 V
5 m	2261.40 V	2170.944 V

Table 5.6: Maximum induced overvoltages for different DC cable lengths – Case Study 2

Induced Overvoltages (V_{max}) Case study 2		
Cable Length	**8/20 µs**	**10/350 µs**
1 m	5802.90 V	5512.90 V
2 m	5792.5 V	5502.50 V
5 m	5711.40 V	5311.60 V

5.5 Chapter Summary

The results from this investigation yielded the appearance of induced overvoltages on the DC cables of the solar panel when impulse current was injected at different positions. It is

also important to notice the influence of changing the lightning current stroke location. The simulation indicated that the induced overvoltages increase rapidly as the distance between the panel and the lightning strike is reduced. In general, variations in the magnitudes of overvoltages were observed by varying the location through different case studies. Greater magnitudes of induced overvoltages were observed when the lightning strike was near the panel. The current model makes it possible to predict LIOs on solar panels for different protection scenarios and current amplitudes, thus ensuring that the necessary protection measures for microinverters are taken.

This chapter has presented the results of the first simulation model. LIOs were measured across the DC cables of the PV panel in both components of the study. The observed induced overvoltages were subjected to different magnitudes of lightning currents while in different stroke locations.

6 Experimental Validation

6.1 Introduction

This chapter presents the findings from the experimental investigation. The magnitude of LIOs was investigated with impulse current injected at different positions (protection scenarios) with 8/20 μs and 10/350 μs standard lightning waveforms. It was also of considerable interest to perform measurements under DM and CM configurations to validate the simulation model. A thorough analysis and interpretation of these waveforms are considered one of the first steps in developing overvoltage protection measures.

6.2 Case Study 1 Experimental Results

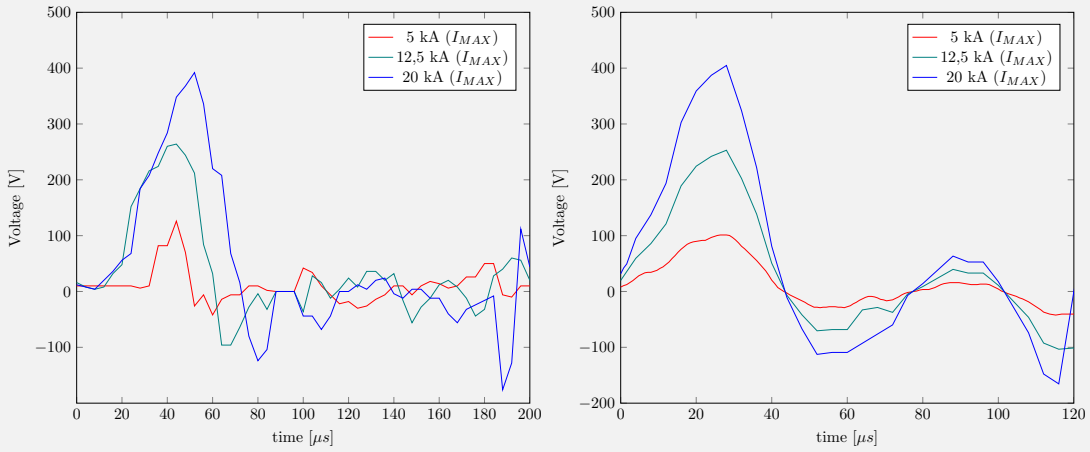
The first case study tested the PV panel with 8/20 μs and 10/350 μs standard current waveforms. The current was injected into the external LPS under different current magnitudes. The induced voltages were measured for three different impulse currents (5 kA, 12.5 kA and 20 kA) for open DC cables in 8/20 μs and 10/350 μs standard impulse waveforms. The induced overvoltage waveforms for the DM configuration are shown in figures 6.1 (a) and (b). The highest induced voltages for 8/20 μs and 10/350 μs lightning impulses were 430 V and 415 V, respectively, when a 20 kA impulse current was injected. When a 12.5 kA impulse current is injected, the induced overvoltages were 284 V and 267 V. For a 5 kA impulse current, the voltages were 126 V and 116 V for 8/20 μs and 10/350 μs lightning impulses, respectively. Thus, no significant amplitude differences were observed between the 8/20 μs and 10/350 μs standard lightning waveforms. The highest voltages measured in 8/20 μs and 10/350 μs current waveforms in CM were 980 V and 890 V for a 20 kA impulse current (Figure 6.2 (a) and (b)). When the LPS was injected with a 12.5 kA impulse current, the highest voltages were 660 V and 732 V, and for a 5 kA impulse, 272 V and 293 V were measured for 8/20 μs and 10/350 μs current waveforms, respectively. The CM-measured induced voltages were greater than the DM induced voltages.

Table 6.1 and 6.2 show the maximum induced voltages for case study 1 in open DC cables for impulse currents for 5 kA, 12,5 kA, and 20 kA) and with a microinverter (for 1 kA, 2 kA,

and 5kA) respectively. Similar to the simulation study in chapter 5, the voltage waveforms appear to increase linearly with the impulse current increase. This indicates that the induced overvoltage strongly depends on the impulse current, showing a linear proportional increase. It was observed that the CM configuration measured overvoltages greatly exceeding that of the DM configuration, similar to the simulation model. This important factor can be considered for different earthing systems. The relative error between the simulation and experimental results (maximum induced voltage) for case study one does not exceed 17 %.

The experiment further demonstrated that the induced overvoltages start from zero and peak, then go below zero, oscillating between the negative and positive before stabilising at zero. The oscillations are due to the circuit's parameters, including the circuit's inductive and capacitive components.

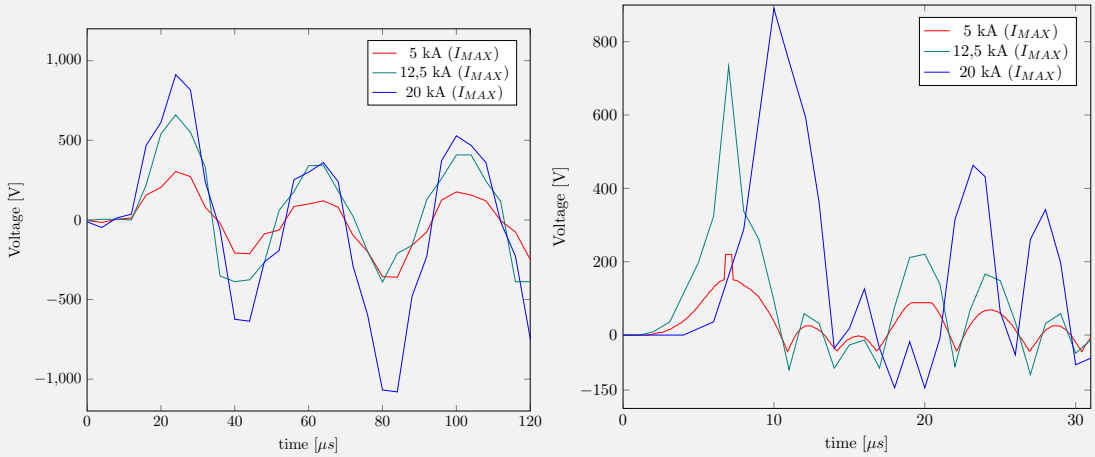
The open-circuit measurements were not the induced overvoltages that appeared on the microinverter; therefore, measurements with a microinverter connected to the DC cables were taken. In the experimental investigation with a microinverter connected between the DC cables, the impulse current injected was 1 kA, 2 kA and 5 kA. A 5 kA impulse current induced overvoltage of 58 V was measured across the DC cables. The induced overvoltages with a microinverter connected to the DC cables are summarised in table 6.2. The increased oscillation and reduced overvoltages observed with a microinverter connected to the circuit (Figures 6.3 (a) and (b)) are due to the microinverter's inductive and capacitive components.



(a) Induced overvoltages, 8/20 μs impulse

(b) Induced overvoltages, 10/350 μs impulse

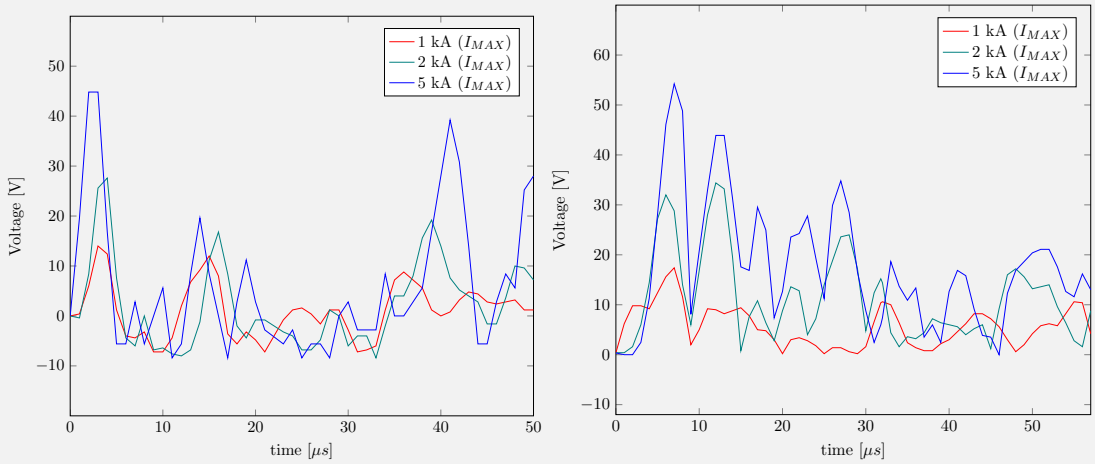
Figure 6.1: Experimental case study 1: Induced overvoltages DM



(a) Induced overvoltages, 8/20 μs impulse **(b)** Induced overvoltages, 10/350 μs impulse

Figure 6.2: Experimental case study 1: Induced overvoltages CM

The experimental case study 1 results are summarised in table 6.1.



(a) Induced overvoltages, 8/20 μs impulse **(b)** Induced overvoltages, 10/350 μs impulse

Figure 6.3: Experimental case study 1: Induced overvoltages with a microinverter

Table 6.1: Case study 1 experiment results

Induced Overvoltage ($Vmax$)				
Impulse current (I_{max})	**DM**		**CM**	
	8/20 µs	**10/350 µs**	**8/20 µs**	**10/350 µs**
5 kA	126 V	116 V	272 V	293 V
12,5 kA	284 V	267 V	660 V	732 V
20 kA	430 V	415 V	980 V	890 V

Table 6.2: Experimental case study 1 maximum induced overvoltages with a microinverter connected to the DC cables

Induced Overvoltage (V_{max})		
Impulse current (I_{max})	**8/20 µs**	**10/350 µs**
1 kA	14.4 V	17,4 V
2 kA	30.8 V	32 V
5 kA	58 V	57.6 V

6.3 Case Study 2 Experimental Results

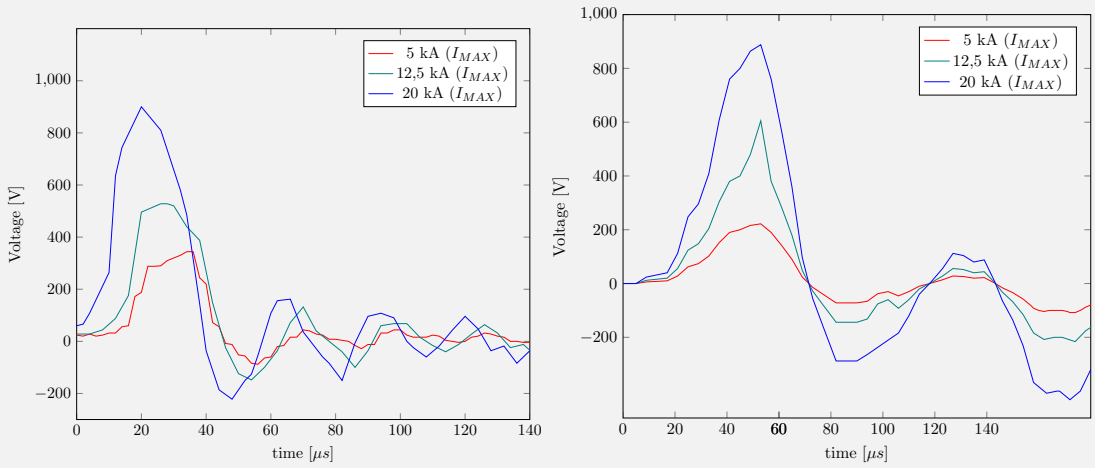
The induced overvoltages were measured when an impulse current was injected into the PV system's frame. This case study represents a scenario where there is no external LPS. The induced overvoltages were almost double that with an external LPS connected. Thus, the lightning strike location is one of the several parameters influencing lightning-induced overvoltages.

In the DM configuration, the highest induced voltages were 970 V and 950 V, respectively, with a 20 kA current impulse (Figures 6.4 (a) and (b)). When a 12.5 kA impulse current was injected into the frame, the induced voltages were 590 and 610 V, and lower voltages of 280 and 244 V were measured for a 5 kA current impulse, with the 8/20 μs and 10/350 μs impulse current waveforms, respectively. In the CM configuration, the highest induced overvoltages were measured under an impulse current of 20 kA. These voltages for the 8/20 μs and 10/350 μs impulse current waveforms were 1.71 kV and 1.68 kV, respectively. The induced overvoltages showed a linear proportional increase with increasing impulse current. The peak voltages measured for a 12.5 kA impulse current were 992 V and 1.16 kV, and for a 5 kA impulse current, the voltages were 460 and 483 V for the 8/20 μs and 10/350 μs impulse current waveforms, respectively (Figures 6.5 (a) and (b)).

The voltages measured in case study 2 indicated an increased risk of a PV system without

an LPS, as these voltages were higher than obtained in case study 1. This is due to a stronger magnetic field interacting with the PV panel, inducing greater overvoltages on the PV panel's DC cables (Table 6.3). A similar observation was noted in the simulations (Chapter 5).

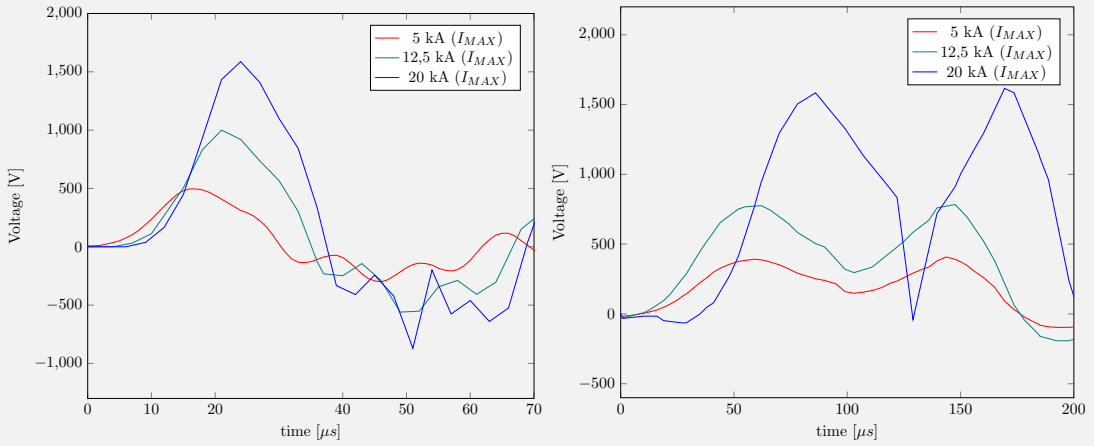
When a microinverter was applied to the second case study, a 5 kA impulse current caused an overvoltage on the DC cables to reach a maximum of 130 V (10/350 μs waveform). A linear increase in impulse current caused a linear increase in the induced overvoltage. In general, the induced overvoltage circuit reaches a peak voltage and travels to below zero, and after that oscillates until it reaches zero (Figures 6.6 (a) and (b)). Similar to case study 1, voltage oscillation increased due to the circuit characteristics when a microinverter is connected. The induced overvoltages with a microinverter connected to the DC cables are summarised in table 6.4.



(a) Induced overvoltages, 8/20 μs impulse

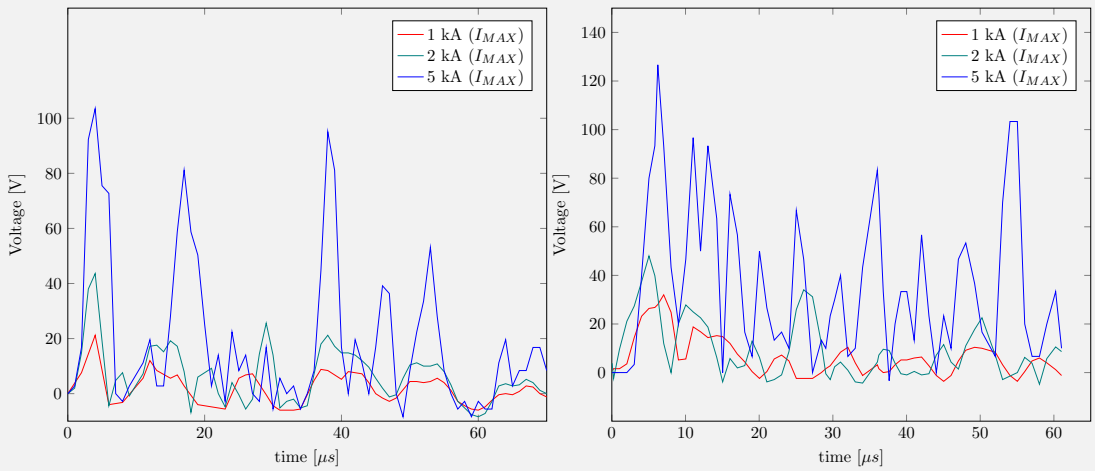
(b) Induced overvoltages, 10/350 μs impulse

Figure 6.4: Experimental case study 2: Induced overvoltages DM



(a) Induced overvoltages, 8/20 μs impulse **(b)** Induced overvoltages, 10/350 μs impulse

Figure 6.5: Experimental case study 2: Induced overvoltages CM



(a) Induced overvoltages, 8/20 μs impulse **(b)** Induced overvoltages, 10/350 μs impulse

Figure 6.6: Experimental case study 2: Induced overvoltages with a microinverter

Table 6.3: Case study 2 experiment results

Induced Overvoltage (V_{max})				
Impulse current (I_{max})	**DM**		**CM**	
	8/20 µs	**10/350 µs**	**8/20 µs**	**10/350 µs**
5 kA	280 V	244 V	460 V	483 V
12,5 kA	590 V	610 V	992 V	1.16 V
20 kA	970 V	950 V	1.71 kV	1.68 kV

Table 6.4: Experimental case study 2 maximum induced overvoltages with a microinverter connected to the DC cables

Induced Overvoltage (V_{max})		
Impulse current (I_{max})	**8/20 µs**	**10/350 µs**
1 kA	21.2	21.12 V
2 kA	43,6 V	46,08 V
5 kA	128,6 V	123,33 V

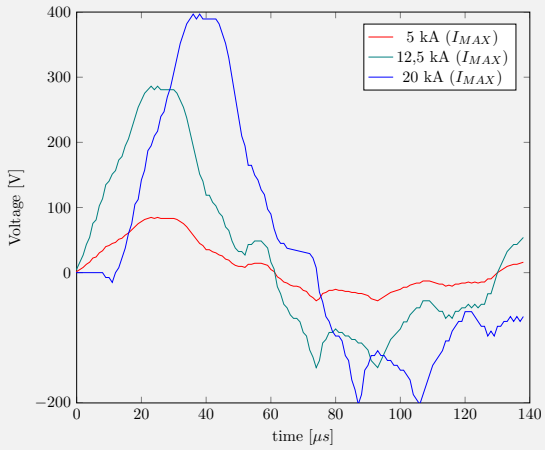
6.4 Twisted-pair Configuration

The magnetic influence of the wires was investigated with the twisted pair configuration of the DC cables. In this configuration, the DC cables are twisted together to reduce the electromagnetic radiation between the pair.

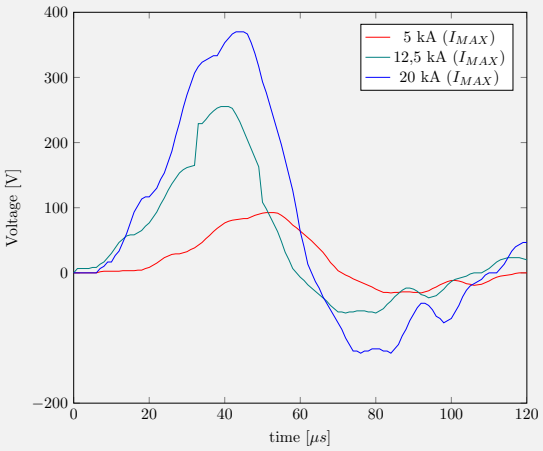
The induced voltages measured with a twisted pair configuration with 8/20 μs and 10/350 μs impulse waveforms when impulse current was injected onto the external LPS are shown in figure 6.7 (a) and (b), respectively. The highest induced voltages were 390 V and 395 V, respectively, with a 20 kA current impulse. When a 12.5 kA impulse current was injected into the frame, the induced voltages were 281 V and 250 V, and lower voltages of 98 V and 102 V were measured for a 5 kA current impulse, with the 8/20 μs and 10/350 μs impulse current waveforms, respectively. The induced overvoltages were measured when an impulse current was injected into the PV system's frame with a twisted pair configuration. The highest voltages measured in 8/20 μs and 10/350 μs current waveforms in DM were 810 V and 840 V for a 20 kA impulse current (Figure 6.8 (a) and (b)). When the LPS was injected with a 12.5 kA impulse current, the highest voltages were 550 V and 590 V, and for a 5 kA impulse, 220 V and 230 V were measured for 8/20 μs and 10/350 μs current waveforms, respectively.

The overall results of the twisted pair configuration showed no significant difference in

the open circuit voltages; thus, the magnetic influence of twisting the cable pair has no significant effect on the induced voltages. Case study 1 and 2 induced voltages with twisted pair configuration are shown in tables 6.5 and 6.6, respectively.

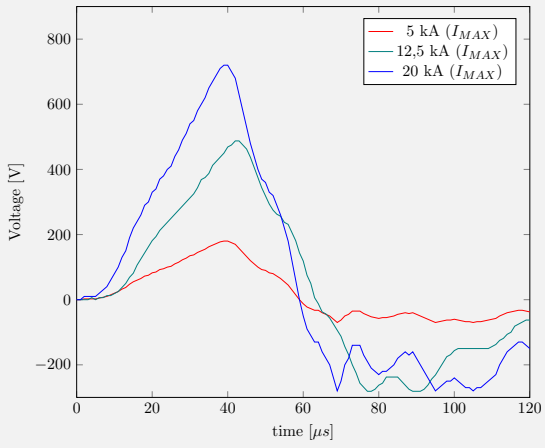


(a) Experimental case study 1: Induced overvoltages DM, twisted-pair, 8/20 μs impulse

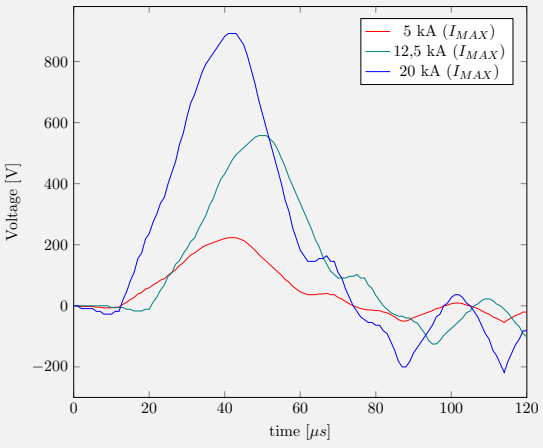


(b) Induced overvoltages, 10/350 μs impulse

Figure 6.7: Case study 1, DM Induced voltages: twisted-pair



(a) Induced overvoltages, 8/20 μs impulse



(b) Induced overvoltages, 10/350 μs impulse

Figure 6.8: Case study 2, DM Induced voltages: twisted-pair

Table 6.5: Experimental case study 1 maximum induced overvoltages with a twisted pair configuration

Induced Overvoltage (V_{max})		
Impulse current I_{max}	**8/20 µs**	**10/350 µs**
5 kA	98 V	102 V
12,5 kA	281 V	250 V
20 kA	390 V	395 V

Table 6.6: Experimental case study 2 maximum induced overvoltages with a twisted-pair configuration

Induced Overvoltage (V_{max})		
Impulse current (I_{max})	**8/20 µs**	**10/350 µs**
5 kA	220 V	230 V
12,5 kA	550 V	590 V
20 kA	810 V	840 V

6.5 Validation

6.5.1 Measured values in experiment and simulation

The induced overvoltages measured in the experiments and simulations generally agreed between the two studies. The results of maximum induced voltages are summarised in Tables 6.7 and 6.8. The simulation predictions were compared with experimental data, and the minimal discrepancies can be attributed to:

- The simulated impulse currents are based on mathematical expressions, which generally give pure waveforms. In the experimental setting, the impulse generator's components, the measuring equipment, along with the connecting circuit components generally form part of the overall circuit. These additional circuit components may affect the measured induced voltages.
- In the experimental setting, maximum impulse currents were attained by manual control; a small margin of human error can be accepted due to the sensitivity of handling experimental equipment. Attaining perfect maximum impulse currents may be challenging, especially at higher impulse currents. Such differences, although minor, may also influence the induced overvoltages measured.

Table 6.7: Summary of induced overvoltages on open DC cables in DM

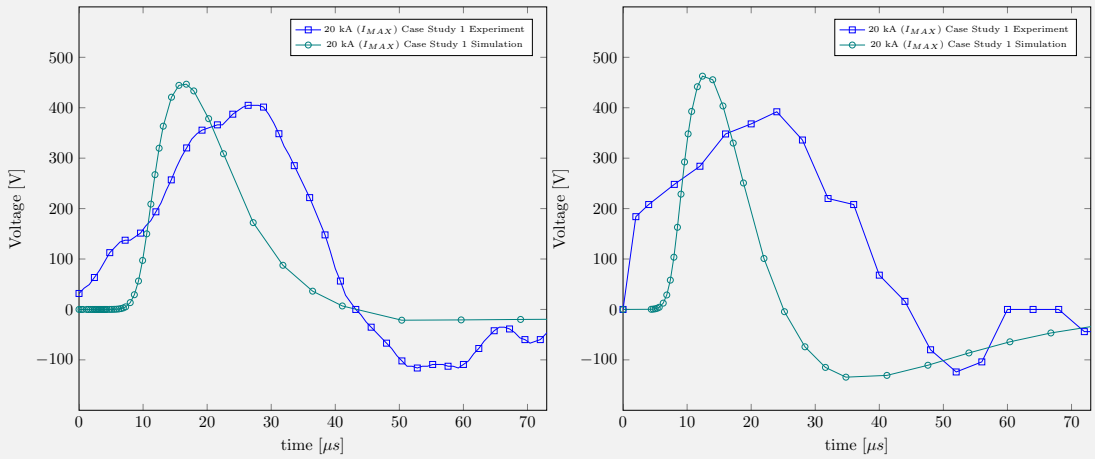
Open DC Cables in DM								
Impulse Current (I_{max})	**Experiment (V_{max})**				**Simulation (V_{max})**			
	8/20 µs		**10/350 µs**		**8/20 µs**		**10/350 µs**	
	CS1	**CS2**	**CS1**	**CS2**	**CS1**	**CS2**	**CS1**	**CS2**
5 kA	126 V	280 V	116 V	244 V	115,65 V	275 V	113,25 V	244,75 V
12,5 kA	284 V	590 V	267 V	610	289,12 V	687,5 V	280,70 V	611,85 V
20 kA	430 V	970 V	415 V	950 V	462 V	1.1kV	448,54 V	0,99 kV
100 kA	-	-	-	-	2.31 kV	5,8 kV	2.24 kV	5,16 kV

Table 6.8: Summary of induced overvoltages on open DC cables in CM

Open DC Cables in CM								
Impulse Current (I_{max})	**Experiment (V_{max})**				**Simulation (V_{max})**			
	8/20 µs		**10/350 µs**		**8/20 µs**		**10/350 µs**	
	CS1	**CS2**	**CS1**	**CS2**	**CS1**	**CS2**	**CS1**	**CS2**
5 kA	272 V	460 V	293V	483 V	252 V	455 V	260 V	404,95 V
12,5 kA	660 V	992 V	732 V	1.16 kV	650 V	1,14 kV	631,07 V	1,01 kV
20 kA	980 V	1,71 kV	890 V	1,68 kV	1.01 kV	1,82 kV	1040 V	1,61kV
100 kA	-	-	-	-	5.2 kV	9.1 kV	5.04 kV	8.1 kV

*CS - Case Study

Figures 6.9 (a) and (b)compares the experimental and simulation induced overvoltages at 20 kA for case study 1, showing their similarity.



(a) Case study 1: 10/350 μs impulse **(b)** Case study 1: 8/20 μs impulse

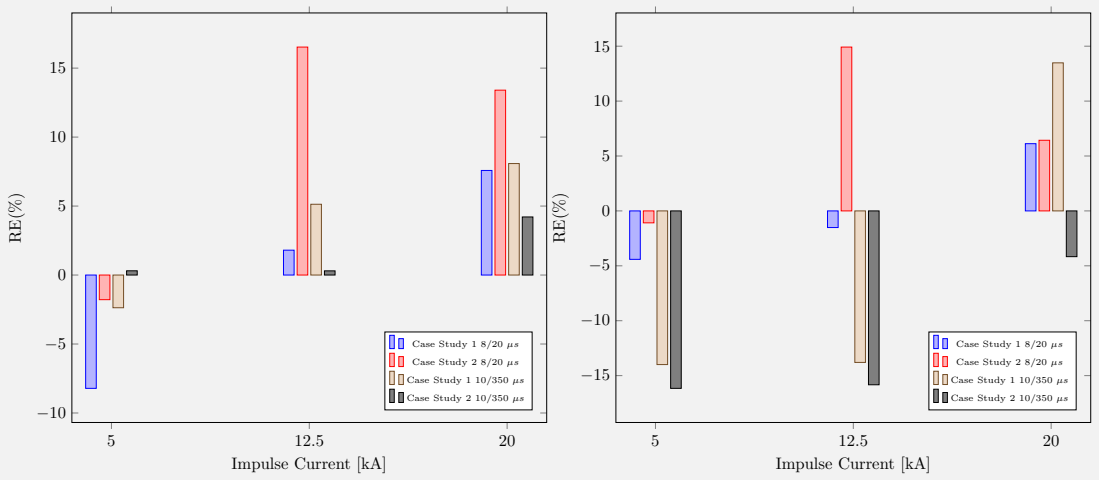
Figure 6.9: Comparison of induced voltages in experiment and simulation, 20 kA

6.5.2 Relative error

The simulation results were compared with experimental results for each case study, and the relative error was computed using:

$$RE(\%) = \frac{V_{sim} - V_{exp}}{V_{exp}} \tag{6.1}$$

Figures 6.10 (a) and (b) show the relative error between the simulated and experimental results. The relative error did not exceed 17% for the DM and 15% for the CM induced voltages. Much has already been discussed regarding these minor discrepancies.



(a) DM **(b)** CM

Figure 6.10: Relative error at different impulse currents

6.6 Chapter Summary

The magnitude of LIOs was investigated in different positions in an experimental setting. The validation method has also been introduced. The stroke locations on the lightning rod and PV frame were studied under different impulse currents at the open DC cables (DM) and the between ground and a DC cable (CM) to reveal different surge characteristics of the setup when lightning strikes different positions. These results further indicated that the circuit characteristics, the mode of measurement, and lightning parameters were the most important factors determining the magnitude of induced overvoltages to microinverters.

As the electrical characteristics of the simulation are linear, the relationship between the lightning stroke amplitudes will have proportional changes in the induced overvoltages. This

linearity was observed in the results where the series of tests involved the step-changing of the current's magnitude. The limitation of the experimental study naturally includes using limited laboratory equipment, such as the limitations in injecting lightning currents greater than 20 kA from the impulse generator. When an impulse current strikes the external LPS, the affected object develops an alternating magnetic field that produces an induction emf on the circuits. The induced overvoltage is the voltage generated by the coupling between the lines and the electromagnetic field induced by the impulse current during the period of a lightning strike.

7 Simulation 2 Results: Protection Performance (PSCAD)

7.1 Introduction

The need for a good quality power supply in PV systems makes lightning protection one of the primary requirements in PV installations (PVIs). SPDs are connected to the DC and AC cables in PVIs to protect the electronic components against lightning transients. In this regard, MOVs can effectively protect sensitive low-voltage electrical equipment. However, to ensure an adequate protection approach for microinverters, it is necessary to analyse LIO stresses' influence on them.

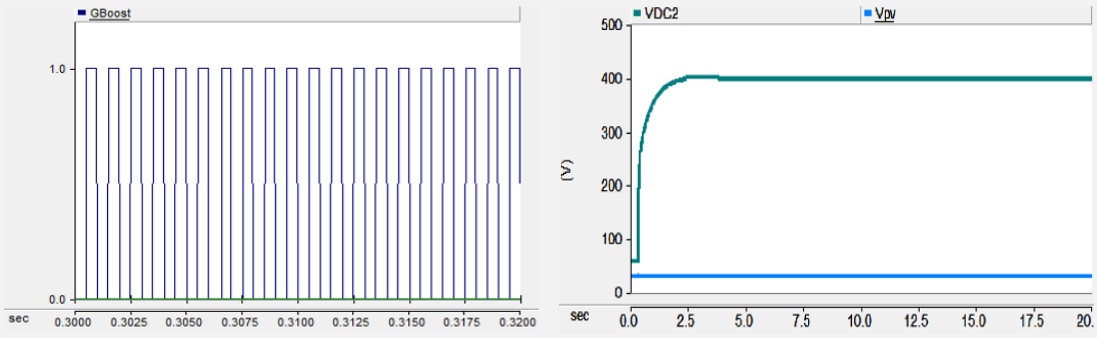
This investigation, therefore, began with an analysis of the overcurrents appearing on the microinverter when exposed to indirect lightning transients without an SPD. Two approaches are analysed: 1) the influence of induced voltages which were measured when an impulse current was injected on the external LPS; 2) the influence of induced voltages which were measured when an impulse current was injected into the frame of the PV system. Simulations followed this with the selected SPD connected to the DC cables, and subsequently, the protection performance of the SPD's microinverter circuit was analysed. The results of energy load simulations for an SPD installed at the connections to the DC cables are presented in this chapter.

7.2 Simulation Results of PV Panel with microinverter at Steady State

The steady-state operation of the PV system was modelled to ensure the correct functionality of the system. The steady-state operation of the DC-DC and DC-AC stage of the microinverters are commonly analysed using the current and voltage waveforms, obtaining their mean values and the amplitude of their ripples. The microinverter circuit was implemented with the methodology described in Chapter 4 (section 4.5).

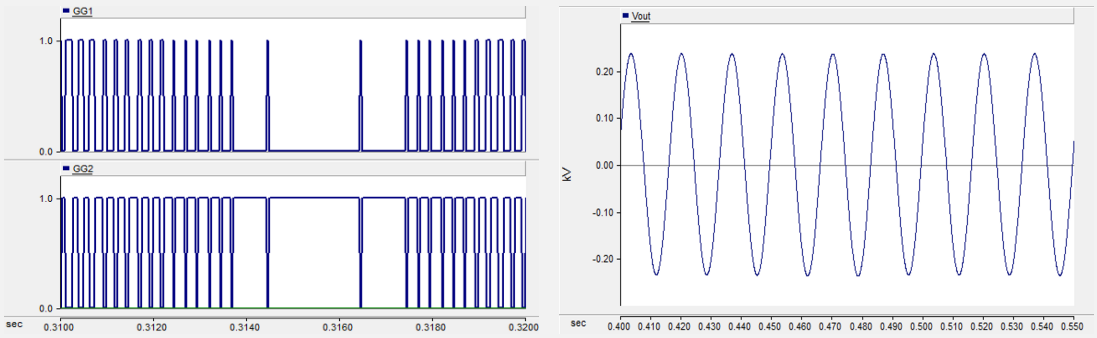
On the DC-DC converter stage, the input was 30 V, and the output voltage was 400 V.

The control circuit was implemented to control the switching of the MOSFET (metal-oxide-semiconductor field-effect transistor). This switching is illustrated in figure 7.1a, and the input and output voltages are shown in figure 7.1b. A 100 W prototype of the full-bridge grid-connected inverter was implemented to work with an input voltage of 400 V DC and a grid voltage of 230 V and 50 Hz. The gate control waveforms and the output voltage waveform are illustrated in figures 7.2 (a) and (b), respectively.



(a) Boost converter MOSFET gate control **(b)** Input and output voltages – Boost converter

Figure 7.1: Boost converter waveforms



(a) Inverter gate control waveforms **(b)** Output voltage

Figure 7.2: Inverter waveforms

7.3 Measurements of overcurrents appearing at the microinverter

A lightning stroke radiates quickly and changes the electromagnetic fields in the surrounding areas. The overcurrents appearing at the microinverter without surge protection were measured during an indirect lightning transient period. This analysis was performed with the two case studies using both the 8/20 μs and 10/350 μs standard current waveforms. The

simulations were performed by injecting the induced overvoltages at different impulse current amplitudes measured from the COMSOL Multiphysics® simulation (Chapter 5). These voltages were applied to the DC cables of the microinverter, and overcurrents were measured. The simulation results were obtained under each protection scenario described in Chapter 4.

7.3.1 Case 1: overcurrents appearing on the microinverter

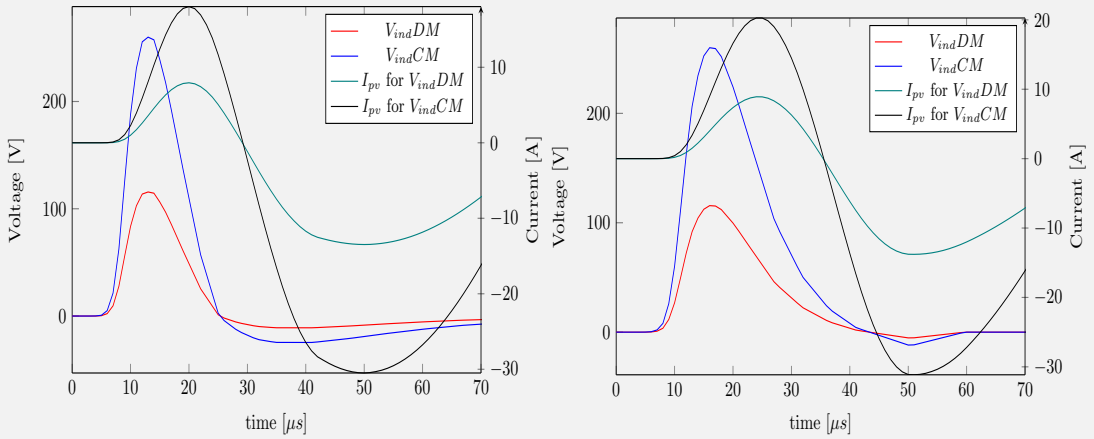
The system is tested in the first case study with overvoltages measured with an external LPS connected under CM and DM configurations. For the 5 kA impulse current, the induced maximum voltages of 115 V and 260 V were recorded for the DM and CM configurations in 8/20 μs impulse current, respectively. The maximum currents flowing through to the microinverter (I_{pv}) on the microinverter with an 8/20 μs impulse current were 8 A and 18 A for DM and CM, respectively. When a 10/350 μs impulse current was injected on the lightning rod, the maximum overcurrents measured were 9 A and 20 A (Figures 7.3 (a) and (b)). The currents on the microinverter oscillated between the zero line while moving from negative to positive values before disappearing. This oscillation was due to the microinverter's reactive components (inductive and capacitive).

When the lightning rod was injected with a 12.5 kA impulse current, the maximum induced voltages were 289 V and 650 V for the DM and CM configurations in 8/20 μs impulse current waveform, respectively. The resulting overcurrents on the microinverter were 20 A and 44 A for 8/20 μs impulse current waveform, and 22 A and 47 A for 10/350 μs impulse current waveform (Figure 7.4 (a) and (b)). There was no significant difference between the overcurrent with 8/20 μs and 10/350 μs impulse currents. When the lightning rod was injected with a 20 kA impulse current, the overcurrents increased proportionally to the induced overvoltage. The peak currents measured in DM and CM were 32 A and 73 A for the 8/20 μs impulse current, respectively, and similarly, 36 A and 80 A for the 10/350 μs impulse current (Figures 7.5 (a) and (b)).

The results of overcurrents appearing on the microinverter when a 100 kA extreme impulse current was injected on the rod are shown in figures 7.6 (a) and (b) for 8/20 μs and 10/350 μs impulse current waveforms respectively. In the DM configuration, a 158 A oscillating overcurrent was measured between the DC lines, and for the CM configuration, the overcurrent reached a maximum of 413 A for an 8/20 μs impulse current. Similarly, the maximum overcurrent in the DC cables reached 167 A and 429 A for the DM and CM configurations, respectively, using a 10/350 μs impulse current. It has to be noted in this scenario that the waveforms oscillate much longer than in the case of an 8/20 μs waveform. It can also be noted that at 100 kA impulse current, there is a slight change in the current waveform at 20 μs; this change occurs around the same time when there is a polarity reversal in the induced voltage and is highly visible in 8/20 μs. The overcurrents measured at the microinverter in

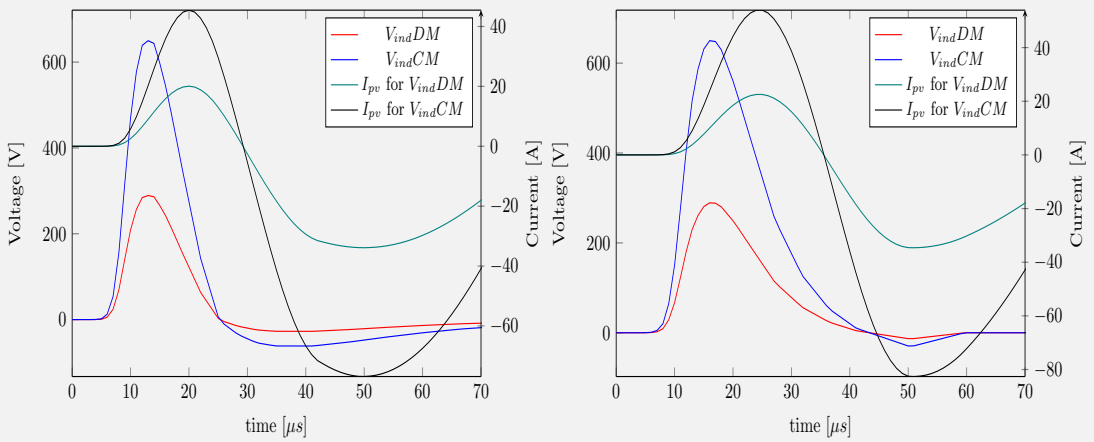
case study 1 are summarised in Table 7.1.

The results generally show an increase in current flow to the microinverter with increased overvoltages caused by lightning currents. At higher impulse currents (e.g. 100 kA), the overcurrents potentially exceed the maximum destructive currents to the microinverter, thus posing a risk of damage to the electronic components. The need for an SPD to be connected to the DC cables of a microinverter is very clear from these findings.



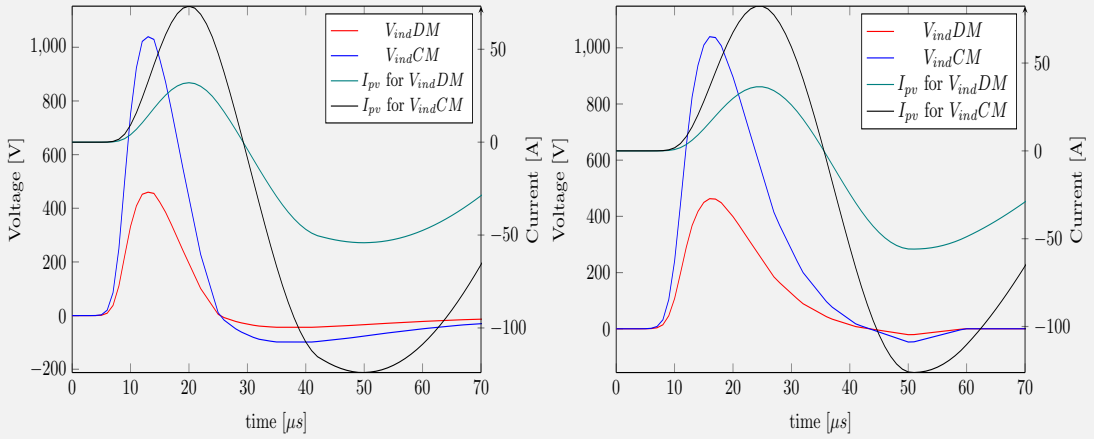
(a) 8/20 μs impulse current **(b)** 10/350 μs impulse current

Figure 7.3: Case study 1: Overcurrents at the microinverter, 5 kA



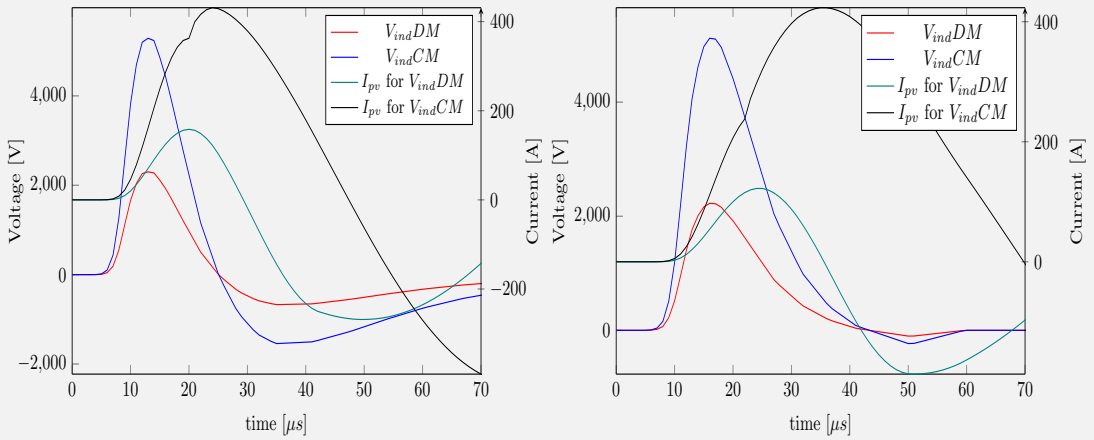
(a) 8/20 μs Impulse current **(b)** 10/350 μs Impulse current

Figure 7.4: Case study 1: Overcurrents at the microinverter, 12.5 kA



(a) 8/20 μs impulse current **(b)** 10/350 μs impulse current

Figure 7.5: Case study 1: Overcurrents at the microinverter, 20 kA



(a) 8/20 μs impulse current **(b)** 10/350 μs impulse current

Figure 7.6: Case study 1: Overcurrents at the microinverter, 100 kA

Table 7.1: Overcurrents at the microinverter in case study 1

8/20 µs Standard Waveform								
	5kA		**12.5 kA**		**20 kA**		**100 kA**	
Mode of Measurement	V_{max}	I_{pv}	V_{max}	I_{pv}	V_{max}	I_{pv}	V_{max}	I_{pv}
DM	115.6 V	8 A	289.12 V	20 A	462 V	32 A	2.31 kV	158 A
CM	260 V	18 A	650	44 A	1.04 kV	73 A	5.2 kV	413 A
10/350 µs Standard Waveform								
	5kA		**12.5 kA**		**20 kA**		**100 kA**	
Mode of Measurement	V_{max}	I_{pv}	V_{max}	I_{pv}	V_{max}	I_{pv}	V_{max}	I_{pv}
DM	113.25 V	9 A	280.70 V	22 A	448.54 V	36 A	2.24 kV	167 A
CM	252 V	20 A	631.07 V	47 A	1.01 kV	80	5.04 kV	429 A

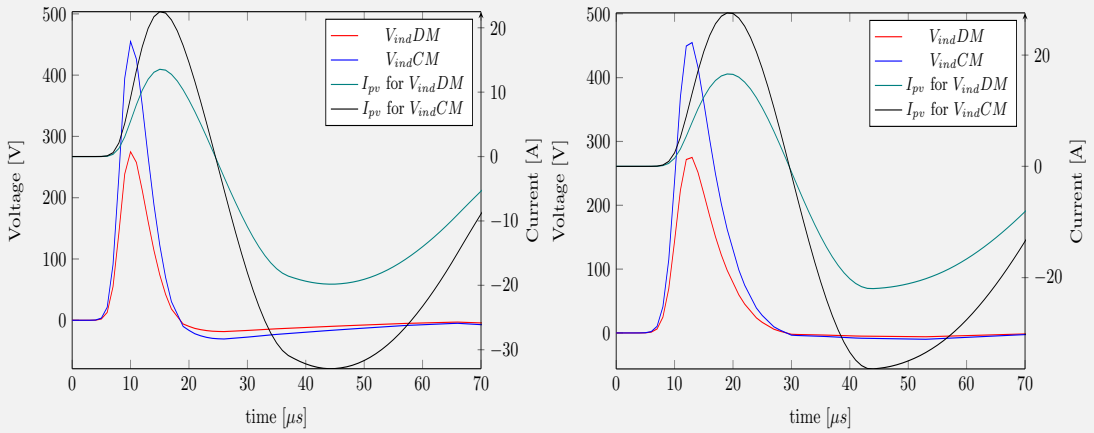
7.3.2 Case 2: overcurrents appearing at the microinverter

For case study 2, the impulse current injected into the frame of the PV system showed high voltages on the DC cables in extreme currents. These voltages, measured in the COMSOL Multiphysics® simulation, were injected into the PSCAD model, and overcurrents were measured on the microinverter's DC cables. The induced overvoltages across the DC cables were the highest in the investigations in DM and CM.

When a 5 kA impulse current was injected into the frame of the PV panel, the induced overvoltages measured in DM and CM were 275 V and 455 V, respectively, for an 8/20 μs impulse current waveform. The resulting overcurrents on the microinverter were 13 A and 22 A for an 8/20 μs impulse current, and 16 A and 27 A for a 10/350 μs impulse current in DM and CM, respectively (Figures 7.7 (a) and (b)). When the impulse current was increased to 12.5 kA, the induced overvoltages were 687 V and 1.1 kV for DM and CM, respectively. The overcurrent flowing to the microinverter was 34 A and 56 A for an 8/20 μs impulse current and 40 A and 64 A for a 10/350 μs impulse current (Figures 7.8 (a) and (b)). The currents increased proportionally to the induced overvoltages measured across the DC cables. When a 20 kA maximum impulse current was injected into the PV panel, the induced overvoltages measured in DM and CM were 1.1 kV and 1.82 kV. The overcurrents across the microinverter were 73 A and 90 A for an 8/20 μs impulse current and 77 A and 102 A for a 10/350 μs impulse current in DM and CM, respectively (Figures 7.9 (a) and (b)). When a 100 kA extreme impulse current of 8/20 μs was injected into the PV system's frame, the overcurrents on the DC cables reached 291 A and 713 A in DM and CM, respectively. For the 10/350 μs current waveform, the overcurrents appearing on the DC cable were 306 A and 723 A for the DM and CM configurations, respectively (Figures 7.10 (a) and (b)). The overcurrents at the microinverter in case study 2 are summarised in table 7.2.

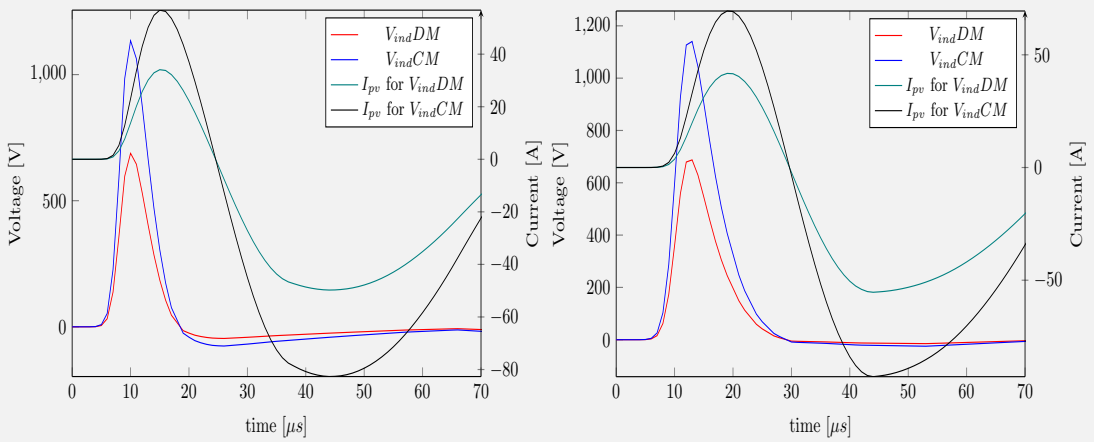
The overcurrents appearing on the microinverter in this case study showed an increase

with induced voltages., similar to case study 1. However, the results are higher than in the previous case study, thus showing that without an external LPS, the microinverter will be at a higher risk of damage due to lightning currents. Additionally, the overcurrent waveforms have different rise and fall times determined by the type of induced voltage or lightning current injected into the frame. This is to be expected with different waveforms for lightning transients.



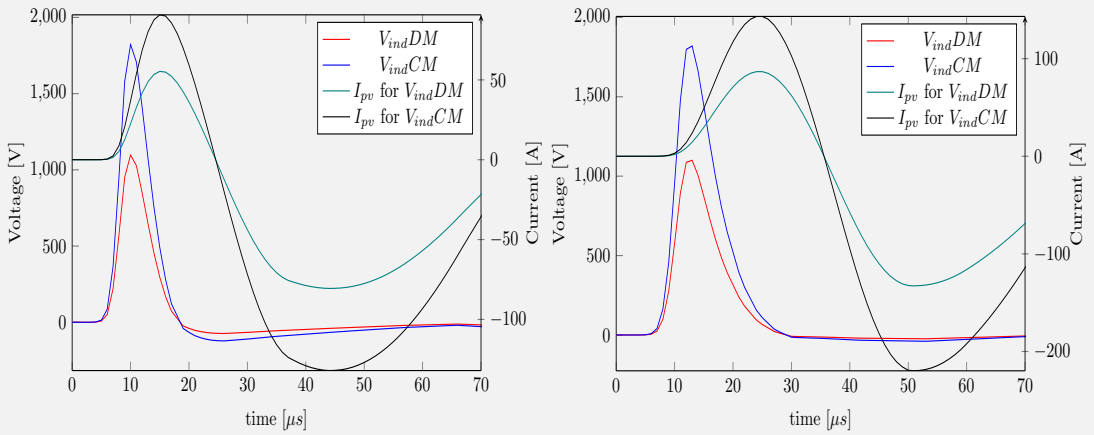
(a) 8/20 μs impulse current **(b)** 10/350 μs impulse current

Figure 7.7: Case study 2: Overcurrents at the microinverter, 5 kA



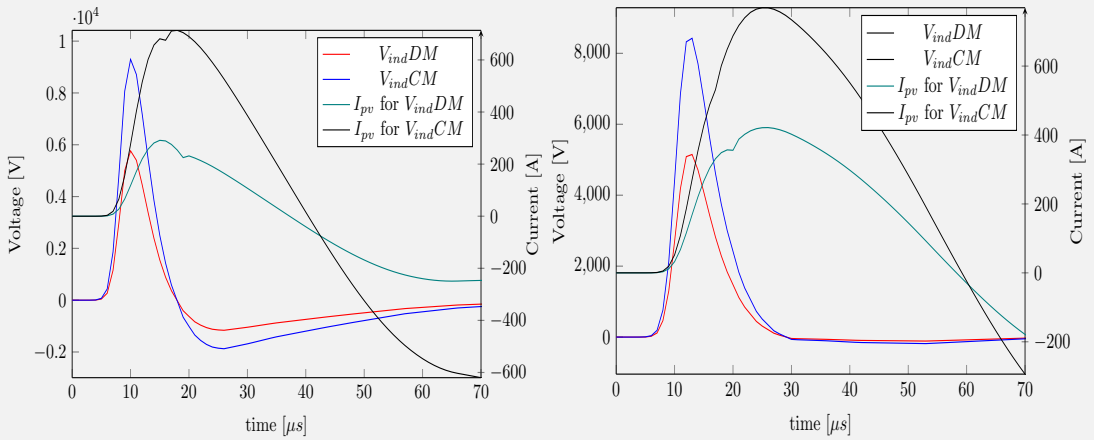
(a) 8/20 μs impulse current **(b)** 10/350 μs impulse current

Figure 7.8: Case study 2: Overcurrents at the microinverter, 12.5 kA



(a) 8/20 μs impulse current **(b)** 10/350 μs impulse current

Figure 7.9: Case study 2: Overcurrents at the microinverter, 20 kA



(a) 8/20 μs impulse current **(b)** 10/350 μs impulse current

Figure 7.10: Case study 2: Overcurrents at the microinverter, 100 kA

Table 7.2: Overcurrents at the microinverter in case study 2

8/20 µs Standard Waveform								
	5kA		**12.5 kA**		**20 kA**		**100 kA**	
Mode of Measurement	V_{max}	I_{pv}	V_{max}	I_{pv}	V_{max}	I_{pv}	V_{max}	I_{pv}
DM	275 V	13 A	687,5 V	34 A	1.1 kV	73 A	5.8 kV	291A
CM	455 V	22 A	1.14 kV	56 A	1.82 kV	90 A	9.1 kV	713 A
10/350 µs Standard Waveform								
	5kA		**12.5 kA**		**20 kA**		**100 kA**	
Mode of Measurement	V_{max}	I_{pv}	V_{max}	I_{pv}	V_{max}	I_{pv}	V_{max}	I_{pv}
DM	244.75 V	16 A	611.85 V	40 A	0.99 kV	77 A	5.16 kV	306 A
CM	404.95 V	27 A	1.01 kV	64 A	1.61 kV	102 A	8.1 kV	723 A

7.4 Simulation Results with SPD connected on the DC cables

SPDs are installed in protected circuits to divert surge currents to limit transient overvoltages. In this simulation case, the SPD was connected between the DC cables of the microinverter. Induced overvoltages were applied across the DC cables. This investigation focused on the peak values and waveforms of currents flowing through the SPD and the energy absorbed by the SPD for induced voltages measured for 20 kA and 100 kA impulse currents for the 8/20 μs and 10/350 μs impulse current-induced overvoltages under DM and CM configurations. In this section, the current flowing through the SPD and the energy by the SPD are reported in two scenarios.

7.4.1 Case study 1 with SPD

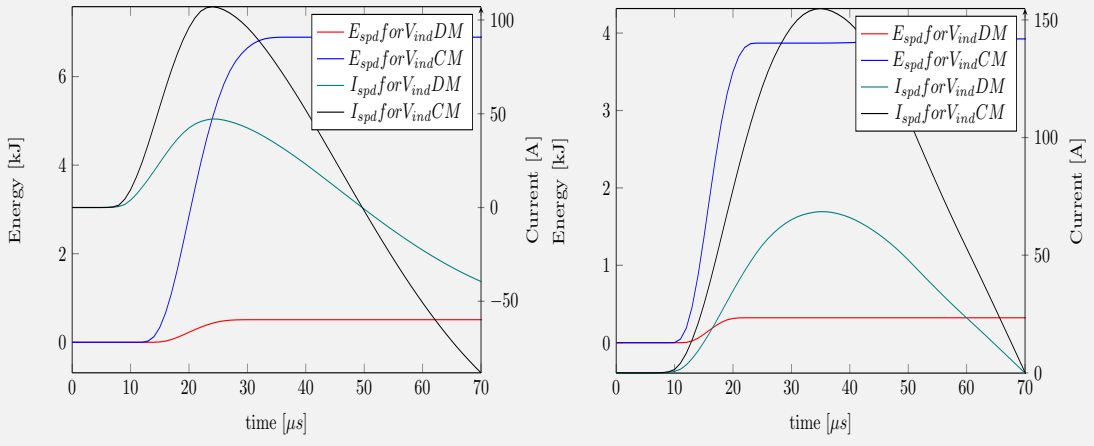
The SPD current and energy were assessed with impulse voltage measured when the impulse current was injected into the external LPS. No energy overload for induced voltages with maximum impulse currents of 5 kA and 12.5 kA was detected due to the induced voltage not exceeding the U_p value of the SPD.

The SPD energy and current for the 8/20 μs and 10/350 μs standard induced current waveforms under 20 kA maximum current are shown in Figures 7.11 (a) and (b), respectively, in DM and CM. For an 8/20 μs standard waveform, the maximum energy measured was 0.32 kJ, and the maximum current was 47.2 A for DM configuration. Similarly, 3.9 kJ and 106.54 A for CM configuration. The polarity reversal of the 8/20 μs waveform increased the energy absorbed by the SPD. For a 100 kA extreme impulse current in the DM configuration, the energy absorbed by the SPD was 29.56 kJ for an 8/20 μs waveform, and 238.54 A of current flowed through the SPD. For a 10/350 μs impulse current, the energy absorbed was 40.47 kJ, and a current of 345.11 A flowed through the SPD (Figures 7.12 (a) and (b)). When

CM-induced voltages were applied to the circuit, on an 8/20 μs impulse current, the energy absorbed by the SPD was 180.4 kJ, and the current reached a peak of 535.85 A. For a 10/350 μs waveform impulse current, the energy absorbed was 221.22 kJ, and the current reached a peak of 775.57 A (Figures 7.12 (a) and (b)). The results of the current and energy absorbed by the SPD are summarised in Table 7.3.

These results show that the current flowing through the SPD (I_{spd}) depends on the amplitude and shape of the induced overvoltage appearing on the microinverter. The waveshape and the polarity reversal of the induced voltage increased the energy absorbed by the SPD. At higher impulse currents, the current flowing through the SPD rises, and so does the energy absorbed by the SPD. Moreover, with 8/20 μs impulse current waveshape, which showed a high undershoot value as described in chapter 5, the energy continues to increase when the reverse polarity voltage exceeds the U_p value of the SPD. For lower impulse current amplitudes, depending on the type of SPD installed, the current through the SPD was lower, and the microinverter may be protected against the effects of lightning.

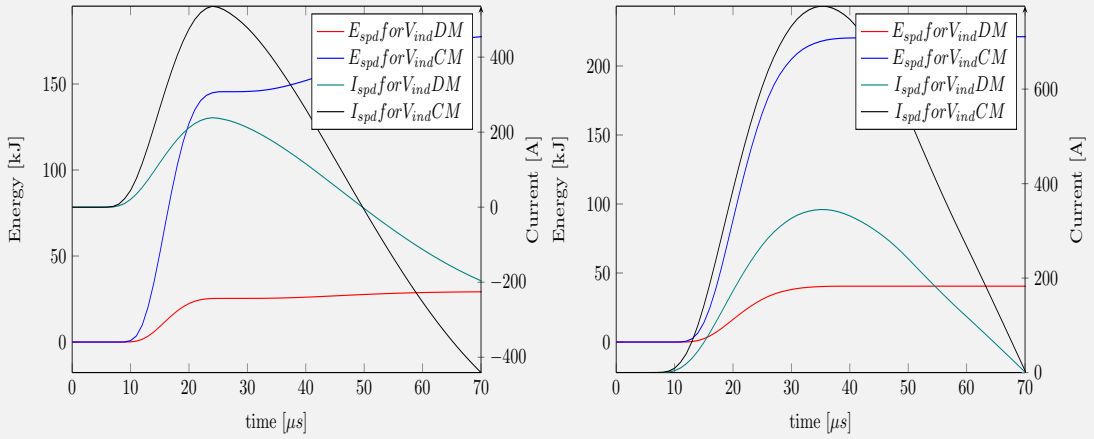
However, it should be noted that the current and energy absorbed by the SPD with 10/350 μs were higher than the current and energy absorbed by the 8/20 μs; thus, more heat will be dissipated with a 10/350 μs. However, since the 10/350 μs is an extreme waveform used to test class I SPDs, it will have a low probability of occurrence, and therefore the 8/20 μs impulse values are likely more practical.



(a) 8/20 μs impulse current

(b) 10/350 μs impulse current

Figure 7.11: Case study 1: SPD current and energy absorbed, 20 kA



(a) 8/20 μs impulse current **(b)** 10/350 μs impulse current

Figure 7.12: Case study 1: SPD current and energy absorbed, 100 kA

Table 7.3: SPD energy and current overload case study 1

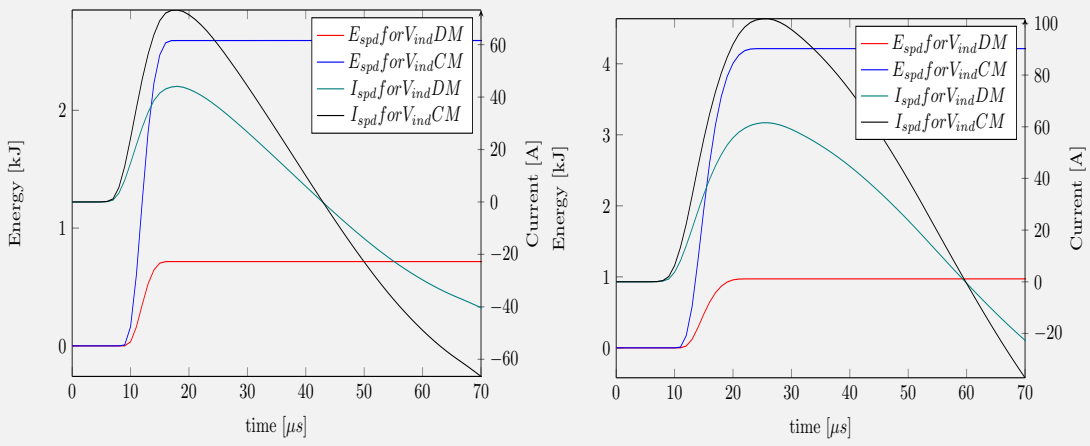
8/20 µs Impulse Current Waveform				
	20 kA		**100 kA**	
Mode of Measurement	E_{spd}	I_{spd}	E_{spd}	I_{spd}
DM	0.32 kJ	47.20 A	29.56 kJ	238.54 A
CM	3.9 kJ	106.54 A	180.40 kJ	535.85 A
10/350 µs Impulse Current Waveform				
	20 kA		**100 kA**	
Mode of Measurement	E_{spd}	I_{spd}	E_{spd}	I_{spd}
DM	0.5 kJ	68.45 A	40.47 kJ	345.11 A
CM	6.8 kJ	154.82 A	221.22 kJ	775.57 A

7.4.2 Case study 2 with SPD

The results of energy load simulations for an SPD connected to the DC cables when impulse current is injected into the PV frame are presented in this section. For a maximum impulse current of 5 kA, there was little to negligible energy overload on the SPD in both the DM and CM configurations as these voltages did not exceed or slightly exceed the U_p value of the SPD. Maximum currents of 12.5 kA, 20 kA and 100 kA showed energy overloads on the SPD when connected to the DC cables. For a 12.5 kA impulse current of 8/20 μs, the current flowing through the SPD was 44.08 A for DM and 73.20 A for CM. The corresponding energy flowing through the SPD was 0.71 kJ for the DM and 2.59 kJ for the CM configurations (Figure 7.13 (a) and (b)).

The induced voltages measured when an impulse current was injected into the frame of the PV system were higher than in the previous case study. When a 20 kA 8/20 μs impulse current was injected into the frame in the DM configuration, the induced voltage was 1.1 kV, the resulting peak current measured on the SPD was 70.69 A, and the energy absorbed by the SPD was 2.81 kJ. When a 10/350 μs impulse current was injected, the energy absorbed by the SPD was 4.21 kJ. When applying CM-induced voltages, the resulting energy absorbed by the SPD increased to 8.73 kJ, and the overcurrent increased to 117.19 A for the 8/20 μs waveform. For a 10/350 μs waveform, the current was 163.42 A, and the energy absorbed by the SPD was 12.09 kJ (Figures 7.14 (a) and (b)). When an extreme current of 100 kA was injected into the frame of the PV panel, the current on the SPD was 369.86 A and energy of 119.28 kJ was absorbed. The results show that more energy needs to be absorbed by the SPD for higher voltages. The highest currents flowing through the SPD were measured in the CM configuration for case study 2. For 8/20 μ impulse current-induced voltage, the peak current was 581.88 and energy of 310 kJ was absorbed. When the induced voltages for a 10/350 μ impulse current were applied, the current was 814.14 A, and the absorbed energy was 372 kJ (Figures 7.15 (a) and (b)). The current and energy absorbed by the SPD are summarised in table 7.4.

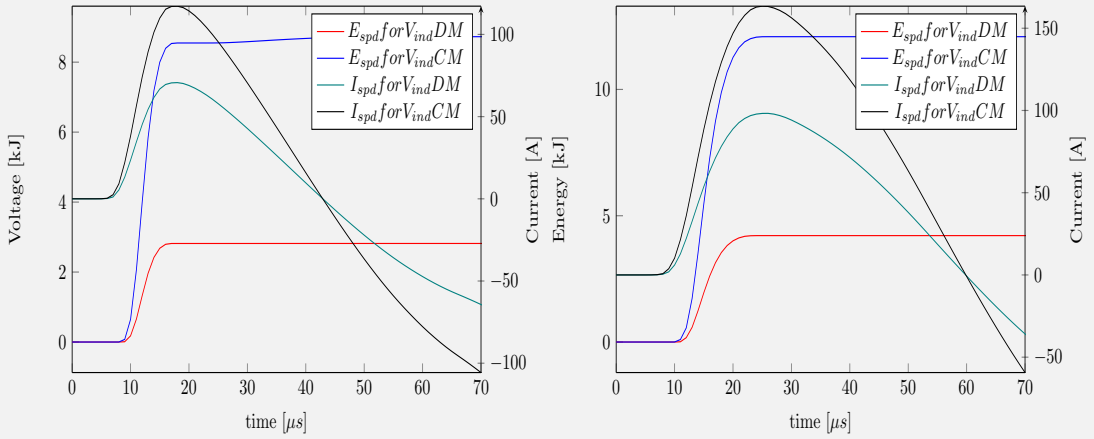
It can be deduced that case study 2 is the most severe for microinverters installed in PV systems. When the impulse is injected directly onto the frame of the PV panel, the current across the SPD and the energy were higher compared to case study 1. Additionally, CM configuration showed the most severe configuration compared to DM configuration.



(a) 8/20 μs impulse current

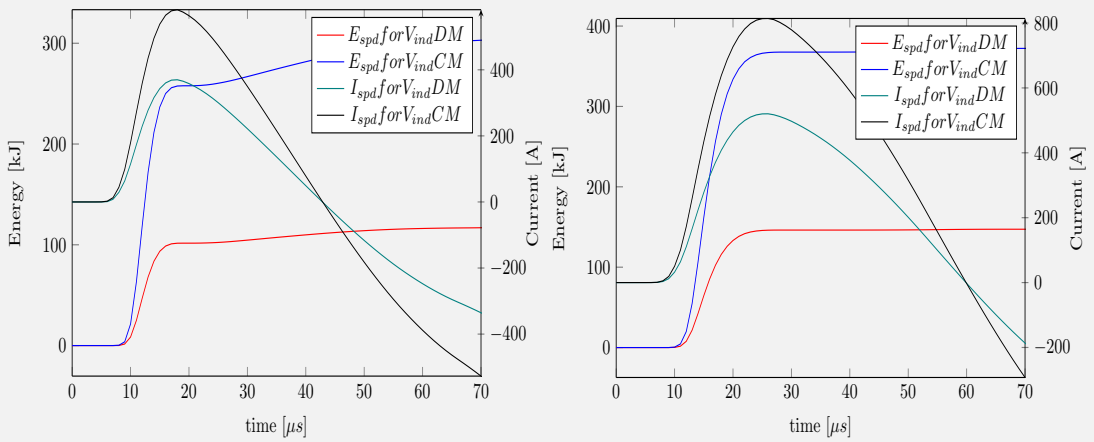
(b) 10/350 μs impulse current

Figure 7.13: Case study 2: SPD current and energy absorbed, 12.5 kA



(a) 8/20 μs impulse current **(b)** 10/350 μs impulse current

Figure 7.14: Case study 2: SPD current and energy absorbed, 20 kA



(a) 8/20 μs impulse current **(b)** 10/350 μs impulse current

Figure 7.15: Case study 2: SPD current and energy absorbed, 100 kA

Table 7.4: SPD energy and current overload case study 2

8/20 µs impulse Current Waveform						
	12.5 kA		**20 kA**		**100 kA**	
Mode of Measurement	E_{spd}	I_{spd}	E_{spd}	I_{spd}	E_{spd}	I_{spd}
DM	0.71 kJ	44.08 A	2.81 kJ	70.69 A	119.28 kJ	369.86 A
CM	2.59 kJ	73.20 A	8.73 kJ	117.19 A	310.61 kJ	581.88A
10/350 µs Impulse Current Waveform						
	12.5 kA		**20 kA**		**100 kA**	
Mode of Measurement	E_{spd}	I_{spd}	E_{spd}	I_{spd}	E_{spd}	I_{spd}
DM	0.97 kJ	61.54 A	4.21 kJ	98.24 A	147.23 kJ	520.28 A
CM	4.21 kJ	101.80 A	12.09 kJ	163.42 A	372.23 kJ	814.14 A

7.5 Chapter Summary

Under high impulse currents, the overcurrents, which can exceed the maximum allowed currents, may affect the connected microinverter. The currents notably oscillated for an extended time, far exceeding the duration of the induced waveforms. However, with the introduction of the SPD to the DC cables, the high transient current and its relative energy were absorbed by the SPD. The effects of the SPD connected to the microinverter's DC cables when excited by indirect lightning phenomenon were investigated.

In this chapter, the current and the absorbed energy for each case study when applying impulse currents were computed using PSCAD. The energy overload of the SPD was greatly affected by the induced voltages on the SPD and the characteristics of the impulse current's waveform. For example, when an extreme surge occurred, the energy overload of the SPD was exceeded. But when a surge with a lower magnitude occurs, which is more likely, the SPD energy overload was not exceeded.

8 Discussion

8.1 Introduction

Lightning-induced overvoltages caused by indirect lightning strokes may affect nearby PV panels in a PVI. In this research, it was possible, through simulations and experiments, to measure the characteristics of lightning-induced voltages in PV systems. Such characteristics include the waveform's amplitudes and steepness. These induced voltages were then used to test an SPD connected to the DC cables of a PV panel with a microinverter, and the resulting energy overload and the current flowing through the SPD were analysed.

This chapter will begin with analysing factors considered influential in the magnitude of LIOs based on experimental and simulation investigations conducted, followed by the discussions on the energy overload and currents flowing through the SPD when connected to the DC cables. Additionally, recommendations for microinverter protection practices are proposed, solely driven by the results and carefully analysed to minimise lightning risk to the microinverter.

8.2 Influence factors for induced overvoltages

The simulation and experimental studies conducted in this research (Chapters 5 and 6) have shown the influence of the electromagnetic coupling concept on PV systems caused by lightning transients in empirical data. This concept was explored in a linear medium (air), where the time-varying current flows through the rod or PV frame, creating a time-varying magnetic field and an induced electric field, thereby producing an emf on the PV panel's DC cables.

Several conditions influence the induced overvoltages on the PV panel's DC cables. LIO's amplitudes depend on parameters such as the lightning current amplitude, the LPS, and the lightning strike location [10, 86, 87, 89, 91]. The results from this present work demonstrated the presence of induced overvoltages on the PV panel's DC cables when subjected to impulse current. These measurements further showed that the circuit characteristics, the protection scenario and lightning parameters were the most important factors that govern

the magnitude of induced overvoltages appearing on the PV panel's DC cables and, thus, directly to microinverters. Table 8.1 shows the measured parameters and their influence on LIOs obtained from the simulation and experiment.

Table 8.1: Factors influencing lightning-induced overvoltages

Parameter	**Method**	**Results**	**Lightning Induced overvoltage**
Lightning Current Amplitude	Simulation and Experiment	**Case Study 1**: 5-100 kA, V_{max}: 115 V - 2.3 kV in DM	Lightning-induced overvoltages (DM and CM) increase proportionally with an increase in injected impulse current.
LPS distance	Simulation	**Case Study 1** LPS distance: 1-3 metres, V_{max}: 2.3 kV - 384 V in DM	Lightning-induced overvoltages (DM and CM) decrease with increasing distance between the LPS and PV panel.
Lightning Strike Location (protection scenario)	Simulation and Experiment	**Case Study 1 - Case Study 2**, V_{max}: 2.3 kV - 5.8 kV @ 100 kA impulse	LIOs (DM and CM) decrease with strike distance. Case study 2, where the impulse current was injected on the PV frame, indicated a significant increase in induced overvoltages.
Wire Lengths	Simulation	**Case Study 1** Wire lengths: 1-5 metres, V_{max}: 2.3 kV - 2.26 kV at 100 kA impulse current	Had little impact on lightning-induced overvoltages (DM and CM).
Lightning Current Waveform	Simulation and Experiment	Slight change in V_{max} between 8/20 μs and 10/350 μs lightning current waveforms	Induced overvoltages decrease with increasing front time of the lightning waveform. However, no significant difference between the induced voltages amplitudes between 8/20 μs and 10/350 μs lightning current waveforms
Mode of Measurements (CM and DM)	Simulation and Experiment	**Case Study 1** : V_{max}: 2.3 kV (DM)- 5.2 kV (CM)	CM measured lightning-induced overvoltages were significantly greater than that in DM.
Microinverter connected on the DC cables	Experiment	**Case Study 1**, V_{max}: 58 V - 126 V (Open DC) at 5 kA impulse current	Decrease with load impedance. When a microinverter was connected, lightning-induced overvoltages (DM) were reduced due to the internal circuit characteristics.
Twisted Pair Configuration	Experiment	**Case Study 1**, V_{max} : 430 (Open DC)- 390 V (twisted-pair) in DM at 20 kA impulse current	DM lightning-induced overvoltages reduced, however not significantly ($\tilde{4}$0 V difference at 20 kA). As the measurements are performed with cables close to each other, no significant change in induced overvoltages was observed.

8.2.1 The effect of changing current amplitude

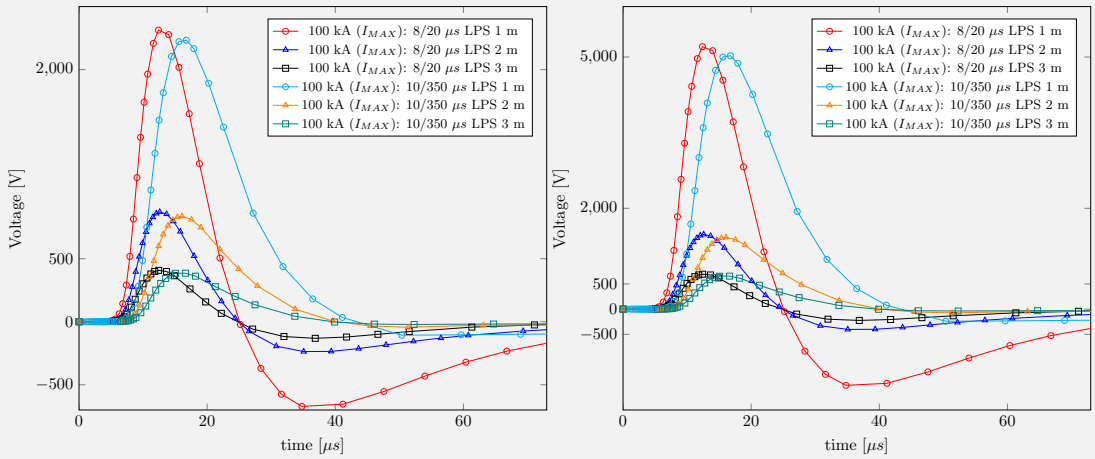
The interconnection of solar cells creates an internal loop, and the induced voltage is highly influenced by the magnetic flux passing through the loop [86, 88]. The magnetic flux density (**B**) as shown in equation 3.26 is highly dependent on the maximum current flowing through the current-carrying conductor. The proportional increase of induced voltages with impulse current, as demonstrated by [10, 87, 90, 91], signifies the risk of high lightning currents to PV panels. In this current study, it was fairly easy to notice that the induced overvoltage increased with increasing lightning current amplitude, as the simulation (Chapter 5) and experiments (Chapter 6) showed. This linearity was observed with the change in impulse current amplitudes. The measurements were conducted experimentally using a step-current approach with 5 kA, 12.5 kA and 20 kA impulse currents and, additionally, a 100 kA impulse current in a simulation setting. In the induced voltage simulation model (Chapter 5), the maximum value of the induced voltage at a 5 kA impulse current was 115 V, and an induced voltage of 2.3 kV at a 100 kA impulse was recorded. In case study 2, the induced voltages were 275 V at 5 kA impulse current and 5.8 kV at 100 kA impulse current. This linear increase in induced voltage is consistent with previous studies, where [87] found this value to range from 0.5 - 14 kV with impulse currents from 20-50 kA at different striking points and authors in [86] measured 4.29 kV with an impulse current of 110 kA. Additionally, investigations by [10] showed that the induced voltages from 0.5 kA/μs to 120 kA/μs oscillating currents increased from 14.8 V to 3.5 kV. Other investigations [90] measured this change of induced voltages against impulse currents injected directly at the different points, where the induced voltages using 2 to 200 kA impulse currents increased from 390 V to 3.19 kV.

8.2.2 The effect of changing LPS separation distance

The induced overvoltages with 100 kA impulse currents, as shown in figures 8.1 (a) and (b) in DM and CM configurations, respectively, suggest that the induced voltage is dependent on the distance from the LPS to the PV panel. The reduction in induced voltage was readily seen by moving the LPS two metres and three metres away from the panel. The highest induced voltages were recorded when the external LPS was 1 meter from the PV panel. These voltages were as high as 2.3 kV and 5.2 kV in DM and CM, respectively, at 100 kA impulse current. When the same impulse current was applied at a distance of 2 metres, the voltage dropped to 837 V and 1.4 kV in DM and CM, respectively. The reduction in induced voltages as the distance between the LPS and the PV panel is in accordance with previously reported work [10, 86, 89]. In [89], the induced voltages varied from 1.3 kV to 4.29 kV at 100 kA impulse current given different distances, and [86] showed that the induced voltage decreased given 1 - 2.5 metres lightning strike location. Investigations by [10] further indicated that the induced voltage at 120 kA/μs oscillating current with a separation distance of 0.5 metres

was 9.7 kV but reduced to 840 V when the separation distance was increased to 2 metres from the panel.

This observation from this work and previous work indicate that the distance from the panel is crucial in the induced voltages measured across the DC cables of a PV panel. In addition, this observation is critical in PV systems with microinverters as multiple panels in an array will have separate microinverters, which will be subjected to different induced voltages depending on the distance between the external LPS and the panels. When the LPS is closer to the panel, a higher magnetic intensity may arise due to the lightning current. This will further result in a higher magnetic flux passing across the internal loop and, therefore, greater induced voltages. These results show how nearby lightning strikes may affect other PV panels within a distance from the LPS system.



(a) Induced overvoltages in DM **(b)** Induced overvoltages in CM

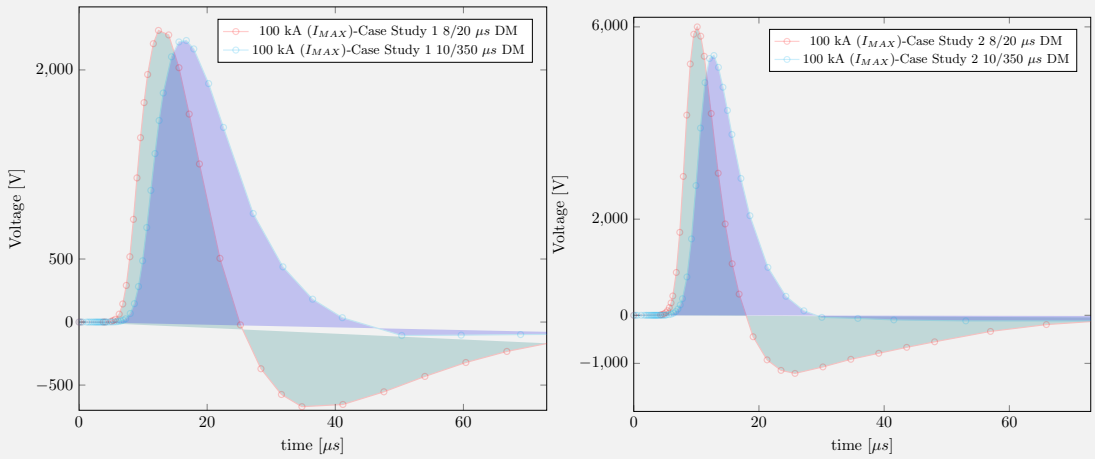
Figure 8.1: The effect of changing LPS distance on induced overvoltage

8.2.3 The effect of changing protection scenario

The protection scenario, as investigated through the different case studies, significantly influenced the induced overvoltages. In case study 2, with impulse current being injected directly into the panel's frame, the induced overvoltages were higher compared to when the impulse current was injected on the external LPS (Case study 1), a metre away from the panel. The condition of current injected on the PV frame results in the highest magnitude of induced voltages as there is a high concentration of current and the resultant magnetic flux closer to the PV panel. It is apparent that the introduction of the LPS (in the form of a lightning rod) greatly influenced the overvoltages. It is important to notice the influence of changing the lightning current stroke location, where the location closest to the panel resulted in higher

voltages on the DC cables.

Figures 8.2 (a) and (b) show the induced voltage waveforms at 100 kA impulse current in case study 1 and case study 2, respectively. Maximum amplitudes measured were 2.3 kV and 5.8 kV in DM configuration. Comparing the induced overvoltages' rise and fall times in figures 8.2 (a) and (b) shows that this was highly dependent on the protection scenario (Case study 1 and Case study 2) and impulse current waveform, where a quick rise and fall times were recorded when the impulse current was injected on the PV panel's frame (Case Study 2). The protection scenario in PV systems has been formerly investigated by [61] suggesting that at 10 kA impulse current, the maximum induced voltages measured were 680 V in a non-isolated LPS system and 475 V in an isolated LPS system. This finding is consistent with the study's observation. In the simulation model, the induced voltage at 12,5 kA impulse current was measured to be 687.5 V when there is no external LPS and 289 V in an isolated LPS in differential mode. Several research studies have concluded that lightning striking closer to the panel may be destructive due to the high voltages associated with the lightning surges [20, 85–87].



(a) Induced overvoltages, case study 1

(b) Induced overvoltages, case study 2

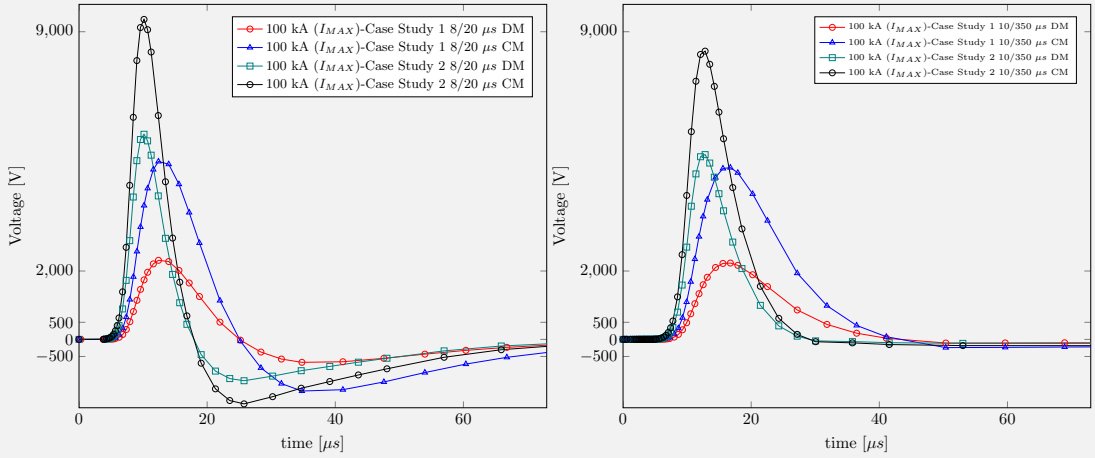
Figure 8.2: The effect of changing the protection scenario

8.2.4 The effect of mode of measurement

While most previous contributions [20, 85–87] have mainly focussed on DM mode induced voltages, in this present study, both DM and CM induced voltages are presented. Notably, very few studies have attempted to compare DM and CM-induced voltages [20, 88]. The induced voltages results from this current study are shown in figures 8.3 (a) and (b) in 8/20 μs and 10/350 μs impulse current waveforms at 100 kA, respectively. The results have

indicated significant differences in both modes of measurement, where induced overvoltages were significantly higher in CM. In case study 1, the difference between induced voltage in DM and CM was 2.9 kV, and 3.3 kV in case study 2, at 100 kA impulse current. This represents an average factor of about 2.3 between DM and CM-induced voltages. Several studies have made a similar observation in their investigations of DM and CM-induced voltages [20, 88]. The studies have similarly found that induced voltages in CM have a much higher amplitude than DM-induced voltages and have suggested that the CM-induced voltages can be 1.1 - 3 times the DM-induced voltages.

The frame of the PV panel creates a geometric loop in addition to the loop created by the interconnections of the cells. Since the loop created by the loop is connected to ground, it creates a short circuit current close to the internal loop, therefore reducing the magnetic field of the internal loop [10, 86]. This explains the reduction in induced voltages in DM. The reason for high induced voltages in CM is due to high ground potential [20]. It is important to note that induced overvoltages may appear in both modes, wherein PV systems, DM voltages appear between the DC cables and CM voltages appear between one of the DC cables and ground. SPDs can, therefore, be connected in either of the modes and will be subjected to these voltages. Understanding the difference in these voltages will be very crucial for protection engineers in the selection of the SPD's mode of protection.



(a) Induced overvoltage with 8/20 μs waveform **(b)** Induced overvoltages with 10/350 μs waveform

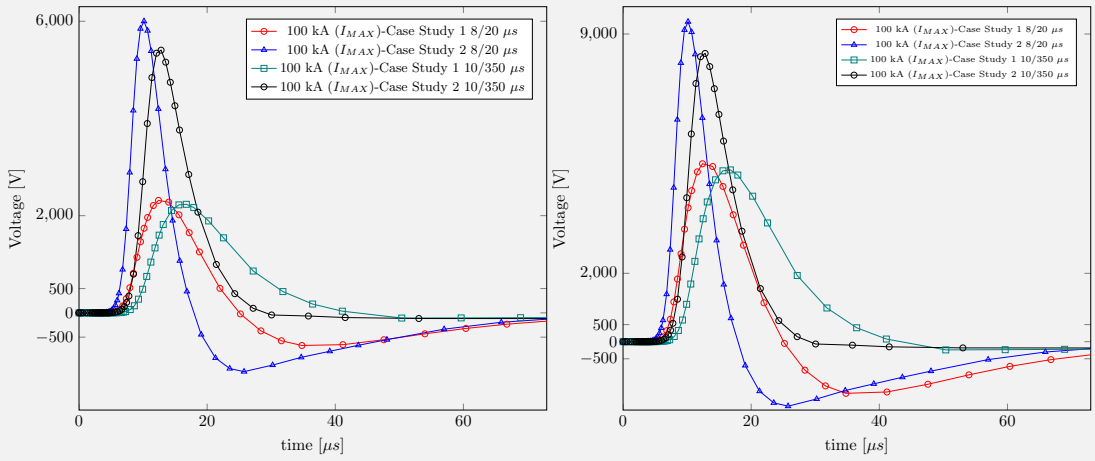
Figure 8.3: The effect of mode of configuration on induced overvoltage

8.2.5 The effect of changing impulse current wave shape

The 10/350 μs and 8/20 μs impulse current waveforms used in this research have been applied to measure induced voltages in PV systems in previous works [61, 87, 90–93]. Most of these

studies have used one of the two waveforms; very few published studies have attempted to compare various waveforms [20]. Regarding the lightning current waveforms (10/350 μs and 8/20 μs standard waveforms), there were no significant differences in induced overvoltages amplitudes; however, the rise and the fall times of the induced voltages were different (see figures 8.4 (a) and (b) for Case studies 1 and 2, respectively). The induced voltage rise and fall times depend on the current waveform's characteristics. Measurements performed with an 8/20 μs impulse current waveforms showed a quick rise and fall times in the induced voltages compared to the measurements performed with a 10/350 μs impulse current waveforms. The average steepness of induced voltage at 20 kA impulse current was measured to be 19.61 V/μs for 8/20 μs standard waveform and 18.35 V/μs for 10/350 μs standard waveform for case study 1. For case study 2, values of average steepness at 20 kA were 102.4 V/μs and 75.9 V/μs for 8/20 and 10/350 μs impulse current waveforms, respectively. Since the rise and fall times tested with different waveforms significantly affect the peak magnitude of the induced overvoltages, the rise and fall times of induced voltages considerably impact the energy content. A high negative undershoot of induced voltage was observed in 8/20 μs impulse current compared to the voltages induced with a 10/350 μs impulse current. This represents the differential of the impulse current.

Authors in [20] similarly found that the induced voltage waveforms varied with lightning current waveforms. Their investigations measured the induced using 1/200 μs, 6/50 μs, and 10/350 μs impulse current waveforms suggested that the induced voltages with a 10/350 μs have a longer rise and fall time compared to induced voltages with 1/200 μs and 6/50 μs impulse current waveforms.



(a) DM induced voltages **(b)** CM Induced voltages

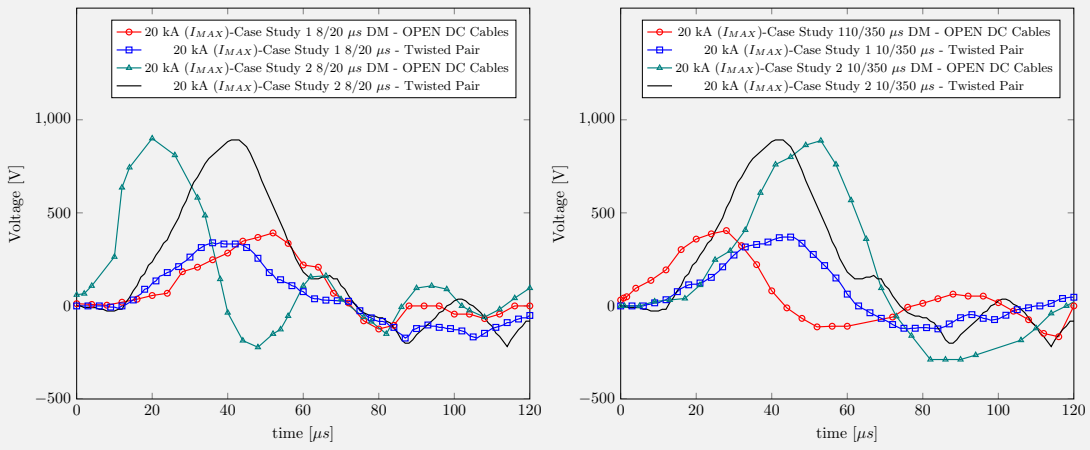
Figure 8.4: The effect of changing current waveforms

8.2.6 The effect of wire lengths

The other factor measured for induced voltages is the effect of wire lengths. In PV systems, this effect has been formerly investigated by [90,91]. While the previous report by [91] claim no change in induced voltages for wire lengths not exceeding 20 m, where at 19 kA impulse current, the induced voltage was constant (11.7 kV), authors in [90] suggested that a slight voltage drop was measured when the wire lengths were increased from 5 metres to 10 metres at 100 kA impulse current, this voltage reduced from 2.19 kV to 2.17 kV. This observation from [90] is consistent with this present work. The results in this present study show a slight voltage reduction due to increased resistance of the wires, where a slight decrease in induced voltage was observed with increased wire lengths. This, however, does not cause a significant change. In both case studies 1 and 2, only a 2% reduction in induced voltages has been recorded at 1-meter cable length and 5 metres cable length.

8.2.7 The effect of twisting DC cables

The induced voltages with twisting the DC cables to form a twisted pair configuration showed no significant reduction in induced voltages (Figures 8.5 (a) and (b)) as was tested experimentally. In case study 1, only a slight induced voltage reduction of 40 V was measured between open dc cables and twisted-pair cables. Therefore, It can be concluded that the magnetic influence between the two DC cables plays no significant role in the magnitude of induced voltages. This investigation has not been reported in previous studies.



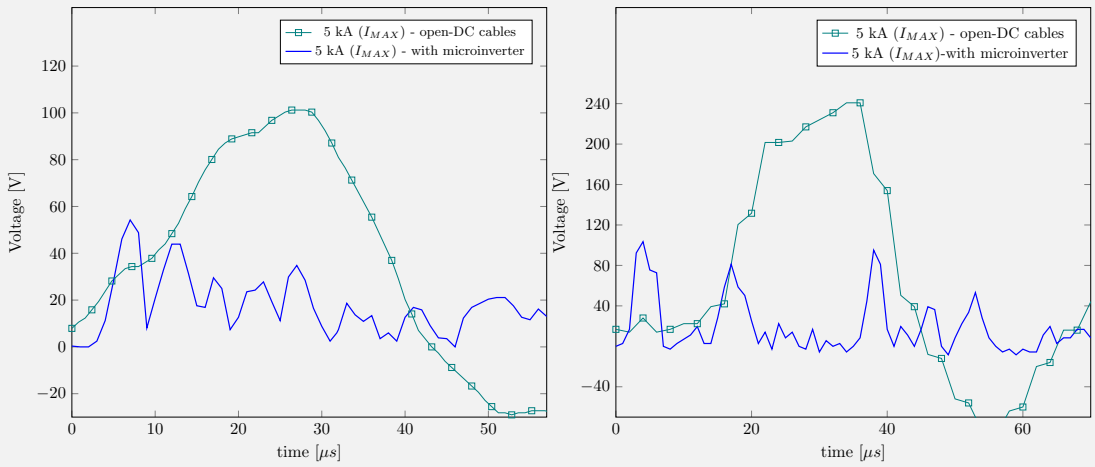
(a) Induced overvoltages, 8/20 μs Impulse **(b)** Induced overvoltages, 10/350 μs Impulse

Figure 8.5: The effect of twisting the DC Cables (10/350 μs Impulse)

8.2.8 Measurements with a microinverter

With a microinverter connected on the DC side, a reduced voltage was measured between the DC cables to approximately half of the open DC voltage magnitude. This is due to the effective impedance of the microinverter reacting to the induced voltages. The increased impedance of the circuit notably resulted in increased oscillations between the circuit's inductive and capacitive elements. It must be noted that the oscillations are a secondary phenomenon excited by the circuit characteristics and not primarily caused by the impulse lightning current. It is evident, therefore, that the circuit's electrical and physical characteristics can influence the induced voltages' characteristics.

Figures 8.6 (a) and (b) illustrates the comparisons between the induced voltages measured in open-DC cables to that measured with a microinverter connected in both case study 1 and 2, respectively.



(a) Experimental case study 1: 10/350 μs impulse **(b)** Experimental case study 2: 8/20 μs impulse

Figure 8.6: Induced voltages, open DC cables vs with a microinverter, 5 kA

8.3 SPD energy overload and protection performance

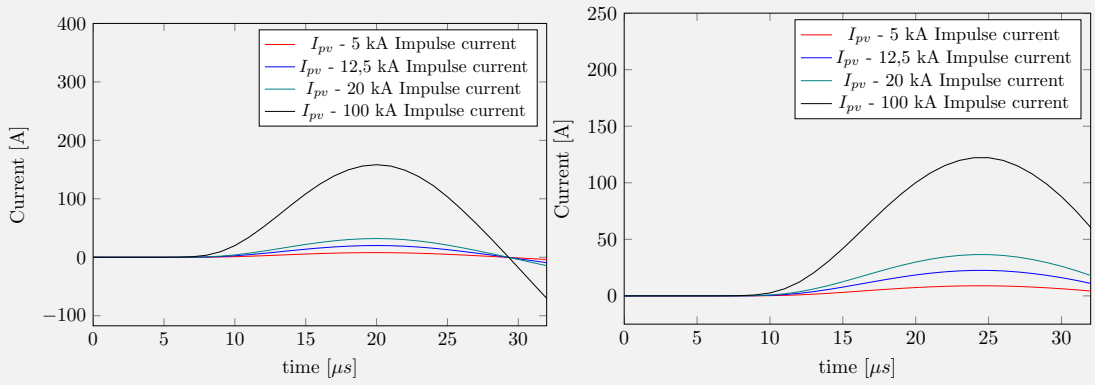
8.3.1 Overcurrents appearing on the microinverter

As discussed, the induced voltages measurements obtained in chapter 5 made it possible to predict maximum induced voltages as a function of several parameters. In the assumption that impulse current flows through the lightning rod or the frame of the PV panel, the influence of these voltages was further investigated with and without an SPD connected to the DC cables of the PV panel with a microinverter. Previous studies, however, have not

empirically examined the effects of induced voltages on microinverters installed in PVIs.

A previous report by [92] indicated that the maximum induced current in a PV system with a 5 kA indirect current near the PV structure was estimated to be 200 A. In this current study, the overcurrents appearing on a microinverter during a period of lightning impulse caused by the induced voltages were investigated in PSCAD for different current amplitudes. Results of the overcurrents appearing on the microinverter caused by induced voltages as shown in figures 8.7 - 8.10 have highlighted that the induced voltage's amplitude and waveshapes can determine the currents amplitude and waveshape as they flow to the microinverter. In case study 1, the overcurrents appearing at the microinverter at 100kA did not exceed 429 A; in case study 2, the maximum current was no more than 723 A. The overcurrents in CM configurations appear to be higher than in DM configurations. The overvoltages excited an oscillation between the inductive and capacitive components of the circuit and persisted far longer than the duration of the induced voltage. It was observed that the overcurrents might exceed the magnitude without surge protection, which can damage the microinverter.

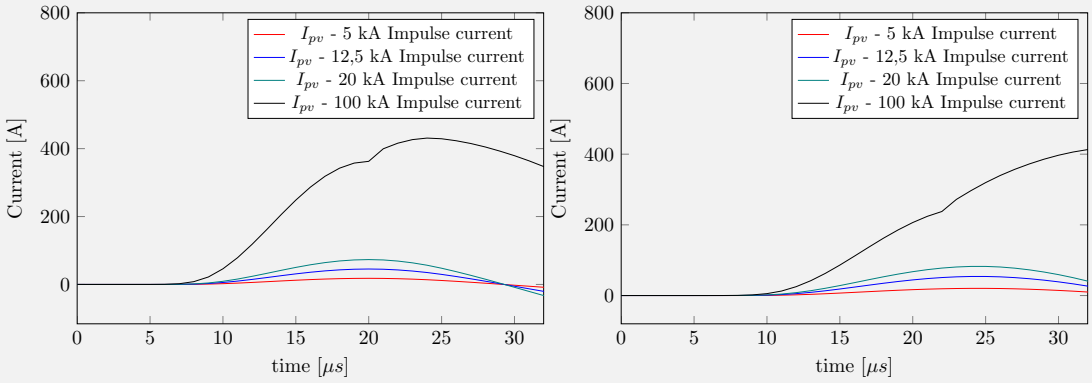
To protect the microinverters' internal components, an SPD with a protection level lower than the impulse withstand voltage of the microinverter should be installed between the DC cables. This is discussed in the next section.



(a) Overcurrents, 8/20 μs waveform

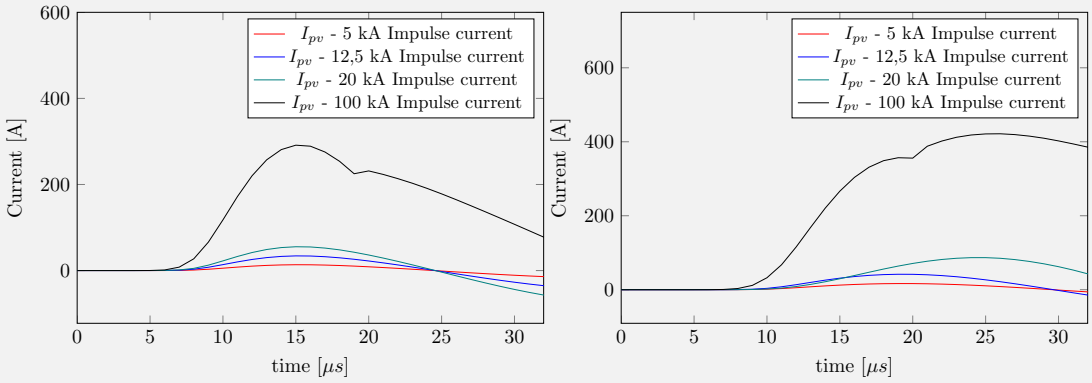
(b) Overcurrents, 10/350 μs waveform

Figure 8.7: Case study 1 overrcurrents appearing at the microinverter, DM



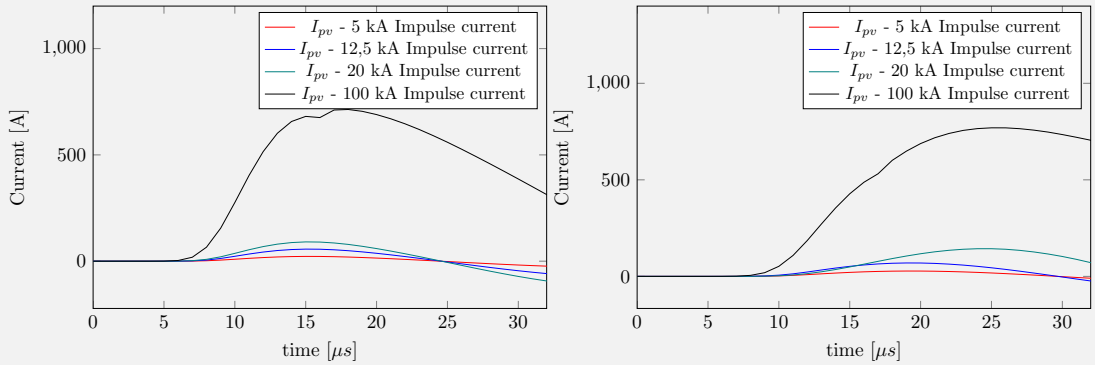
(a) Overrcurrents, 8/20 μs waveform **(b)** Overrcurrents, 10/350 μs waveform

Figure 8.8: Case study 1 overrcurrents appearing at the microinverter, CM



(a) Overrcurrents, 8/20 μs waveform **(b)** Overrcurrents, 10/350 μs waveform

Figure 8.9: Case study 2 overrcurrents appearing at the microinverter, DM



(a) Overcurrents, 8/20 μs waveform

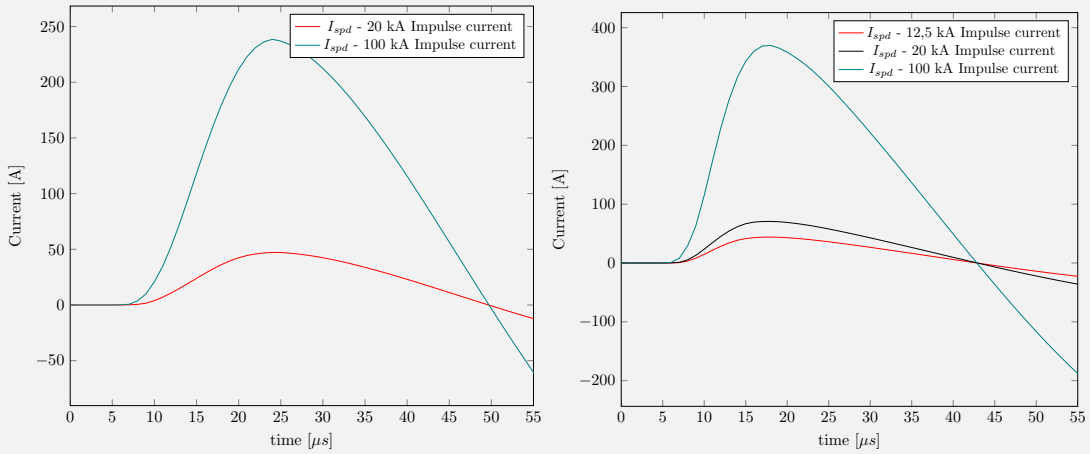
(b) Overcurrents, 8/20 μs waveform

Figure 8.10: Case study 2 overcurrents appearing at the microinverter, CM

8.3.2 SPD stress due to lightning currents

Generally, two categories may be used to measure the stress on the SPD due to lightning currents; overload and flashover [63]. Energy overloads may be caused by the energy absorbed by the SPD exceeding the capabilities of the SPD. Investigations performed by [20, 90, 93] have shown how SPDs can partially protect the PV inverters against lightning transients. However, it must be noted that most of these accounts have not investigated the magnitudes of the overcurrents studies in SPDs to protect PV systems.

The overcurrents across the SPDs of a PV system were previously investigated by Zhang *et al.* [20], suggesting that with a 5 kV induced overvoltage, the maximum current through the SPD was 500 A. These previous investigations' findings are consistent with this current study showing a linear increase in overcurrents, where the maximum current flowing through the SPD with a 5.8 kV (DM) was 369 A in case study 2 for a 100 kA impulse current injection. In case study 1, with an induced voltage of 2.3 kV, the maximum current through the SPD was 238 A. As shown in Figures 8.11 (a) and (b), the current flowing through the SPD during a period of impulse voltage changes from less than 1 mA to hundreds of amperes at high impulse currents injection. The results in this research with surge protection (MOV) connected to the DC cables showed how microinverters could be protected from lightning strikes. As illustrated, the impulse currents injected into different protection cases showed different induced voltage waveforms, the current flowing through the SPD, and the energy absorbed by the SPD. Since the CM configuration showed higher voltages than the DM configuration, the energy absorbed by the SPD was also affected, thus, the increase in energy overload of the SPD.



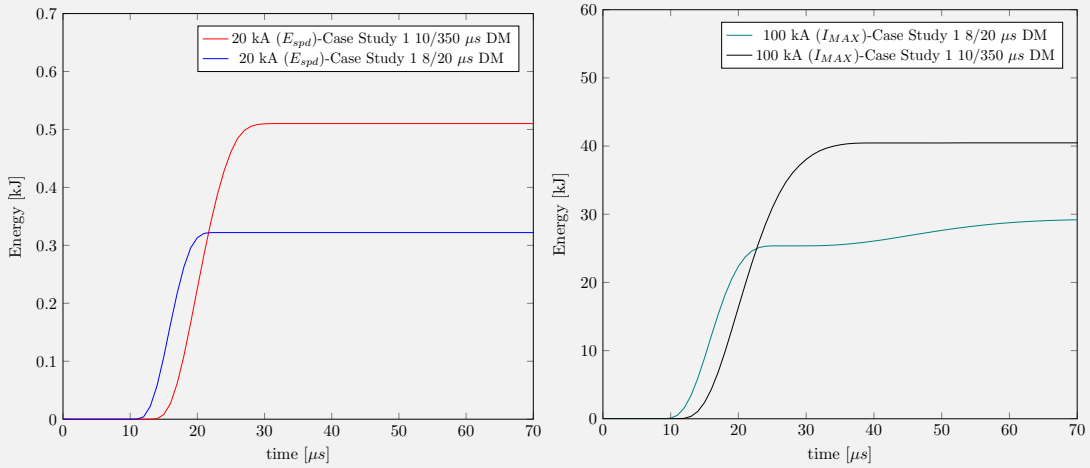
(a) Case study 1 **(b)** Case Study 2

Figure 8.11: Currents flowing through the SPD, DM, 8/20 μs waveform

The energy absorbed by the SPD under different current waveforms was also investigated. The simulation results confirm the influence of different parameters determining the stress experienced by the SPD during a lightning strike as prescribed by standard IEC 62305-4: 2010 [21] standard, including the lightning current and the type of waveshape being considered. The quantitative measurement of these factors is essential in developing effective protective measures to protect microinverters in PV systems. While some previous studies in PV lightning protection have provided recommendations for SPDs installed in PV systems [20, 90, 92], they do not address the energy absorption measurements of SPDs connected to PVIs. For example, authors in [93] have reported that the energy absorbed by the SPD connected to the DC cables of a PV system increase with increased directly injected impulse currents and is dependent on the lightning current injected. This finding is consistent with this current present work finding, although it has to be noted that this work focussed on induced voltages near the PV structure.

In this present study, the energy absorbed by the SPD varied as a function of the impulse current injected into the nearby structure of the PV panel. The energy and current increased with the amplitude of the impulse current injected. This analysis further showed that the energy absorbed by the SPD for induced voltage waveforms caused by an 8/20 μs standard waveform was less than those under 10/350 μs waveforms. This can also be due to the fall times of the 10/350 μs waveform being longer than the 8/20 μs waveforms (Figure 8.12a). It was noted that under extreme currents of 100 kA, the energy overload of the SPD may be exceeded as tens of kilojoules are recorded (Figure 8.12b). This is due to the high voltages appearing on the DC cables. However, it also has to be noted that the probability of these

extreme lightning currents is very low; according to the IEC 62305-1: 2010 [63] standard, this probability (P) is 0.05.



(a) Energy absorbed by the SPD (20kA) **(b)** Energy absorbed by the SPD (100kA)

Figure 8.12: Energy absorbed by the SPD

8.4 Recommendations

8.4.1 Lightning-induced overvoltages risk for microinveters

Microinverters have lower voltage and current rating characteristics than central or string inverters, and therefore, on this basis, they become more sensitive to lightning stresses. Therefore, evaluation of the waveforms, representing the equivalent lightning surges, is primal in developing the necessary protection measures. The experiments and the simulation models proposed in this research have shown that microinverters are susceptible to lightning stresses, in all cases, including with and without external LPS. However, the risk is lowered when an LPS is in place. Based on the experimental and simulation results, it has been confirmed that the induced voltages on the DC cables of a solar panel can exceed the U_w of microinverters. Voltages as high as several kilovolts were induced on the panel and measured under extreme currents.

8.4.2 Lightning Protection Systems

To provide full protection for microinverters installed in PV systems against lightning transients, available strategies and techniques may be evaluated and employed to safeguard buildings. These techniques, which include internal and external LPSs, should also align with the

location and design of a PVI. Furthermore, they should be adequate to protect a PVI against both direct and indirect lightning transients. Through different case studies, the results further confirmed that external LPSs play an essential role in protecting the PV panel by reducing the amplitudes of induced voltages on the DC cables.

This study explored using a lightning rod as a part of the LPS. External lightning protection measures divert the lightning strikes near the protected object to ground. This is achieved using arresters, air termination and the grounding system. The selection and coordination of an effective LPS depending on the area to be protected in microinverter configurations will be essential in reducing the effects of lightning transients on PVIs as the simulation and experiment showed. Different air termination systems may be evaluated based on the structure and the materials of the roof where microinverters are installed. The methods which have been prescribed by standards are; the rolling sphere method (RSM), protection angle method (PAM), and the mesh method (MM), each being installed under different conditions to offer effective protection [65].

8.4.3 SPDs for microinverters

To obtain full protection for PV systems with microinverters, SPDs should be installed on PVIs, with or without an external LPS. The experiments and simulations have shown the appearance of LIOs in PV systems with microinverters. The key parameter in the design of an SPD is the U_p, which is related to the equipment's U_w. This rated U_w is defined by the equipment's manufacturer based on its ability to withstand overvoltages.

The study results show that the DC side of the microinverter can also be affected by LIOs. Despite this, most microinverters are not protected against LIOs. Regarding the DC side of the microinverter, the following recommendations should suffice:

- The space limitation of the microinverter should be considered, as most installations are installed close to the panels with less DC wiring. It also becomes important to avoid unnecessary conductor loops. Therefore, the DC side of a microinverter should be installed with an internal surge protection device (Figure 8.13).
- The type of microinverter installed should be reviewed, considering the internal components. Protection of these devices is of practical importance. Microinverters should be designed with internal voltage clamping devices, e.g., MOVs. This should allow the microinverter to be partially protected against the effects of lightning currents. The internal protection circuit's U_p should not exceed the U_w of the microinverter. It is also important to note that the selection of the SPD is based on a risk assessment. A certain level of failure may be accepted based on some economic and technical criteria.
- The IEC 62305-4:2010 [21] standard stipulates 'selection and installation of a coordinated SPD system' using U_p. The selection of a proper U_p of the SPD depends on the U_w, the connecting conductors' length and the routing circuit's length from the SPD to the microinverter. When an SPD is installed, the total U_p is a summation of the inductive ΔU of the connecting conductors and the SPDs U_p. For this research, a U_p of 400 V was selected based on a U_w of 500 V. However; this will depend on the characteristics of a connected microinverter.

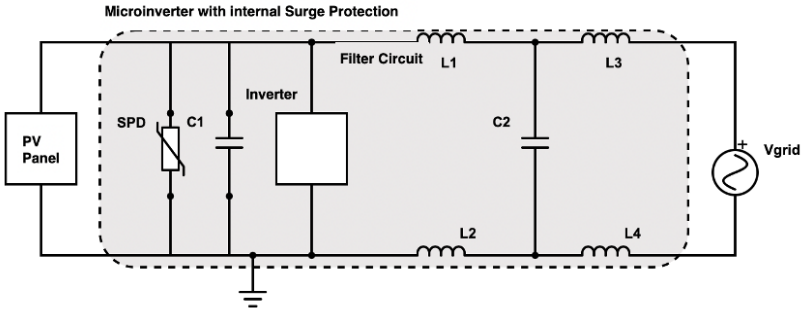
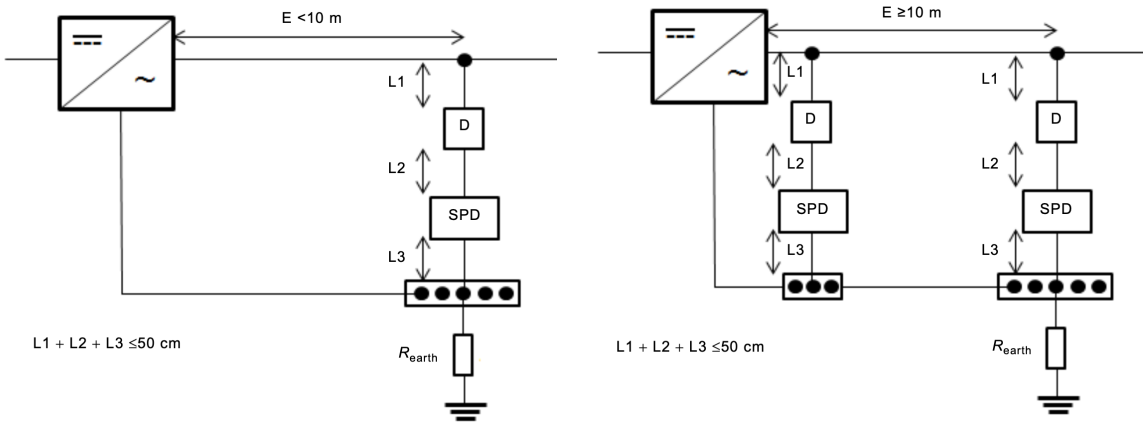


Figure 8.13: Microinverter with SPD connected on the DC side. Concept adapted from [5]

Regarding the AC side of the microinverter, the following recommendations may suffice:

- The AC side of the microinverter is no different from the normal SPD recommendation for central inverters. Since the AC side of the microinverter (or a string of microinverters) is connected to the grid or supply mains (230/400 V AC), it should be installed with an SPD. If the length of the routing conductor is greater than 10 m, an additional SPD should be installed close to the main circuit board (Figure 8.14 (a) and (b)) [77].
- In general, a safety margin of at least 20% between the rated impulse voltage of the equipment and the U_p up to 0,8 times U_w should be maintained (IEC 61643-12 [75], and IEC 62305-4:2010 [21]). See IEC 60364-5-53:2015, Clause 534 for possible exceptions. If not otherwise specified, the acceptable overvoltage category is category II. The maximum impulse voltage expected to reach the equipment is 2.5 kV for 230/400 V AC systems. This generally requires a protection scheme with several coordinated SPDs. The manufacturers of SPDs may provide the necessary information for such coordination.



(a) SPD Installation on the AC side of the inverter with short distance (< 10m)

(b) SPD Installation on the AC side of the inverter with long-distance (≥ 10m)

Figure 8.14: AC side SPD recommendations for inverters [77]

9 Conclusion

9.1 Conclusion

Several theoretical texts on the nature of lightning have been published, and protection measures for electrical equipment have been subsequently established. But despite this knowledge, protection measures for microinverters installed in PVIs have not been standardised. This research attempted to close this void by providing an exposition for suitable protection measures in the scope of PVI's protection.

This dissertation paid special attention to the lightning-induced overvoltages on microinverters used on PV systems and is based on the theoretical knowledge of lightning effects on electrical systems. It has been found that lightning currents flowing through LPS structures or the PV frame can cause induced overvoltages. These results can be generalised to cover different protection scenarios for PVIs with microinverters. The magnitude of these voltages varied as a function of lightning current parameters and protection cases. These parameters, including lightning current amplitude, protection scenario, mode of measurements, and circuit characteristics, indicated a variation in overvoltage magnitudes appearing on the DC cables. It was observed that the magnitude of induced overvoltages increased based on the strike location of the panel. Higher magnitudes were observed in locations closer to the panel, for instance, when the lightning was injected into the frame. In addition, the distance between the LPS and the PV panel also influenced the induced overvoltages on the DC cables. Other parameters such as wire lengths on the DC cabling showed no significant effect on the induced overvoltages due to low resistances. It is also expected that, since microinverters are usually coupled to the PV panel or installed near the panel, the DC cable wire lengths would not be long and, as such, will not contribute significantly to the magnitude of induced voltages. However, microinverters are sensitive electronics; it can be concluded that these induced overvoltages can exceed the microinverters' U_w. The proposed simulation model has been verified experimentally in a laboratory setting.

The results with surge protection connected to the DC cables of the PV panel showed the energy absorbed by the SPD and the current. Based on performed analyses, the following conclusions were formulated:

- The high induced overvoltage confirms the need to install an SPD on the DC cables of a microinverter.
- A proper SPD type II connected to the DC cables of the microinverter may divert the surge current to ground and protect the microinverter against lightning transients.
- The current and energy absorbed by the SPD depend on the impulse current characteristics. The induced overvoltage waveform's rise and fall times may be associated with the energy absorbed by the SPD.
- CM-induced overvoltages, which are greater than DM-induced overvoltages, may overload the SPD at high impulse currents.
- In extreme currents (e.g., 100 kA impulse currents), the energy absorption capabilities of the SPD may be exceeded, which may cause SPD failure to protect the microinverter.

Finally, several issues should be covered by surge protection standards. The standards should provide reliable recommendations for manufacturers and consumers to protect microinverters. In relation to this work, the standards have to address the following shortcomings in the protection of microinverters:

- Voltage withstand levels for microinverters should be introduced. This purpose is to have a set of values that should be the basis for insulation coordination and should be used by other technical committees of the IEC in charge of product standards. Despite this, the maximum U_w for microinverters operating in nominal voltages of less than 50 V has not been defined. Furthermore, the current standards have not provided details on the protection of these devices.
- Although current standards refer to the distance between the PV panel and the microinverter, it is known that microinverters are usually installed close to the panel. Therefore, the distance between the panel and the inverter is less than 10 metres (sometimes these devices are fitted directly to the panel), and specifically, such protection should be specified.
- In addition, since microinverters rely on internal lightning protection, the standards should address the requirements for internal lightning protection for microinverters.

This research has provided information on the protection of microinverters in PV systems. It has been noted that the protection of microinverters has not been covered in well-known standards. Protection engineers and SPD manufacturers may use the induced overvoltages measured along with the recommendations to enhance lightning protection for microinverters on PV systems.

9.2 Principal Contributions

The principal contributions of this work are:

1. Simulations of induced overvoltages on a microinverter's DC cables on a PV system were performed. The simulation introduced higher currents that the experimental study could not generate. The empirical data of the induced overvoltages can be used to properly select protection d evices, such as SPDs, using the knowledge of overvoltages that can be subjected to equipment. In addition, this analytical study makes it possible to note the influence factors for induced voltages.

2. Experimentally, different lightning stroke locations were tested to measure their effect on overvoltages induced on the DC cables of a solar panel and subsequently on the microinverters. Experimental results were used as a primary validation method for the simulation predictions.

3. The simulation and experimental settings explored the induced overvoltages under DM and CM configurations. This is important for protection engineers to decide on the configuration mode for SPDs in PV installation.

4. The simulation explored the use of the SPD connected to the DC cables and its protection performance against lightning-induced overvoltages. The protection performance section of this research provided the following useful information:

    - The overcurrents appearing at the microinverter were measured under different protection scenarios without the SPD connected. This information is helpful for selecting and coordinating SPDs.
    - The energy overload and current flowing through the SPD were measured. The simulation showed increased energy and current through the SPD under different induced overvoltages for different protection scenarios and configurations. This information is crucial for SPD manufacturers in the design of surge protection for microinverters.

9.3 Suggested Future Work

The limitations of this research have made it necessary to leave aside further studies in the field that could be important. Suggestions for future work are:

1. This study used a single earth connection between the protection system and the panel; future research may also focus on the influence of overvoltages on microinverters using different soil resistivities.

2. Different surge protection devices have different $I-V$ characteristics; future work may investigate different SPDs and their influence on the induced overvoltages regarding their characteristics.

3. It has also become common to use more than one type of protective device to obtain the best possible combination of desirable characteristics. These are usually referred to as multistage hybrid circuits. Since this research only explored MOVs as a protective device, future research may explore using more than one protective device combination.

4. The effect of the type of the external LPS on the induced voltages was not investigated in this research. More work can be conducted in this regard, where the different materials used in the design of these LPSs' may be investigated, along with their geometries and separation distances.

5. This research elicited simulation and experimental investigation. However, several theoretical models have been applied to calculate lightning-induced overvoltages, such as the Taylor, Rusck, Rachidi, Chowdry, and many others. Future research may also theoretically explore the protection of microinverters through overvoltage calculation using these models.

6. Further work may also focus on finding the average U_w for different microinverters. It has been noted that microinverter manufacturers do not make this information available.

Bibliography

[1] H. A. Sher and K. E. Addoweesh, "Micro-inverters—promising solutions in solar photovoltaics," *Energy for Sustainable Development*, vol. 16, no. 4, pp. 389–400, 2012.

[2] D. L. Caiza, S. Kouro, F. Flores-Bahamonde, and R. Hernandez, "Unfolding pv microinverter current control: Rectified sinusoidal vs sinusoidal reference waveform," in *2018 IEEE Energy Conversion Congress and Exposition (ECCE)*. IEEE, 2018, pp. 7094–7100.

[3] Ö. Çelik, A. Teke, and A. Tan, "Overview of micro-inverters as a challenging technology in photovoltaic applications," *Renewable and Sustainable Energy Reviews*, vol. 82, pp. 3191–3206, 2018.

[4] T. Shimizu, K. Wada, and N. Nakamura, "Flyback-type single-phase utility interactive inverter with power pulsation decoupling on the dc input for an ac photovoltaic module system," *IEEE transactions on power electronics*, vol. 21, no. 5, pp. 1264–1272, 2006.

[5] O. Lopez-Santos, G. García, and L. Martinez-Salamero, "Derivation of a global model of a two-stage photovoltaic microinverter using sliding-mode control," in *2015 IEEE 13th Brazilian Power Electronics Conference and 1st Southern Power Electronics Conference (COBEP/SPEC)*. IEEE, Conference Proceedings, pp. 1–6.

[6] A. Khan, L. Ben-Brahim, A. Gastli, and M. Benammar, "Review and simulation of leakage current in transformerless microinverters for pv applications," *Renewable and Sustainable Energy Reviews*, vol. 74, pp. 1240–1256, 2017.

[7] F. Heidler, W. Zischank, Z. Flisowski, C. Bouquegneau, and C. Mazzetti, "Parameters of lightning current given in iec 62305–background, experience and outlook," in *29th ICPL conference*, Conference Proceedings.

[8] E. M. Bazelyan and Y. P. Raizer, *Lightning physics and lightning protection*. CRC Press, 2000.

[9] M. Uman, V. Rakov, G. Schnetzer, K. Rambo, D. Crawford, and R. Fisher, "Time derivative of the electric field 10, 14, and 30 m from triggered lightning strokes," *Journal of Geophysical Research: Atmospheres*, vol. 105, no. D12, pp. 15 577–15 595, 2000.

[10] H.-J. Stern and H. C. Karner, "Lightning induced emc phenomena in photovoltaic modules," in *1993 International Symposium on Electromagnetic Compatibility.* IEEE, Conference Proceedings, pp. 442–446.

[11] Y. Fuangfung, S. Sinthusonthishat, and P. Yutthagowith, "A software tool for induced voltages and currents calculation caused by lightning electromagnetic field in pv systems," in *2015 12th International Conference on Electrical Engineering/Electronics, Computer, Telecommunications and Information Technology (ECTI-CON).* IEEE, Conference Proceedings, pp. 1–4.

[12] J. He, *Metal oxide varistors: from microstructure to macro-characteristics.* John Wiley & Sons, 2019.

[13] DEHN, *LIGHTNING PROTECTIONGUIDE 3rd updated Edition ed*, 2014.

[14] J. Runge, "Design and control of resilient micro-inverter system," Ph.D. dissertation, 2016.

[15] D. Z. Gao and K. Sun, "Dc–ac inverters," *Electric Renewable Energy Systems*, pp. 354–381, 2015.

[16] O. Lopez Santos, "Contribution to the dc-ac conversion in photovoltaic systems: Module oriented converters," Ph.D. dissertation, Toulouse, INSA, 2015.

[17] IEC, *61442:2010 - Safety of power converters for use in photovoltaic power systems: Part 1: General requirements*, 2010.

[18] C. Gomes, "On the selection and installation of surge protection devices in a tt wiring system for equipment and human safety," *Safety Science*, vol. 49, no. 6, pp. 861–870, 2011.

[19] R. Maltione, V. M. dos Reis, D. I. Narvaez, M. G. Villalva, and L. C. Kretly, "Small size inverters: Development challenges for pv, renewable energy applications, as well iot, emc, lightning and robustness tradeoffs," in *2018 13th IEEE International Conference on Industry Applications (INDUSCON).* IEEE, Conference Proceedings, pp. 1150–1157.

[20] Y. Zhang, H. Chen, and Y. Du, "Lightning protection design of solar photovoltaic systems: Methodology and guidelines," *Electric Power Systems Research*, vol. 174, p. 105877, 2019.

[21] IEC, *62305-4: 2010 - Protection against Lightning: Part 4: Electrical and Electronic Systems within structures*, 2010.

[22] R. Hasan and S. Mekhilef, "Highly efficient flyback microinverter for grid-connected rooftop pv system," *Solar Energy*, vol. 146, pp. 511–522, 2017.

[23] S. Jiang, D. Cao, Y. Li, and F. Z. Peng, "Grid-connected boost-half-bridge photovoltaic microinverter system using repetitive current control and maximum power point tracking," *IEEE Transactions on power Electronics*, vol. 27, no. 11, pp. 4711–4722, 2012.

[24] O. Nezamuddin, J. Crespo, and E. C. dos Santos, "Design of a highly efficient microinverter," in *2016 IEEE 43rd Photovoltaic Specialists Conference (PVSC)*. IEEE, 2016, Conference Proceedings, pp. 3463–3468.

[25] S. Öztürk and I. Çadırcı, "A generalized and flexible control scheme for photovoltaic grid-tie microinverters," *IEEE Transactions on Industry Applications*, vol. 54, no. 1, pp. 505–516, 2017.

[26] A. Vasan, L. Laskai, and M. Ilic, "Defining humidity test duration for microinverter reliability assessment: A physics-of-failure approach," in *2017 IEEE Applied Power Electronics Conference and Exposition (APEC)*. IEEE, Conference Proceedings, pp. 2336–2340.

[27] G. TamizhMani, "Standardization and reliability testing of module-level power electronics (mlpe)," in *Proc. NREL Rel. Workshop*, 2015, pp. 1–18.

[28] Y. Li and R. Oruganti, "A low cost high efficiency inverter for photovoltaic ac module application," in *2010 35th IEEE Photovoltaic Specialists Conference*. IEEE, Conference Proceedings, pp. 002 853–002 858.

[29] S. Jain and V. Agarwal, "A single-stage grid connected inverter topology for solar pv systems with maximum power point tracking," *IEEE transactions on power electronics*, vol. 22, no. 5, pp. 1928–1940, 2007.

[30] B. Sahan, A. N. Vergara, N. Henze, A. Engler, and P. Zacharias, "A single-stage pv module integrated converter based on a low-power current-source inverter," *IEEE Transactions on Industrial Electronics*, vol. 55, no. 7, pp. 2602–2609, 2008.

[31] T. Kerekes, R. Teodorescu, P. Rodríguez, G. Vázquez, and E. Aldabas, "A new high-efficiency single-phase transformerless pv inverter topology," *IEEE Transactions on industrial electronics*, vol. 58, no. 1, pp. 184–191, 2009.

[32] M. E. Ahmed, M. Orabi, and O. M. AbdelRahim, "Two-stage micro-grid inverter with high-voltage gain for photovoltaic applications," *IET Power Electronics*, vol. 6, no. 9, pp. 1812–1821, 2013.

[33] R. Hasan, W. Hassan, M. Farhangi, S. Mekhilef, and W. Xiao, "Enhanced soft-switching strategy for flyback-based microinverter in pv power systems," *IET Renewable Power Generation*, vol. 13, no. 15, pp. 2830–2839, 2019.

[34] F. Evran, "Plug-in repetitive control of single-phase grid-connected inverter for ac module applications," *IET Power Electronics*, vol. 10, no. 1, pp. 47–58, 2017.

[35] D. Meneses, F. Blaabjerg, O. Garcia, and J. A. Cobos, "Review and comparison of step-up transformerless topologies for photovoltaic ac-module application," *IEEE Transactions on Power Electronics*, vol. 28, no. 6, pp. 2649–2663, 2012.

[36] W. Li, X. Lv, Y. Deng, J. Liu, and X. He, "A review of non-isolated high step-up dc/dc converters in renewable energy applications," in *2009 Twenty-Fourth Annual IEEE Applied Power Electronics Conference and Exposition*. IEEE, 2009, pp. 364–369.

[37] L.-S. Yang, T.-J. Liang, and J.-F. Chen, "Transformerless dc–dc converters with high step-up voltage gain," *IEEE Transactions on Industrial Electronics*, vol. 56, no. 8, pp. 3144–3152, 2009.

[38] M. N. Bhukya and V. R. Kota, "A quick and effective mppt scheme for solar power generation during dynamic weather and partial shaded conditions," *Engineering Science and Technology, an International Journal*, vol. 22, no. 3, pp. 869–884, 2019.

[39] A. Kihal, F. Krim, A. Laib, B. Talbi, and H. Afghoul, "An improved mppt scheme employing adaptive integral derivative sliding mode control for photovoltaic systems under fast irradiation changes," *ISA transactions*, vol. 87, pp. 297–306, 2019.

[40] S. Li, "A mppt speed optimization strategy for photovolatic system using vwp interval based on weather forecast," *Optik*, vol. 192, p. 162958, 2019.

[41] M. A. Uman, *The lightning discharge*. Courier Corporation, 2001.

[42] J. R. Dwyer and M. A. Uman, "The physics of lightning," *Physics Reports*, vol. 534, no. 4, pp. 147–241, 2014.

[43] P. Chowdhuri, J. Anderson, W. Chisholm, T. Field, M. Ishii, J. Martinez, M. Marz, J. McDaniel, T. McDermott, and A. Mousa, "Parameters of lightning strokes: a review," *IEEE Transactions on Power Delivery*, vol. 20, no. 1, pp. 346–358, 2005.

[44] V. Cooray, "The lightning flash, vol. 34," *Institution of Engineering and Technology (IET), Stevenage, UK*, 2003.

[45] Z. Yu, T. Zhu, Z. Wang, G. Lu, R. Zeng, Y. Liu, J. Luo, Y. Wang, J. He, and C. Zhuang, "Calculation and experiment of induced lightning overvoltage on power distribution line," *Electric Power Systems Research*, vol. 139, pp. 52–59, 2016.

[46] C. Gomes and V. Cooray, "Concepts of lightning return stroke models," *IEEE Transactions on Electromagnetic Compatibility*, vol. 42, no. 1, pp. 82–96, 2000.

[47] W. Jia and Z. Xiaoqing, "Double-exponential expression of lightning current waveforms," in *The 2006 4th Asia-Pacific Conference on Environmental Electromagnetics.* IEEE, 2006, pp. 320–323.

[48] F. Heidler, J. Cvetic, and B. Stanic, "Calculation of lightning current parameters," *IEEE Transactions on power delivery*, vol. 14, no. 2, pp. 399–404, 1999.

[49] S. Wang, S. Xie, C. Zhuang, Y. Ouyang, Y. Geng, R. Zeng, G. Liu, H. Cai, and T. Li, "Analysis of lightning-induced overvoltage waveform parameters," in *2018 34th International Conference on Lightning Protection (ICLP).* IEEE, Conference Proceedings, pp. 1–5.

[50] R. Bansal, *Fundamentals of engineering electromagnetics.* CRC press, 2018.

[51] M. Paolone, "Modeling of lightning-induced voltages on distribution networks for the solution of power quality problems, and relevant implementation in a transient program," *Department of Electrical Engineering Bologna, Italy: University of Bologna*, p. 117, 2001.

[52] Q. Yang, L. Yin, H. Liu, K. Wang, and J. Huang, "Measurement of lightning-induced overvoltage in power distribution lines using ceramic-capacitor insulator," *IEEE Transactions on Electromagnetic Compatibility*, vol. 61, no. 3, pp. 788–795, 2019.

[53] S. Rusck, "Induced lightning over-voltages on power-transmission lines with special reference to the over-voltage protection of low voltage networks," *Trans. Royal Intitute of Technology, Stockholm*, 1958.

[54] A. K. Agrawal, H. J. Price, and S. H. Gurbaxani, "Transient response of multiconductor transmission lines excited by a nonuniform electromagnetic field," *IEEE Transactions on electromagnetic compatibility*, no. 2, pp. 119–129, 1980.

[55] P. Chowdhuri and E. T. Gross, "Voltage surges induced on overhead lines by lightning strokes," in *Proceedings of the Institution of Electrical Engineers*, vol. 114, no. 12. IET, 1967, pp. 1899–1907.

[56] C. Nucci, F. Rachidi, M. Ianoz, and C. Mazzetti, "Comparison of two coupling models for lightning-induced overvoltage calculations," *IEEE Transactions on power delivery*, vol. 10, no. 1, pp. 330–339, 1995.

[57] J. C. Hernández, P. G. Vidal, and F. Jurado, "Lightning and surge protection in photovoltaic installations," *IEEE Transactions on power delivery*, vol. 23, no. 4, pp. 1961–1971, 2008.

[58] T. Noda, "A numerical simulation of transient electromagnetic fields for obtaining the step response of a transmission tower using the fdtd method," *IEEE Transactions on power delivery*, vol. 23, no. 2, pp. 1262–1263, 2008.

[59] V. Cooray and V. Scuka, "Lightning-induced overvoltages in power lines: Validity of various approximations made in overvoltage calculations," *IEEE transactions on electromagnetic compatibility*, vol. 40, no. 4, pp. 355–363, 1998.

[60] N. Ahmad, M. Ab-Kadir, M. Izadi, N. Azis, M. Radzi, N. Zaini, and M. Nasir, "Lightning protection on photovoltaic systems: A review on current and recommended practices," *Renewable and Sustainable Energy Reviews*, vol. 82, pp. 1611–1619, 2018.

[61] C. A. Charalambous, N. D. Kokkinos, and N. Christofides, "External lightning protection and grounding in large-scale photovoltaic applications," *IEEE transactions on electromagnetic compatibility*, vol. 56, no. 2, pp. 427–434, 2013.

[62] R. Zoro, "Tropical lightning current parameters and protection of transmission lines," *International Journal on Electrical Engineering and Informatics*, vol. 11, no. 3, pp. 506–514, 2019.

[63] IEC, *62305-1: 2010 - Protection against Lightning: Part 1: General Principles*, 2010.

[64] IEC, *62305-2: 2010 - Protection against Lightning: Part 2: Risk Management*, 2010.

[65] IEC, *62305-3: 2010 - Protection against Lightning: Part 3: Physical damage to life structures and life hazard*, 2010.

[66] M. Mitolo, "Protective bonding conductors: an iec point of view," in *IEEE Systems Technical Conference on Industrial and Commercial Power 2005.* IEEE, Conference Proceedings, pp. 178–183.

[67] C. A. Christodoulou, L. Ekonomou, A. Mitropoulou, V. Vita, and I. Stathopulos, "Surge arresters' circuit models review and their application to a hellenic 150 kv transmission line," *Simulation Modelling Practice and Theory*, vol. 18, no. 6, pp. 836–849, 2010.

[68] G. L. Piparo, T. Kisielewicz, C. Mazzetti, and R. Pomponi, "Assessment of probability of damage of an apparatus protected by a surge protective devices system," *International Journal of Electrical Power and Energy Systems*, vol. 75, pp. 38–49, 2016.

[69] Z. He and Y. Du, "Influence of different factors on coordination of two cascaded spds," *Electric Power Systems Research*, vol. 139, pp. 139–145, 2016.

[70] T. Kisielewicz, G. L. Piparo, F. Fiamingo, C. Mazzetti, B. Kuca, and Z. Flisowski, "Factors affecting selection, installation and coordination of surge protective devices for low voltage systems," *Electric Power Systems Research*, vol. 113, pp. 220–227, 2014.

[71] A. Bayadi, N. Harid, K. Zehar, and S. Belkhiat, "Simulation of metal oxide surge arrester dynamic behavior under fast transients," in *International Conference on Power Systems Transients, New Orleans, USA*, 2003.

[72] F. Fernandez and R. Diaz, "Metal-oxide surge arrester model for fast transient simulations," in *Proceedings of 2001 International conference on power system transients*. Citeseer, 2001, pp. 681–687.

[73] A. Rousseau and P. Gruet, "Lightning risk assessment for explosives sites taking into account zones 0, 1 and 2 and environmental risk," in *GROUND'2010 and 4. LPE. International Conference on Grounding and Earthing and 4. International Conference on Lightning Physics and Effects*, Conference Proceedings, pp. 86–90.

[74] IEC, *61643-11: 2011 - Low-voltage surge protective devices Part 11: Surge protective devices connected to low-voltage power systems — Requirements and test methods*, 2011.

[75] IEC, *61643-12: 2008 - Low-voltage surge protective devices Part 12: Surge protective devices connected to low-voltage power distribution systems — Selection and application principles*, 2008.

[76] IEC, *61643-31: 2018 - Low-voltage surge protective devices: Part 31: Requirements and test methods for SPDs for photovoltaic installations*, 2018.

[77] IEC, *61643-32: 2017 - Low-voltage surge protective devices: Part 32: Surge protective devices connected to the d.c side of photovoltaic installations - Selection and application principles*, 2017.

[78] M. Wetter, J. Schimanski, C. Birkholz, and K. Scheibe, "Energetic coordination of mov-based surge protective devices," in *2010 30th International Conference on Lightning Protection (ICLP)*. IEEE, Conference Proceedings, pp. 1–5.

[79] C. A. Christodoulou, F. A. Assimakopoulou, I. F. Gonos, and I. A. Stathopulos, "Simulation of metal oxide surge arresters behavior," in *2008 IEEE Power Electronics Specialists Conference*. IEEE, 2008, pp. 1862–1866.

[80] V. Milardić, I. Uglesic, and I. Pavić, "Selection of surge protective devices for low-voltage systems connected to overhead line," *IEEE Transactions on Power Delivery*, vol. 25, no. 3, pp. 1530–1537, 2010.

[81] P. Unahalekhaka and S. Phonkaphon, "Simulation of surge protective devices for low-voltage systems connected to digital subscriber line access multiplexer."

[82] F. Fiamingo, M. Marzinotto, C. Mazzetti, Z. Flisowski, G. L. Piparo, and G. Amicucci, "Evaluation of spd protection distance in low-voltage systems," *Journal of electrostatics*, vol. 65, no. 5-6, pp. 363–370, 2007.

[83] A. Gomes, M. Ab Kadir, C. Gomes, and Z. Khurshid, "Development of a portable type i to iii lightning surge protective device for compact structures," in *2018 34th International Conference on Lightning Protection (ICLP)*. IEEE, 2018, pp. 1–9.

[84] J. He, "Discussions on factors influencing the effective protection distance of spd to loads," in *2015 Asia-Pacific Symposium on Electromagnetic Compatibility (APEMC)*. IEEE, Conference Proceedings, pp. 420–423.

[85] P. Vangala, M. Ropp, K. Haggerty, K. Lynn, and W. Wilson, "Field measurements of lightning-induced voltage transients in pv arrays," in *2008 33rd IEEE Photovoltaic Specialists Conference*. IEEE, Conference Proceedings, pp. 1–4.

[86] Q. Sun, X. Zhong, J. Liu, F. Wang, S. Chen, L. Zhong, and X. Bian, "Three-dimensional modeling on lightning induced overvoltage for photovoltaic arrays installed on mountain," *Journal of Cleaner Production*, vol. 288, p. 125084, 2021.

[87] Y. Tu, C. Zhang, J. Hu, S. Wang, W. Sun, and H. Li, "Research on lightning overvoltages of solar arrays in a rooftop photovoltaic power system," *Electric power systems research*, vol. 94, pp. 10–15, 2013.

[88] A. Formisano, C. Petrarca, J. C. Hernández, and F. J. Muñoz-Rodríguez, "Assessment of induced voltages in common and differential-mode for a pv module due to nearby lightning strikes," *IET Renewable Power Generation*, vol. 13, no. 8, pp. 1369–1378, 2019.

[89] N. H. A. Rahim, Z. A. Baharudin, and M. N. Othman, "Investigation of wave propagation to pv-solar panel due to induced overvoltage generated by lightning impulse generator," *Adv. Sci. Technol. Lett.(Energy)*, vol. 38, pp. 15–22, 2013.

[90] N. Zaini, M. Ab-Kadir, M. Radzi, M. Izadi, N. Ahmad, N. Azis, and M. Nasir, "On the effect of surge protection devices (spds) placement for grid-connected solar pv farm," in

2018 34th International Conference on Lightning Protection (ICLP). IEEE, Conference Proceedings, pp. 1–5.

[91] N. I. Ahmad, Z. Ali, M. Osman, N. H. Zaini, and M. H. Roslan, "Impacts of lightning-induced overvoltage on a hybrid solar pv–battery energy storage system," *Applied Sciences*, vol. 11, no. 8, p. 3633, 2021.

[92] E. Pons and R. Tommasini, "Lightning protection of pv systems," in *2013 4th International Youth Conference on Energy (IYCE)*. IEEE, Conference Proceedings, pp. 1–5.

[93] Z. Mohammed, H. Hizam, and C. Gomes, "Lightning-induced transient effects in a hybrid pv–wind system and mitigation strategies," *Electric Power Systems Research*, vol. 174, p. 105882, 2019.

[94] J. Woodworth and D. Limburg, "Arrester v–i characteristics tool," in *Arresterworks. com, US*, 2017.

List of Publications

Conference Proceedings

Mosamane, S. and Gomes, C. (2022). *Lightning-induced Overvoltages Risk for Microinverters in Photovoltaic Installations.* 30th South African Universities Power Engineering Conference (SAUPEC), Durban.

Mosamane, S. and Gomes, C. (2022). *Lightning-induced overvoltage protection for microinverters using surge protection devices.* 36th International Conference on Lightning Protection (ICLP), Cape Town.

Journal

Mosamane, S. and Gomes, C. (2022). Simulations and Experimental Validation of lightning-induced voltages on a PV system in both Common Mode and Differential Mode. *IEEE Access.* (Under Review)